



**NAVAL
POSTGRADUATE
SCHOOL**

MONTEREY, CALIFORNIA

THESIS

**A SOLAR BRAYTON CYCLE WITH METAL PHASE
CHANGE THERMAL STORAGE**

by

Barrett C. Roof

June 2017

Thesis Advisor:
Second Reader:

Anthony J. Gannon
Garth V. Hobson

Approved for public release. Distribution is unlimited.

THIS PAGE INTENTIONALLY LEFT BLANK

REPORT DOCUMENTATION PAGE			<i>Form Approved OMB No. 0704-0188</i>	
Public reporting burden for this collection of information is estimated to average 1 hour per response, including the time for reviewing instruction, searching existing data sources, gathering and maintaining the data needed, and completing and reviewing the collection of information. Send comments regarding this burden estimate or any other aspect of this collection of information, including suggestions for reducing this burden, to Washington headquarters Services, Directorate for Information Operations and Reports, 1215 Jefferson Davis Highway, Suite 1204, Arlington, VA 22202-4302, and to the Office of Management and Budget, Paperwork Reduction Project (0704-0188) Washington, DC 20503.				
1. AGENCY USE ONLY <i>(Leave blank)</i>	2. REPORT DATE June 2017	3. REPORT TYPE AND DATES COVERED Master's Thesis		
4. TITLE AND SUBTITLE A SOLAR BRAYTON CYCLE WITH METAL PHASE CHANGE THERMAL STORAGE			5. FUNDING NUMBERS	
6. AUTHOR(S) Barrett C. Roof				
7. PERFORMING ORGANIZATION NAME(S) AND ADDRESS(ES) Naval Postgraduate School Monterey, CA 93943-5000			8. PERFORMING ORGANIZATION REPORT NUMBER	
9. SPONSORING /MONITORING AGENCY NAME(S) AND ADDRESS(ES)			10. SPONSORING / MONITORING AGENCY REPORT NUMBER	
11. SUPPLEMENTARY NOTES The views expressed in this thesis are those of the author and do not reflect the official policy or position of the Department of Defense or the U.S. Government. IRB number <u> N/A </u> .				
12a. DISTRIBUTION / AVAILABILITY STATEMENT Approved for public release. Distribution is unlimited.			12b. DISTRIBUTION CODE	
13. ABSTRACT (maximum 200 words) <p>The Department of the Navy (DON) has prioritized the establishment of a robust renewable energy platform for its installations. Solar energy has emerged in a way that has provided viable alternatives. The use of solar energy, however, poses a problem of maintaining continuity of power during hours when sunlight is not available. The development of Thermal Energy Storage (TES), while addressing this problem, introduces complexities that can reduce overall plant efficiency. This research aims to simplify the plant design in a way that minimizes such complexities and maximizes efficiency.</p> <p>The research in this thesis explores a new design that integrates static molten metal baths with the solar collector. The proposed initial design is centered on a simple open air Brayton cycle. Aluminum was selected as the phase change metal, providing latent heat to the air in the collector during hours of non-daylight through freezing. The research focuses on the thermodynamic analysis of the system, initial collector design requirements, and minimum volumetric requirements of the aluminum phase change metal. An analytical and numerical flow optimization study of the system was performed for comparison to design calculations.</p>				
14. SUBJECT TERMS thermal energy storage, thermodynamics, heat transfer, fluid dynamics			15. NUMBER OF PAGES 129	
			16. PRICE CODE	
17. SECURITY CLASSIFICATION OF REPORT Unclassified	18. SECURITY CLASSIFICATION OF THIS PAGE Unclassified	19. SECURITY CLASSIFICATION OF ABSTRACT Unclassified	20. LIMITATION OF ABSTRACT UU	

THIS PAGE INTENTIONALLY LEFT BLANK

Approved for public release. Distribution is unlimited.

**A SOLAR BRAYTON CYCLE WITH METAL PHASE CHANGE THERMAL
STORAGE**

Barrett C. Roof
Lieutenant, United States Navy
B.S., Thomas Edison State University, 2008

Submitted in partial fulfillment of the
requirements for the degree of

MASTER OF SCIENCE IN MECHANICAL ENGINEERING

from the

**NAVAL POSTGRADUATE SCHOOL
June 2017**

Approved by: Anthony J. Gannon, Ph.D.
Thesis Advisor

Garth V. Hobson, Ph.D.
Second Reader

Garth V. Hobson, Ph.D.
Chair, Department of Mechanical and Aerospace Engineering

THIS PAGE INTENTIONALLY LEFT BLANK

ABSTRACT

The Department of the Navy (DON) has prioritized the establishment of a robust renewable energy platform for its installations. Solar energy has emerged in a way that has provided viable alternatives. The use of solar energy, however, poses a problem of maintaining continuity of power during hours when sunlight is not available. The development of Thermal Energy Storage (TES), while addressing this problem, introduces complexities that can reduce overall plant efficiency. This research aims to simplify the plant design in a way that minimizes such complexities and maximizes efficiency.

The research in this thesis explores a new design that integrates static molten metal baths with the solar collector. The proposed initial design is centered on a simple open air Brayton cycle. Aluminum was selected as the phase change metal, providing latent heat to the air in the collector during hours of non-daylight through freezing. The research focuses on the thermodynamic analysis of the system, initial collector design requirements, and minimum volumetric requirements of the aluminum phase change metal. An analytical and numerical flow optimization study of the system was performed for comparison to design calculations.

THIS PAGE INTENTIONALLY LEFT BLANK

TABLE OF CONTENTS

I.	INTRODUCTION.....	1
A.	ENERGY GOALS	1
B.	BACKGROUND AND LITERATURE REVIEW	3
1.	Sensible Heat Storage	6
2.	Latent Heat Storage.....	8
II.	THERMODYNAMIC ANALYSIS	11
A.	GOVERNING EQUATIONS	11
1.	Continuity	11
2.	First Law of Thermodynamics	12
3.	Second Law of Thermodynamics	12
B.	CYCLE ANALYSIS	13
1.	Pressure and Temperature.....	13
2.	Specific Work and Heat.....	21
3.	Efficiency, Power, and Mass Flow.....	22
III.	SOLAR COLLECTOR DESIGN.....	25
A.	GEOMETRY.....	25
1.	Collector.....	26
2.	Heat Exchanger Ducting	28
B.	ALUMINUM REQUIREMENTS	36
1.	Mass and Volume.....	36
2.	Collector Duct Thickness	37
C.	HEAT FLUX	39
D.	PRESSURE DROP	41
IV.	OPTIMIZATION.....	45
A.	ANALYTICAL MODEL.....	46
B.	NUMERICAL MODEL	52
1.	Model Construction	52
2.	Boundary Conditions.....	54
3.	Initial Run.....	55
4.	Optimization.....	58
V.	DISCUSSION	63
VI.	CONCLUSION	65

VII. RECOMMENDATIONS.....	67
APPENDIX A. MATLAB CODE FOR ANALYSIS OF PRESSURE DROP AND HEAT FLUX OF 50 KW PLANT	69
APPENDIX B. MATLAB CODE FOR ANALYTICAL OPTIMIZATION OF 50 KW PLANT	71
APPENDIX C. ANSYS-CFX SOLUTION REPORT FOR 50KW PLANT	74
APPENDIX D. ANSYS-CFX OPTIMIZATION REPORT FOR 50KW PLANT	85
APPENDIX E. ANSYS-CFX OPTIMIZATION RAW DATA FOR 50KW PLANT	105
LIST OF REFERENCES	107
INITIAL DISTRIBUTION LIST	109

LIST OF FIGURES

Figure 1.	Installed Solar Capacity by Branch. Source: [4].....	2
Figure 2.	Concentrating Solar Resource of the United States. Source: [7].....	4
Figure 3.	Centralized Solar Thermal Plant with Thermal Energy Storage. Source: [9].....	5
Figure 4.	Andasol Parabolic Trough Solar Power Plant with Molten Salt TES. Source: [13].....	7
Figure 5.	Parabolic Trough Solar Power Plant Utilizing Molten Salt TES. Source: [15].....	7
Figure 6.	Open Air Brayton Cycle with Solar Collector.....	13
Figure 7.	Temperature-Entropy Diagram of Brayton Cycle. Adapted from [21].....	14
Figure 8.	Design Cycle Net Work vs. Compressor Pressure Ratio.....	18
Figure 9.	Cycle Net Work vs. Compressor Pressure Ratio for Seasonal Variations.....	19
Figure 10.	Side View of Solar Collector with Multiple Stacked Ducts.	25
Figure 11.	Top Down View of Solar Collector.....	26
Figure 12.	Single 3-D Square Duct with Molten Aluminum.	28
Figure 13.	Collector Length vs. Number of Ducts.....	33
Figure 14.	Heat Flux vs. Number of Ducts (Without Aluminum).	40
Figure 15.	Heat Flux vs. Number of Ducts (With and Without Aluminum).	41
Figure 16.	Collector Pressure Drop vs. Number of Ducts.....	43
Figure 17.	Mean Temperature Profile for Fully Developed Flow, Constant Temperature Wall. Source: [25]	45
Figure 18.	Analytical Solution of Power vs. Mass Flow for a 50 kW Plant.	48
Figure 19.	Analytical Solution of Collector Temperature Difference vs. Mass Flow for a 50 kW Plant.	49

Figure 20.	Analytical Solution of Thermal Efficiency vs. Mass Flow for a 50 kW Plant.....	50
Figure 21.	Analytical Solution of Heat Exchanger Effectiveness vs. Mass Flow for a 50 kW Plant.	51
Figure 22.	SolidWorks Drawing of Single Duct Model.....	53
Figure 23.	ANSYS-CFX Mesh for Single Duct Model.	53
Figure 24.	ANSYS-CFX Default Domain with Boundaries for Single Duct Model.	55
Figure 25.	ANSYS-CFX Mass and Momentum Solution Convergence for Single Duct Model.	56
Figure 26.	Collector Duct Outlet Temperature Profile.....	57
Figure 27.	Collector Duct Outlet Velocity Profile.	58
Figure 28.	Comparison of Analytical and Numerical Solutions for Collector Outlet Temperature vs. Mass Flow.....	59
Figure 29.	Comparison of Analytical and Numerical Solutions for Collector Temperature Rise vs. Mass Flow.....	60
Figure 30.	Comparison of Analytical and Numerical Solutions for Power vs. Mass Flow.....	61

LIST OF TABLES

Table 1.	Efficiencies of Thermal Energy Storage Systems. Adapted from [8].	6
Table 2.	Latent Heat Material Properties of Aluminum and Molten Salt. Adapted from [10, 19].	9
Table 3.	Ideal Gas Properties of Air.	18
Table 4.	Maximum Specific Net Work and Compressor Pressure Ratios.	20
Table 5.	Open Brayton Cycle Design Parameters.	22
Table 6.	Summary of Design Limits.	23
Table 7.	Collector Duct Heat Transfer Parameters.	32
Table 8.	Collector Length Compared to Number of Ducts.	33
Table 9.	Collector Duct Flow Parameters and Hydraulic Diameter.	35
Table 10.	Minimum Aluminum Volumetric Requirement.	37
Table 11.	Aluminum Thickness Compared to Number of Ducts.	38
Table 12.	Ducting Requirements for Heat Flux Orders of Magnitude.	40
Table 13.	Design and Maximum Power Calculations for a 50 kW Plant.	49
Table 14.	Sutherland's Constant and Reference Properties.	54
Table 15.	Maximum Power and Pressure drop Based on Analytical and Numerical Solutions.	62

THIS PAGE INTENTIONALLY LEFT BLANK

LIST OF ACRONYMS AND ABBREVIATIONS

1GW	One Gigawatt
2-D	Two Dimensional
CFD	Computational Fluid Dynamics
DOD	Department of Defense
DON	Department of the Navy
HTF	Heat Transfer Fluid
IRENA	International Renewable Energy Agency
NREL	National Renewable Energy Laboratory
PCM	Phase Change Material
PPA	Power Purchase Agreement
SECNAV	Secretary of the Navy
SEIA	Solar Energy Industries Association
TES	Thermal Energy Storage
T-S	Temperature Entropy

THIS PAGE INTENTIONALLY LEFT BLANK

NOMENCLATURE

<u>Symbols</u>	<u>Description</u>
a	Quadratic Constant
A	Area
b	Quadratic Constant
c	Quadratic Constant
C_p	Specific Heat Capacity (Constant Pressure Process)
C_v	Specific Heat Capacity (Constant Volume Process)
d	Outer Diameter
D_h	Hydraulic Diameter
f	Friction Factor
G	Solar Irradiance
g	Gravitational Constant
h	Enthalpy, Heat Transfer Coefficient
i	Thickness
k	Thermal Conductivity
L	Length
m	Mass
\dot{m}	Mass Flow Rate
N	Number of Ducts
Nu	Nusselt Number
P	Pressure
q	Specific Heat Transfer
Q	Total Heat Transfer
\dot{Q}	Heat Transfer Rate
R	Gas Constant
Re	Reynold's Number
r_p	Pressure Ratio
s	Specific Entropy

T	Temperature
t	Time
u	Velocity
V	Volume
w	Specific Work
\dot{W}	Work Rate
ΔP	Pressure Difference
ΔT	Temperature Difference
α	Scaling Function
ε	Emissivity, Effectiveness
γ	Specific Heat Ratio
η	Thermal Efficiency
ρ	Density, Reflectivity
μ	Dynamic Viscosity
σ	Stefan-Boltzmann Constant

ACKNOWLEDGMENTS

To my wife, Kayla: your love and support have always been the bedrock of my success. To my mother, Linda, and father, Lin, your guidance and sacrifice have paved the way for me to achieve anything to which I set my mind. You all have believed in me, and for that I say, thank you.

THIS PAGE INTENTIONALLY LEFT BLANK

I. INTRODUCTION

The purpose of this thesis is to present an analysis of a new solar thermal plant design that integrates Thermal Energy Storage (TES) into the solar collector heat exchanger. The availability of sunlight is intermittent; therefore, TES systems are required to supplement the solar energy in order to meet the demands of supported installations. TES as separate sub-systems, however, can introduce complexities that are costly and reduce the overall efficiency of the plant. The design of the plant in this thesis focuses on simplicity in a way that eliminates the complexities presented by current TES systems. The goal is to provide a launch pad for continued research and refinement of the design.

The standard Brayton cycle describes the basic design of the plant. The working fluid, air, receives heat directly via the concentration of the sun's radiation into the solar collector heat exchanger. The heat exchanger air ducts in the prototype design are embedded in a static molten aluminum bath. This bath requires no pumping of the metal and simply freezes and thaws around the air ducts. The latent heat energy from this phase change metal continues to heat the air as the metal freezes. This thesis provides a thermodynamic analysis of the plant, minimum volumetric requirements of the aluminum phase change metal, as well as basic geometric design requirements of the solar collector.

In addition to the prototype design requirements, the air flow was optimized to observe plant behavior. Given a specified design power, a basic thermodynamic analysis yields a design mass flow specification. By optimizing the mass flow for power, however, the same plant design could potentially exceed design power, allowing for a transitional operating range between day and night. Analytical and numerical methods were conducted in this study to determine the effects on power while varying mass flow.

A. ENERGY GOALS

The United States Department of Defense (DOD) is the largest consumer of energy of all the federal government agencies, making up at least 80% of the government's energy consumption, as stated by Schwartz [1]. Of the DOD's energy use,

Schwartz [1] also included that installations make up 25% of that share. In response, the DOD has taken action to revise its strategy toward energy, investing heavily in the research and development of renewable energy sources used to supplement commercial grid power for defense installations. Ultimately, the goal of the DOD, as discussed by Feldman [2], is to produce 25% of its energy from renewables by the year 2025.

The Department of the Navy (DON) has responded to the DOD’s energy goals with a more aggressive agenda. In the DON’s *Strategy for Renewable Energy*, Secretary of the Navy (SECNAV) Ray Mabus set five energy goals for the Navy, one that directly applies to energy use by installations. He directed that “by 2020, DON will produce at least 50% of shore based energy requirements from alternative sources; 50% of DON installations will be net-zero” [3]. Security and independence were asserted by Mabus [3] as the Navy’s two energy priorities. Based on these priorities, the DON has taken action to reduce its carbon foot print both operationally and with its installations.

The DON currently leads the DOD in solar energy development, as shown by the Solar Energy Industries Association (SEIA) [4]. Figure 1 illustrates the comparison of the Navy to other branches of service with regard to installed solar energy.

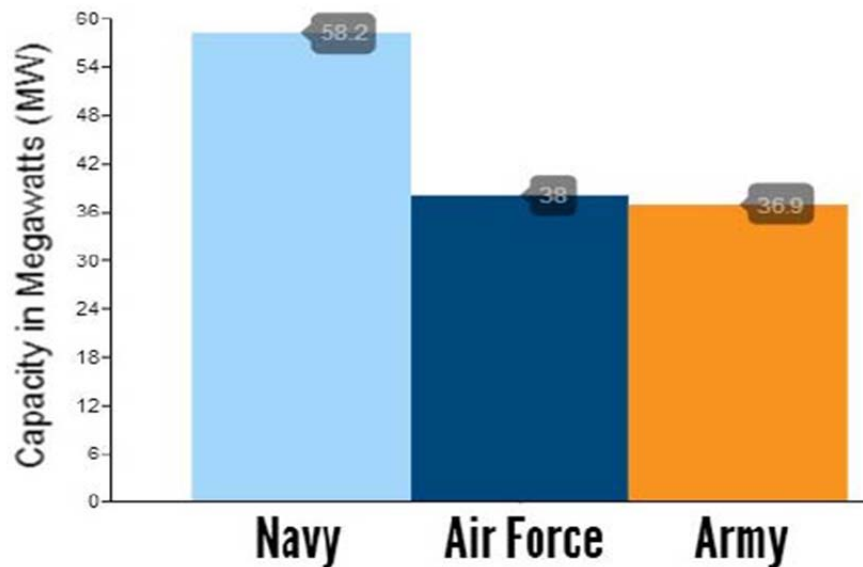


Figure 1. Installed Solar Capacity by Branch. Source: [4].

By comparison, the Navy has made significant gains over its counterparts in the development and implementation of solar energy. As of 2013, due largely in part to the implementation of the Navy's One Gigawatt (1GW) program, the Navy has installed over 58MW for various installations, as stated by SEIA [4]. It is through this program that the Navy executes its goals set by SECNAV. According to McGinn [5], by 2015 the Navy had actually exceeded its energy goals for installations, but not entirely due to organic renewable energy production on its own installations. Part of the 1GW program included provisions known as Power Purchase Agreements (PPA) that allow the procurement of renewable energy from outside commercial sources, according to the DON [6]. While PPAs might be a necessity for some installations where land availability is a challenge, they do not allow installations to operate independently from commercial grids. For true energy security, an installation would need to produce its own power through organic growth of its power production.

Installations continue to be a viable candidate for the development of solar energy. Unlike vessels and other forms of operational equipment where space is limited, shore based installations provide the necessary space to build full-scale plants capable of supplying a significant share of the demand.

While solar power is promising in enabling the DON achieve its strategic goals, it does not come without challenges. The primary concern of utilizing solar energy to power facilities is overcoming the intermittent loss of the power source, the sun. It is during these times that the disruption of power must be addressed, especially as a matter of security for DOD installations.

B. BACKGROUND AND LITERATURE REVIEW

The sun's radiation is an excellent source of clean renewable energy. Many factors, however, can cause disruptions in the power source such as non-daylight hours, adverse weather conditions (cloud cover), and seasonal variations throughout the year. These factors are more prominent in some geographical regions than others that can further complicate the planning and development of solar renewable energy in DOD installations across the nation.

The National Renewable Energy Laboratory (NREL) [7] published a map of the United States that illustrates by color code the variance of concentrating solar resource on an average annual basis. Figure 2 illustrates how the change in local geographic climate across the country can provide either more or less advantage for the utilization of concentrating solar thermal energy.

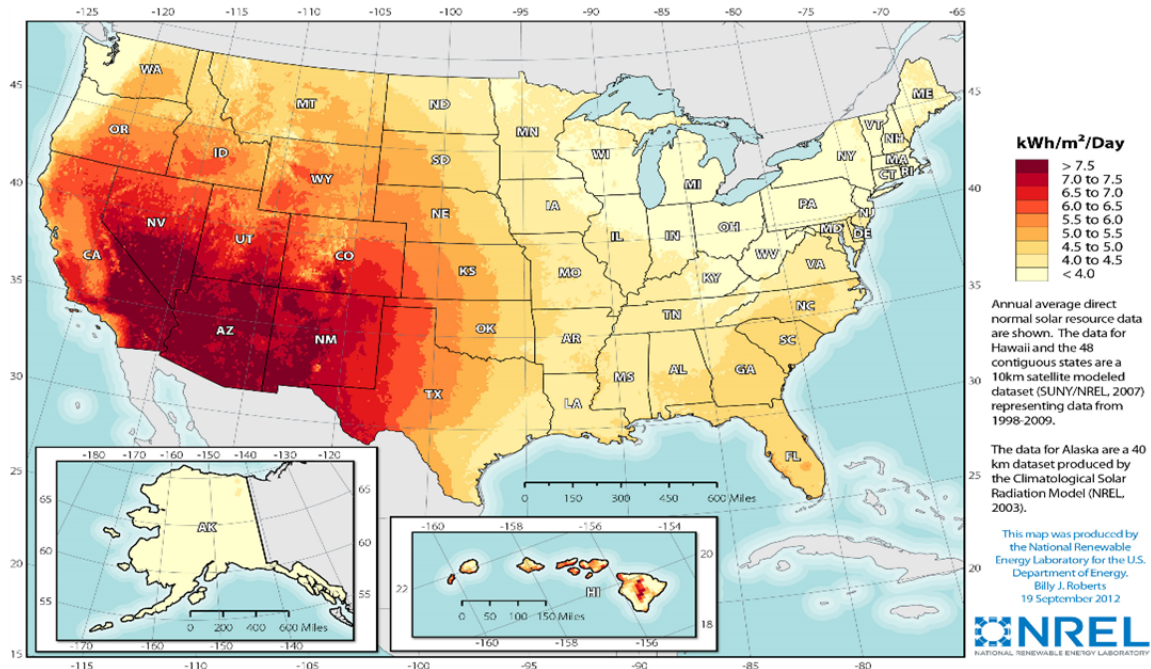


Figure 2. Concentrating Solar Resource of the United States. Source: [7].

The southern regions of California and Nevada, as well as Arizona and New Mexico, provide the best prospects for the development of solar power due to the generally dry and sunny climates. In other regions weather and seasonal variations are more prominent that result in a greater need for efficient TES systems to supplement the solar energy source.

Thermal Energy Storage refers to methods where thermal energy is extracted and stored for later use, as described by the International Renewable Energy (IRENA) [8]. Many design concepts to supplement larger scale concentrating solar power plants currently exist that achieve this purpose and typically fall into two main categories: sensible heat storage and latent heat storage, both of which were discussed by IRENA

[8]. Figure 3 is an example of a centralized solar thermal plant that uses thermal salt thermal energy storage.



Figure 3. Centralized Solar Thermal Plant with Thermal Energy Storage.
Source: [9].

IRENA published general efficiency ratings for TES modes in Table 1. TES systems are not 100% efficient. All forms of TES will lose some heat to the surroundings that can be mitigated through proper insulation technologies. Most forms of TES, however, require energy in the form of pumps or other devices to circulate the energy back into the cycle for continued power. Heat losses and design complexities can therefore impact the efficiency of these systems.

Table 1. Efficiencies of Thermal Energy Storage Systems. Adapted from [8].

TES Mode	Efficiency [%]
Sensible Heat	50-90
Latent Heat	75-90

1. Sensible Heat Storage

Sensible heat TES refers to methods where energy is transferred to a medium without the involvement of a phase change. Many designs using this method have two reservoirs of hot and cold media. Common sensible heat storage systems use water or molten salts as the heat transfer medium.

While the cost of such systems may be relatively low, the volumetric requirements are higher due to the lower energy density of these materials, as discussed by IRENA [8]. These systems require additional energy to circulate the media in order to continue powering the cycle that can lead to lower plant efficiency and increased plant complexity.

Herrmann and Kearney [10] show how sensible heat TES systems are among the most widely used form, with molten salts being the preferred candidate for larger scale plants. Other forms have been investigated, such as water. While hot water storage is inexpensive and easy to procure, its use is typically limited to micro grids, as discussed by Hinke [11]. Water has a low energy density; therefore, the resulting large volumetric requirements could be problematic when scaling up for commercial use. For this reason, existing commercial solar plants have widely been using molten salts, such as the Andasol Power Station in Figure 4, located in Andalusia, Spain. The Andasol Power Station in Spain operates a molten salt sensible heat thermal energy storage system. It consists of three power plants, each rated at 50 MW, and provides heating from thermal storage for up to eight hours [12].



Figure 4. Andasol Parabolic Trough Solar Power Plant with Molten Salt TES. Source: [13].

Current designs of molten salt TES systems are complex, involving the circulation of up to three heat transfer mediums: a heat transfer fluid (HTF), typically oil, the molten salt, and a Rankine cycle working fluid (water), as stated by Herrmann and Kearney [10, 14]. Figure 5 provides an illustration of a typical molten salt TES system powering a Rankine cycle with a parabolic trough collector.

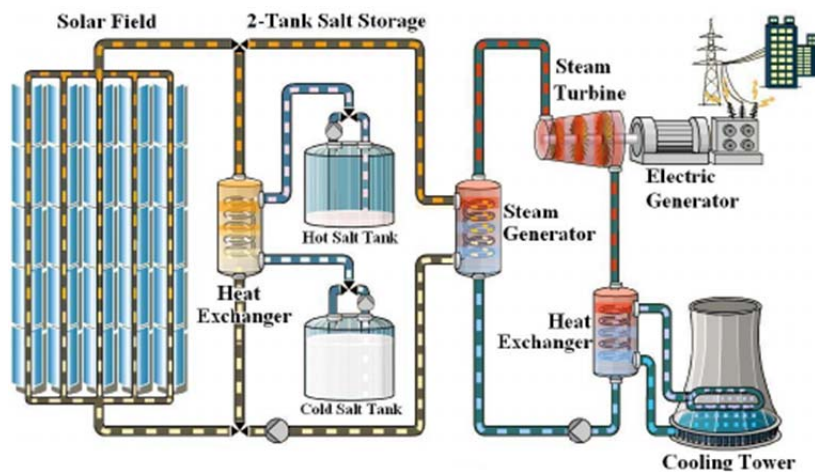


Figure 5. Parabolic Trough Solar Power Plant Utilizing Molten Salt TES. Source: [15].

In this system, the HTF is heated through the parabolic troughs that direct the sun's radiation to heat transfer pipes. The hot HTF is circulated to power the Rankine cycle as well as heat the molten salts that are circulated through a common heat exchanger, shown by Abutayeh et al. [14]. During times when the sunlight is not available, the molten salts are then recirculated while heating the HTF to power the Rankine cycle, as discussed by Abutayeh et al. [14].

Complexity is often the main disadvantage of using molten salts as thermal energy storage, as well as the added volumetric requirements, although efforts have been made to explore design variations that address these problems. For example, Gil et al. [16] proposed a new concept that reduced the molten salt storage volume to one tank that is directly heated by the sun. The design prototype would also remove the need for pumping the salts as a result.

2. Latent Heat Storage

Other forms of TES systems utilize the latent heat of phase change materials (PCM) to provide additional thermal energy needed to power the cycle. In general, the sun's radiation is used to melt a particular PCM at a constant temperature while the energy from the subsequent refreezing process is transferred back into the system. Unlike sensible heat storage, PCMs enable a more controlled form of energy transfer, as discussed by IRENA [8] as the temperature of the medium remains constant throughout the phase change. The energy density of PCMs can be much higher than that of sensible heat media, especially for metals, according to Li et al. [17], resulting in reduced volumetric requirements.

Metals as a phase change material are an excellent form of TES. In addition to the higher energy density compared to sensible heat media, Kotze and von Backstrom [18] discuss how metals typically have a much higher conductivity that greatly enhances the heat transfer rate when the TES is in use. The metal selected for the integrated latent heat thermal storage in this thesis is Aluminum, based on its thermo-physical properties that make it an ideal candidate for Brayton cycle operation.

Jiang et al. [19] researched the possibility of using salt as a phase change material, exploiting its latent heat abilities, vice sensible heat. As shown in Table 2. the molten salt under investigation, Na₂CO₃-NaCl showed comparable melting temperature and heat of fusion specifications to that of standard aluminum. The aluminum, however, has a far superior thermal conductivity for heat transfer.

Table 2. Latent Heat Material Properties of Aluminum and Molten Salt.
Adapted from [10, 19].

Medium	Melting Temperature [C]	Heat of Fusion [kJ/kg]	Thermal Conductivity [W/m-K]
Molten Salt	637	332	2
Aluminum	660	398	205

THIS PAGE INTENTIONALLY LEFT BLANK

II. THERMODYNAMIC ANALYSIS

When designing a new power system, the basic operating limits must first be established as a foundation to guide the design of the components. The first step is to conduct a thermodynamic analysis of the cycle based on known parameters and uncontrolled operating conditions, such as the atmosphere.

A. GOVERNING EQUATIONS

The governing equations of mass, energy, and entropy provide a complete description the cycle. These equations are coupled with reasonable assumptions of the fluid and processes that allow for the calculation of pressure, temperature, heat transfer, and work.

1. Continuity

The mass of a control volume is accounted for by the continuity equation that states that mass can neither be created nor destroyed. The mathematical equation that accounts for the sum of all mass entering the control volume, exiting the control volume, and any rate of change within, is commonly known.

$$\frac{\partial \rho}{\partial t} + \frac{\partial(\rho u)}{\partial x} + \frac{\partial(\rho v)}{\partial y} + \frac{\partial(\rho w)}{\partial z} = 0 \quad (1)$$

This equation describes the continuity of mass in Cartesian coordinates. In thermodynamics, a broader definition is used to account for the sum of the mass flows entering and exiting a system, as well as any change inside.

$$\frac{dm_{c.v.}}{dt} = \sum \dot{m}_i - \sum \dot{m}_e \quad (2)$$

Power systems such as the cycle analyzed in this thesis, are typically analyzed as steady state processes, where the rate of change of mass equals zero. Therefore, the continuity equation, as applied to the analysis of a single entry-single exit system, can be written as:

$$\dot{m}_i = \dot{m}_e = \dot{m} \quad (3)$$

From this expression, the mass flow entering the system equals the mass flow exiting the system, and therefore the subscript can be removed. This key relationship will further guide the first and second law analysis of the plant.

2. First Law of Thermodynamics

The first law of thermodynamics describes the continuity of energy [20]. Similar to the law of conservation of mass, energy can neither be created nor destroyed. This law accounts for all sources of energy entering and exiting a system: heat, work, and flow.

$$\frac{dE_{c.v.}}{dt} = \dot{Q}_{c.v.} - \dot{W}_{c.v.} + \dot{m}_i \left(h_i + \frac{1}{2}V_i^2 + gZ_i \right) - \dot{m}_e \left(h_e + \frac{1}{2}V_e^2 + gZ_e \right) \quad (4)$$

When analyzing plant cycles at steady state, it is assumed that the change in height and the change in velocity are negligible across each process. Additionally, since there is no change in the mass flow throughout the cycle, the first law equation is reduced to the following format and will be used to describe each process of the cycle.

$$\dot{Q}_{c.v.} - \dot{W}_{c.v.} + \dot{m}(h_i - h_e) = 0 \quad (5)$$

3. Second Law of Thermodynamics

The second law of thermodynamics, in conjunction with the first law, provides the total basis for a cycle analysis. While the first law conserves energy, the second law describes the direction a cycle actually occurs.

$$\frac{dS_{c.v.}}{dt} = \dot{m}_i s_i - \dot{m}_e s_e + \frac{\dot{Q}_{c.v.}}{T} + \dot{S}_{gen} \quad (6)$$

This equation describes the entropy that exists in the flow as well as heat generated in the process. The last term describes the rate that entropy is generated in the process. For reversible processes, the generation term is zero but in reality it can never be less than zero, thereby showing that entropy is not necessarily conserved. Based on this phenomenon, the second law can be reduced to the following form that will be used to analyze the power cycle:

$$\dot{m}(s_i - s_e) + \frac{\dot{Q}_{c.v.}}{T} \geq 0 \quad (7)$$

B. CYCLE ANALYSIS

Figure 6 provides a basic illustration of the open air Brayton cycle with the solar collector and the connected turbine and compressor.

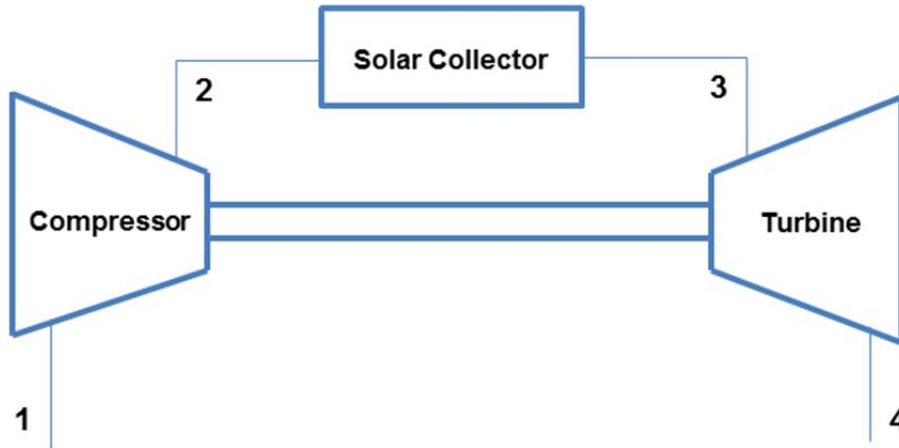


Figure 6. Open Air Brayton Cycle with Solar Collector.

In this cycle, air enters the compressor from the atmosphere (state 1) and is compressed to a high pressure gas before entering the solar collector (state 2). The solar collector transfers heat to the air, increasing its temperature in a constant pressure process (state 3). Finally, the high temperature, high pressure air is used to create work through the turbine process before exhausting to the atmosphere (state 4).

1. Pressure and Temperature

The initial design of the solar plant is based on the concept of an ideal open Brayton cycle. In this cycle, the compressor and turbine processes are assumed to be reversible, meaning there is no change in entropy as losses due to friction or other means are neglected. The heat transfer occurs by raising the temperature of the fluid on a constant pressure line, where state 3 represents an operating limit.

A Temperature-Entropy (T-S) diagram of a standard Brayton Cycle, as shown in Figure 7, illustrates the change of state of the fluid through each process of the cycle. Each number in the diagram represents the corresponding state of the fluid.

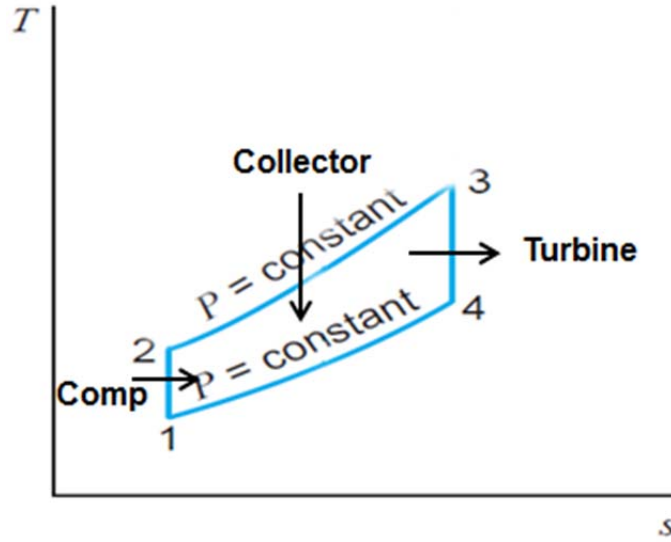


Figure 7. Temperature-Entropy Diagram of Brayton Cycle. Adapted from [21].

The working fluid for this cycle is treated as an ideal gas, where the specific heat is assumed to be constant. Based on these assumptions, equation (7) can be expanded to the following form:

$$s_e - s_i = C_p \ln \frac{T_e}{T_i} - R \ln \frac{P_e}{P_i} . \quad (8)$$

Therefore, the relationship between temperature and pressure for an isentropic ideal gas process becomes:

$$C_p \ln \frac{T_e}{T_i} = R \ln \frac{P_e}{P_i} . \quad (9)$$

This expression is simplified by dividing both sides by the specific heat and taking the inverse of the equality.

$$\frac{T_e}{T_i} = \left(\frac{P_e}{P_i} \right)^{\frac{R}{C_p}} \quad (10)$$

The gas constant for an ideal gas is simply the difference between the specific heat for a constant pressure process and the specific heat for a constant volume process [20].

$$R = C_p - C_v \quad (11)$$

The specific heat ratio is the ratio of the specific heats for a constant pressure process and constant volume process.

$$\gamma = \frac{C_p}{C_v} \quad (12)$$

Combining equations (10), (11), and (12), the relationship between temperature and pressure for an ideal gas process is defined using the specific heat ratio.

$$\frac{T_e}{T_i} = \left(\frac{P_e}{P_i} \right)^{\frac{\gamma-1}{\gamma}} \quad (13)$$

This relationship is used to define the operating parameters for the compressor and turbine processes that are assumed to be isentropic.

Because the air is exhausted from the turbine to the atmosphere, the pressures at the compressor inlet and turbine exit are equal.

$$P_4 = P_1 \quad (14)$$

Assuming the same pressure at these states, and a constant pressure process through the solar collector, the pressure ratios of the compressor and turbine are equal.

$$\frac{P_2}{P_1} = \frac{P_3}{P_4} \quad (15)$$

This relationship between the compressor and turbine is useful because it also shows a similar relationship among the temperatures through these processes.

$$\frac{T_2}{T_1} = \frac{T_3}{T_4} \quad (16)$$

The known values in this case are the temperature of the air entering the compressor (based on atmospheric conditions), and the temperature of the air exiting the solar collector, a fixed design point. There are two unknown values: the temperature of the air exiting the compressor and the temperature of the air exiting the turbine. Solving the equation for the maximum work provides an additional equation that can be used to solve for the relationship between these two unknown values. This will produce the smallest plant possible to generate the desired amount of power.

The specific net work for a Brayton cycle is defined as the difference between the work of the turbine and compressor. For an ideal gas the difference in enthalpy between two states equals the specific heat constant multiplied by the temperature difference.

$$w_{Net} = w_T + w_C = (h_3 - h_4) + (h_1 - h_2) = c_p (T_3 - T_4 + T_1 - T_2) \quad (17)$$

The goal of the design is to achieve maximum power density which occurs when the derivative of the specific net work is zero. Since the compressor inlet and solar collector exit temperatures are fixed constants determined by atmospheric conditions and design constraints respectively, the maximum work can be found by varying the temperature of the compressor outlet, as shown by Greitzer et al.[22].

$$\frac{dw_{Net}}{dT_2} = c_p \left(\frac{dT_3}{dT_2} - \frac{dT_4}{dT_2} + \frac{dT_1}{dT_2} - \frac{dT_2}{dT_2} \right) = c_p \left(0 - \frac{dT_4}{dT_2} + 0 - 1 \right) = 0 \quad (18)$$

After simplification, the relationship between both temperatures is obtained.

$$\frac{dT_4}{dT_2} = 1 \quad (19)$$

From this analysis, the maximum specific net work is achieved when the compressor exit temperature and the turbine exit temperature are equal.

$$T_4 = T_2 \quad (20)$$

Combining equation (20) with equation (16), the design temperatures of the compressor exit and turbine exit are simply a function of the outside air temperature and the specified design temperature of the collector exit.

$$T_2 = \sqrt{T_1 T_3} = T_4 \quad (21)$$

The specific net work of the cycle can be analyzed as a function of the compressor pressure ratio, with the two design points (compressor inlet temperature and collector outlet temperature) as scaling factors. By combining equations (13), (17), and (20), the work equation becomes:

$$w_{Net} = c_p \left[T_3 \left(1 - \left(\frac{P_2}{P_1} \right)^{\frac{1-\gamma}{\gamma}} \right) + T_1 \left(1 - \left(\frac{P_2}{P_1} \right)^{\frac{\gamma-1}{\gamma}} \right) \right] \quad (22)$$

In this equation, the pressure ratio includes the exponential factor that is determined by the specific heat ratio of the ideal gas. By selecting an ideal gas for the cycle and specifying fixed design parameters for the compressor inlet and collector outlet temperatures, the work can be plotted against a range of compressor pressure ratios. This function will provide a visual representation of the compressor pressure ratio required to achieve maximum work.

The metal selected as the phase change material for the latent heat thermal storage is Aluminum. As mentioned before, this is due to its melting temperature and high conductivity. As a starting point, the wall temperature of the collector is assumed to be a constant temperature, equal to that of the aluminum melting point. The collector air outlet temperature was then determined based on a reduced factor of the wall temperature, as the air would never actually reach the wall temperature, so long as there is flow.

$$T_3 = 0.83T_w = 0.83(933K) = 774.39K \quad (23)$$

The compressor inlet temperature was specified as a fixed value, based on average seasonal variation.

$$T_1 = 15^\circ C = 288.15K \quad (24)$$

The cycle uses air as the working fluid that has unique values for the specific heat capacity and specific heat ratios, provided in Table 3.

Table 3. Ideal Gas Properties of Air.

Property	Value	Units
C_p	1.005	[kJ/kg-K]
γ	1.41	[-]

Using the specified values from equations (23) and (24) while applying the ideal gas properties from Table 3. the specific net work of the cycle was plotted as a function of the compressor pressure ratio in Figure 8.

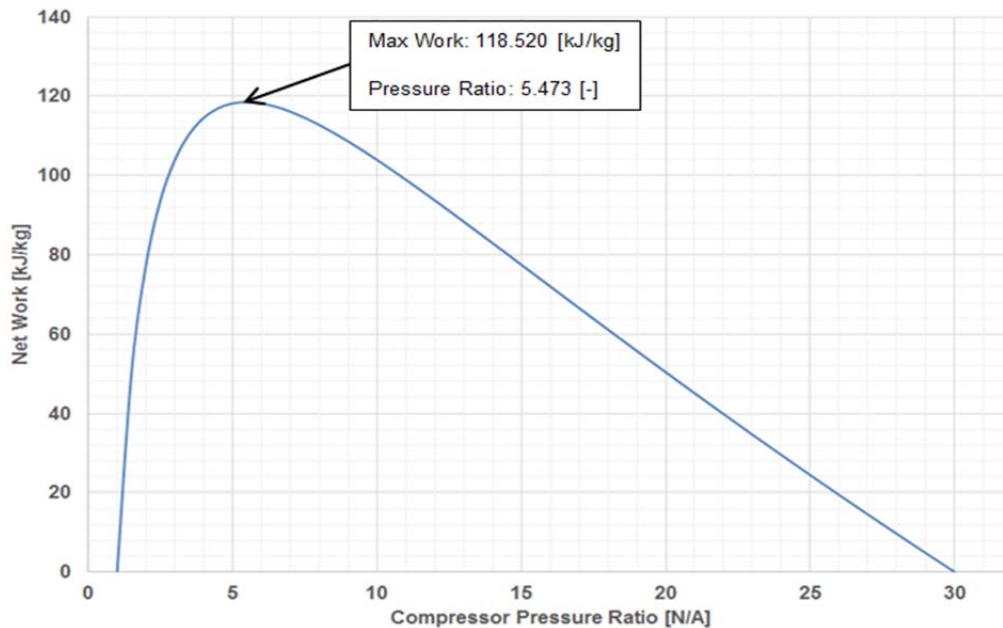


Figure 8. Design Cycle Net Work vs. Compressor Pressure Ratio.

In this case, where the inlet temperature of the compressor is an assumed fixed value, the maximum net work of the cycle corresponds to a compressor pressure ratio of 5.473. Because the cycle is open, where the turbine exit pressure is atmospheric and there

is no assumed pressure drop across the collector, the compressor pressure ratio also corresponds to the pressure drop through the turbine.

The cycle analyzed in Figure 8 is based on an assumed average temperature of the air entering the compressor. For the same plant design, the net work was analyzed to include more extreme temperatures based on colder and warmer seasons throughout the year. Figure 9 illustrates the changes in the cycle net work as a function of the pressure ratio.

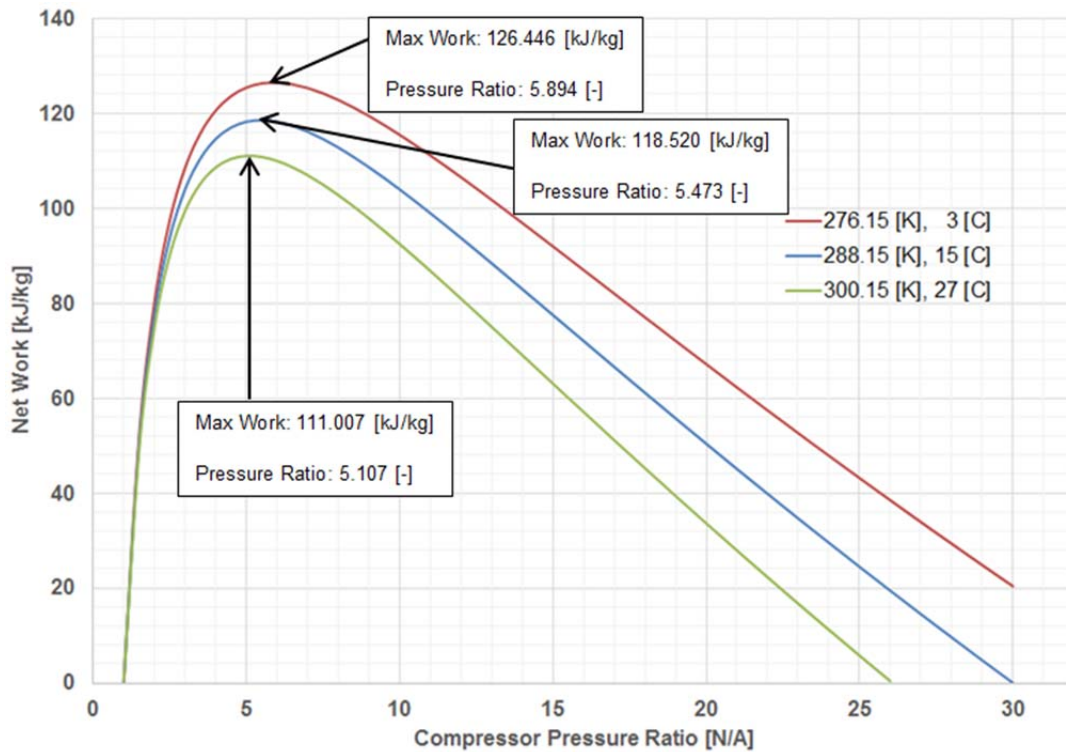


Figure 9. Cycle Net Work vs. Compressor Pressure Ratio for Seasonal Variations.

Based on Figure 9, the cycle achieves a higher maximum net work during times when the air temperature is colder that is attributed by the larger temperature differential through the solar collector. As the outside air temperature gets colder, the compressor pressure ratio required to achieve this maximum work is slightly higher. The computed

values are provided in Table 4. but in summary the compressor would operate in the pressure ratio range of 5–6.

Table 4. Maximum Specific Net Work and Compressor Pressure Ratios.

Average Air Temperature		Max Work [kJ/kg]	Pressure Ratio [-]
[C]	[K]		
3	276.15	126.446	5.894
15	288.15	118.520	5.473
27	300.15	111.007	5.107

Equation (13) can be used to solve for the design temperature of the compressor outlet, based on the assumed average inlet air temperature.

$$T_2 = T_1 \left(\frac{P_2}{P_1} \right)^{\frac{\gamma-1}{\gamma}} = 288.15K (5.473)^{\frac{1.41-1}{1.41}} = 472.377K \quad (25)$$

With the compressor exit temperature known, the temperature at the turbine exit can be solved for using the relationship of equation (16). The result shows that the maximum work occurs when the compressor outlet temperature equals the turbine exit temperature.

$$T_4 = T_3 \frac{T_1}{T_2} = 774.39K \left(\frac{288.15K}{472.377K} \right) = 472.377K = T_2 \quad (26)$$

The lower pressure limit of the cycle is assumed to be atmospheric conditions, 101.3 kPa. In order to determine the upper pressure limit of the cycle, equation (15) is used to solve for the pressure at the compressor exit, knowing that the compressor pressure ratio is equal to the pressure drop across the turbine.

$$P_3 = P_2 = P_1 \frac{P_2}{P_1} = 101.3kPa (5.473) = 554.455kPa \quad (27)$$

2. Specific Work and Heat

The design specific work of the compressor is determined using the First Law of Thermodynamics for a steady state process, adapted for an ideal gas, by using equation (5). Compressor work is expressed as a negative value to indicate the work is put into the system.

$$w_c = h_1 - h_2 = c_p (T_1 - T_2) = 1.005 \frac{kJ}{kg \cdot K} (288.15K - 472.377K) = -185.148 \frac{kJ}{kg} \quad (28)$$

Similarly, the design specific work of the turbine is determined using the specified design temperature of the collector exit, and the fact that the turbine exit temperature is equal to the compressor exit temperature. Turbine work is expressed as a positive value to indicate the work extracted from the system.

$$w_t = h_3 - h_4 = c_p (T_3 - T_4) = 1.005 \frac{kJ}{kg \cdot K} (774.39K - 472.377K) = 303.523 \frac{kJ}{kg} \quad (29)$$

Finally, the specific heat added to the air via the collector process can also be determined using the simple First Law analysis for an ideal gas. For maximum work, this value is equal to the specific work of the turbine.

$$q = h_3 - h_2 = c_p (T_3 - T_2) = 1.005 \frac{kJ}{kg \cdot K} (774.39K - 472.377K) = 303.523 \frac{kJ}{kg} \quad (30)$$

The basic design limits and parameters have been determined for the operation of the cycle. By establishing an average condition of the air, and setting the design temperature limit based on the melting temperature of aluminum, all states were determined for the ideal open cycle and provided in Table 5.

Table 5. Open Brayton Cycle Design Parameters.

Process	Temperature [K]	Pressure [kPa]	Specific Work [kJ/kg]	Specific Heat [kJ/kg]		
Compressor	T_1	288.150	P_1	101.325	-185.148	-
Collector	T_2	472.377	P_2	554.455	-	303.523
Turbine	T_3	774.390	P_3	554.455	303.523	-
	T_4	472.377	P_4	101.325		

3. Efficiency, Power, and Mass Flow

The thermal efficiency of the system is calculated from the specific net work and the specific heat transfer of the collector and corresponds to the maximum work at the associated compressor pressure ratio.

$$\eta = \frac{w_{Net}}{q} = \frac{w_T + w_C}{q} = \frac{303.523 \frac{kJ}{kg} - 185.148 \frac{kJ}{kg}}{303.523 \frac{kJ}{kg}} (100\%) = 39\% \quad (31)$$

Power, defined as the net work rate of the cycle, is a function of mass flow.

$$\dot{W}_{Net} = \dot{m}w_{Net} \quad (32)$$

The initial prototype design is that of a scaled down model, with a design power rating of 50 kW. The specific net work, defined as the sum of the compressor and turbine work, has been calculated, therefore equation (32) can be used to solve for the design mass flow of the cycle.

$$\dot{m} = \frac{\dot{W}_{Net}}{w_{Net}} = \frac{\dot{W}_{Net}}{w_T + w_C} = \frac{50kW}{303.523 \frac{kJ}{kg} - 185.148 \frac{kJ}{kg}} = 0.422 \frac{kg}{s} \quad (33)$$

Having determined the design mass flow rate of the air in the cycle, the individual plant component powers can now be calculated.

$$\dot{W}_C = \dot{m}w_C = 0.422 \frac{kg}{s} \left(-185.148 \frac{kJ}{kg} \right) = -78.204kW \quad (34)$$

$$\dot{W}_T = \dot{m}w_T = 0.422 \frac{kg}{s} \left(303.523 \frac{kJ}{kg} \right) = 128.204kW \quad (35)$$

$$\dot{Q} = \dot{m}q = 0.422 \frac{kg}{s} \left(303.523 \frac{kJ}{kg} \right) = 128.204kW \quad (36)$$

The thermodynamic analysis of the system modeled as an ideal open air Brayton cycle, allowed for the calculation of the initial design limits as well as power ratings for each of the three components of the system. These calculations provide baseline values for sizing the collector as well as selecting a compressor and turbine for the system. Table 6. summarizes the resulting design limits.

Table 6. Summary of Design Limits.

Parameter	Value	Units
Power	50.000	[kW]
Mass Flow	0.422	[kg/s]
Pressure Ratio	5.472	[-]
T _{Hot}	774.390	[K]

THIS PAGE INTENTIONALLY LEFT BLANK

III. SOLAR COLLECTOR DESIGN

In Chapter II, a thermodynamic analysis of the cycle yielded a set of design limits for the system. These calculations are the basis for designing the first iteration of the solar collector's geometry.

A. GEOMETRY

The initial design of the collector is based on the idea of a simple geometry, one where reasonable assumptions of heat transfer and flow can be made, as well as the ability to support the integration of a phase change metal.

In this design, the air exiting the compressor enters the solar collector where the flow is divided among a stack of evenly sized air ducts. These ducts would be wrapped with aluminum phase change metal, so the material is completely integrated into the collector heat exchanger. This system takes advantage of the latent heat of fusion. During the day, the aluminum is in a liquid state as the sun powers the cycle. When the sun is blocked, however, the aluminum undergoes a phase change back to a solid state, but at a constant temperature, as it continues to power the cycle. Figure 10 is a side view of the cycle that illustrates the TES integration.

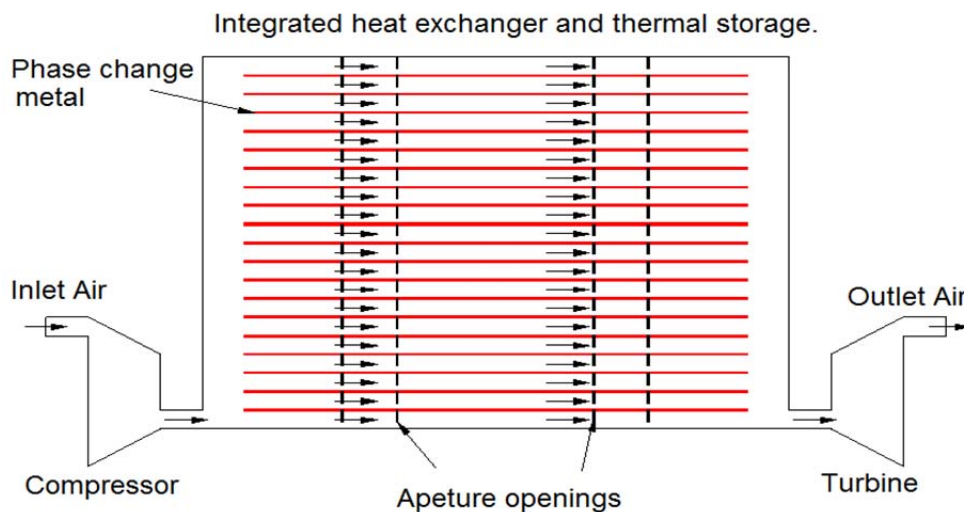


Figure 10. Side View of Solar Collector with Multiple Stacked Ducts.

1. Collector

Similar to a traditional solar collector receiver, the radiation from the sun is directed by an appropriately positioned mirror farm through a small opening or aperture, as shown in Figure 11. The radiation is trapped inside the collector with some assumed minimal losses to the atmosphere. Heat is then transferred over a larger surface area that represents a stack of air ducts. Two design parameters are of particular importance, the required area of the aperture and mirror farm.

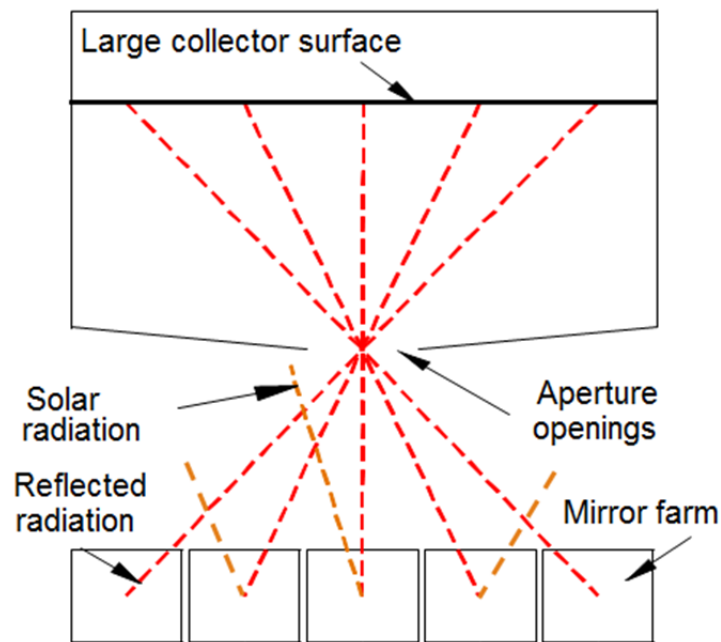


Figure 11. Top Down View of Solar Collector.

a. Aperture

The radiative heat transfer equation describes the relationship of the area in which the radiation passes with the temperatures on each side of the aperture.

$$q = \varepsilon A_{Ap} \sigma (T_0^4 - T_\infty^4) \quad (37)$$

The aperture is a small opening through which the sun's radiation is captured by the mirror farm and then redirected into the collector. The area of the aperture is found by rearranging the radiative heat equation.

$$A_{Ap} = \frac{q}{\varepsilon\sigma(T_0^4 - T_\infty^4)} \quad (38)$$

For this case, the collector is modeled as a black body, where the emissivity equals 1. The radiation equation is a function of the difference of ambient and internal temperatures, both to the fourth power. For the design, the internal temperature is modeled as the melting temperature of aluminum, 933 K. As discussed in Chapter II, the ambient temperature is assumed to be an average based on seasonal variation, 288.15 K. The heat losses through the aperture are assumed to be 5%. Based on these parameters, the aperture area is calculated.

$$A_{Ap} = \frac{0.05(128156W)}{1\left(5.67E-8\frac{W}{m^2 \cdot K^4}\right)(933^4 K^4 - 288.15^4 K^4)} = 0.15m^2$$

In order to provide enough heating to power a 50 kW plant, the area of the aperture would be approximately 0.15 m², assuming minimal losses. These losses can be customizable.

b. Mirror Farm

The area of the mirror farm typically accounts for the bulk of the area required by a solar collector. The equation to calculate this area is a function of the reflectivity of the mirror that can vary depending on the material of the mirror and particulate collection via dust and debris, as well as the losses through the aperture.

$$A_m = \frac{q_{Ap}}{\rho G} \quad (39)$$

In this case, the reflectivity is assumed to be 85%. The sun's irradiance is known as 1000 W/m^2 . The mirror farm must be large enough to direct enough heat for the cycle plus losses from the aperture.

$$A_m = \frac{1.05(128156W)}{0.85\left(1000\frac{W}{m^2}\right)} = 158.31m^2$$

For a 50 kW plant, based on reasonable assumptions of the mirror farm and considering the losses from the aperture, the area of the mirror farm is approximately 158 m^2 .

2. Heat Exchanger Ducting

Having estimated the size of the mirror farm and aperture, the ducting was sized to get a complete picture of the collector. In this design, the air temperature is raised to the desired design temperature through the straight ducting under uniform heating by the by the phase change aluminum. By latent heat phase change, the aluminum maintains near melting temperature through the cyclic melting and re-freezing processes. Figure 12 illustrates the basic model of a single duct.

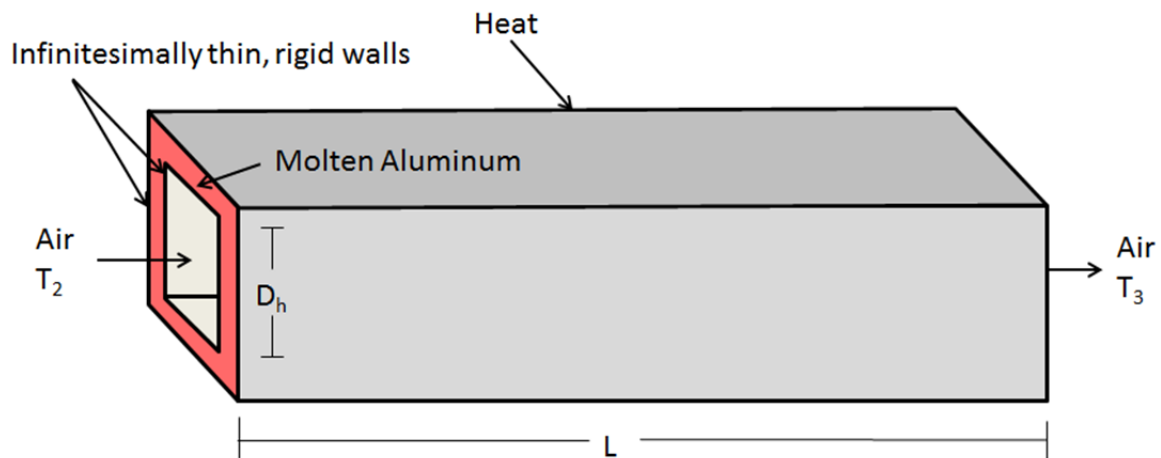


Figure 12. Single 3-D Square Duct with Molten Aluminum.

For the initial design, it was important to estimate the minimum volumetric requirements of the aluminum phase change metal required for thermal energy storage. To this effect, the boundaries that enclose the aluminum around the air duct were considered to be infinitesimally thin rigid walls. In reality, the aluminum would be encased by a non-corrosive and preferably conductive material, such as a ceramic with a high heat transfer coefficient. The thickness and material properties in this case would require additional modeling and would increase the amount of phase change material required.

Since the collector will have a network of stacked ducts, each wrapped with aluminum phase change metal, the cross section was chosen based on a geometry that supports the reasonable stacking of ducts. A square cross section was chosen for uniform heat transfer and flow.

a. Length

The heat equation for the internal flow through a volume is a function of the heat transfer coefficient, the heat transfer surface area, and the temperature difference of the fluid through the duct as it relates to the wall temperature [23].

$$\dot{Q} = hA_s \Delta T_{lm} \quad (40)$$

For internal flow convection where the walls are of a constant temperature, the heat transfer equation is a function of the log mean temperature difference between the inlet and outlet. This relationship accounts for the non-linear temperature rise through a duct where the flow temperature approaches the wall temperature at a rate that is determined by the mass flow.

$$\Delta T_{lm} = \frac{\Delta T_o - \Delta T_i}{\ln \left(\frac{\Delta T_o}{\Delta T_i} \right)} \quad (41)$$

The temperature differences described in this formula are those between the wall temperature and the average temperature of the flow at both the inlet and outlet of the duct.

$$\Delta T_o = T_w - T_3 \quad (42)$$

$$\Delta T_i = T_w - T_2 \quad (43)$$

Substituting equations (42) and (43) into equation (41), the log mean temperature difference can then be expanded and simplified to relate the wall temperature with the temperatures at the inlet and outlet.

$$\Delta T_{lm} = \frac{(T_w - T_3) - (T_w - T_2)}{\ln\left(\frac{T_w - T_3}{T_w - T_2}\right)} = \frac{T_3 - T_2}{\ln\left(\frac{T_w - T_2}{T_w - T_3}\right)} \quad (44)$$

The heat transfer coefficient accounts for the flow properties of the air, including conductivity. For this model, the flow is treated as laminar and fully developed. For a square cross section duct, the Nusselt number is a constant and relates the flow properties with the duct cross section.

$$Nu_D = \frac{hD_h}{k} \quad (45)$$

The Nusselt number, as shown by Incropera et al. [23], based on the specified square cross-section of the duct as well as the assumed flow state, is 3. The heat transfer coefficient can now be rewritten as an expression of the Nusselt number, conductivity, and hydraulic diameter.

$$h = \frac{Nu_D \bar{k}}{D_h} \quad (46)$$

The thermal conductivity of the fluid changes as a function of temperature. Because the temperature changes non-linearly through the duct, the true conductivity may be difficult to model analytically. Therefore, for the initial calculations, a mean conductivity of the inlet and outlet was calculated to approximate the thermal behavior through the duct. Linear interpolation was used to obtain the true conductivity values at the inlet and outlet of the duct.

$$\bar{k} = \frac{k_3 + k_2}{2} \quad (47)$$

$$\bar{k} = \frac{k_3 + k_2}{2} = \frac{5.609E-2 \frac{W}{m \cdot K} + 3.883E-2 \frac{W}{m \cdot K}}{2} = 4.746E-2 \frac{W}{m \cdot K}$$

Since each duct exhibits uniform heating, the total heat transfer area for each duct is the sum of the areas of all four sides.

$$A_s = 4D_h L \quad (48)$$

The heat equation can then be rewritten by substituting equations (44), (46), and (48) in to equation (40).

$$\dot{Q} = \left(\frac{Nu_D \bar{k}}{D_h} \right) (4D_h L) \left(\frac{T_3 - T_2}{\ln \left(\frac{T_w - T_2}{T_w - T_3} \right)} \right) = \frac{4Nu_D \bar{k} L (T_3 - T_2)}{\ln \left(\frac{T_w - T_2}{T_w - T_3} \right)} \quad (49)$$

Using a thermodynamics analysis, the heat transfer can also be described as a function of the mass flow, specific heat, and temperature difference through the collector.

$$\dot{Q} = \dot{m} c_p (T_3 - T_2) \quad (50)$$

When equations (50) and (49) are combined, the collector length is then solved for using the temperature limits identified in Chapter II as well as the flow characteristics modeled in this chapter.

$$L = \frac{\dot{m} c_p (T_3 - T_2)}{4Nu_D \bar{k} (T_3 - T_2)} \ln \left(\frac{T_w - T_2}{T_w - T_3} \right) = \frac{\dot{m} c_p}{4Nu_D \bar{k}} \ln \left(\frac{T_w - T_2}{T_w - T_3} \right) \quad (51)$$

A summary of the flow parameters and the resulting length for a single duct system is provided in Table 7. As mentioned, the wall temperature is modeled based on the melting temperature of Aluminum, and the flow was modeled as laminar and fully developed, which corresponds to a fixed Nusselt number for the square cross sectional duct.

Table 7. Collector Duct Heat Transfer Parameters.

Parameter	Value	Units
Nu_D	2.98	[-]
\dot{m}	0.422	[kg/s]
\bar{k}_{air}	0.047	[W/m-K]
c_p	1005	[J/kg-K]
T_w	933.450	[K]
T_2	472.377	[K]
T_3	774.390	[K]
L (Single Duct)	799.206	[m]

Using the values provided in Table 7. the length of a single duct collector was calculated at 799.206 m. Since the collector is designed based on a multiple duct stacked array, the flow through each duct is proportional to the number of ducts, thus the collector length is inversely proportional. The relationship between the collector length and the number of ducts in the collector is illustrated in Figure 13.

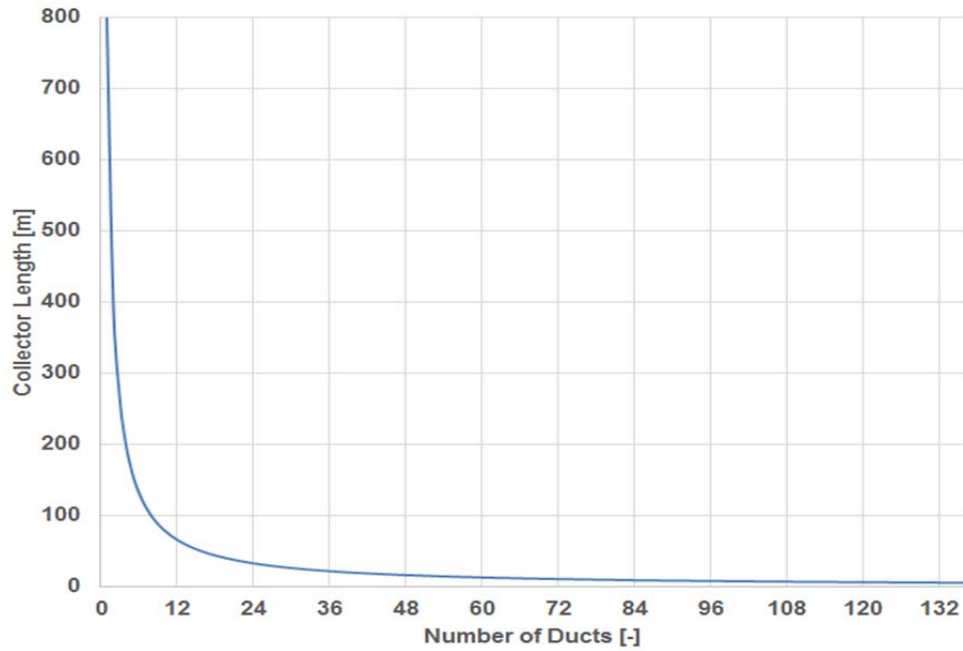


Figure 13. Collector Length vs. Number of Ducts.

By stacking ducts, the length of the collector can be dramatically reduced. Some examples of collector lengths based on the number of ducts are provided in Table 8.

Table 8. Collector Length Compared to Number of Ducts.

Number of Ducts [-]	Collector Length [m]
10	79.921
50	15.984
100	7.992
200	3.996
500	1.598

b. Hydraulic Diameter

Sizing the collector length has been useful in analyzing how the overall length can be reduced as a factor of N (number of ducts). What also must be known is how the length of the collector is related to the hydraulic diameter of the square duct.

The mass flow equation shows how the flow is related to the cross-sectional area of the duct.

$$\dot{m} = \rho A u \quad (52)$$

For the case of the square duct, the cross-sectional area is the square of the hydraulic diameter.

$$A = D_h^2 \quad (53)$$

When the relationship of equation (53) is substituted back into equation (52), the equation still yields two unknowns: the hydraulic diameter and the velocity of the flow. The Reynold's Number for the flow is then used to add an additional equation in order to solve for the hydraulic diameter.

$$\text{Re} = \frac{\rho D_h u}{\bar{\mu}} \quad (54)$$

The Reynold's Number can then be rearranged as an equation expressing the velocity of the flow.

$$u = \frac{\text{Re} \bar{\mu}}{\rho D_h} \quad (55)$$

Equation (55) can then be substituted in to equation (52) to express the mass flow as a function of the Reynold's Number, viscosity, and hydraulic diameter.

$$\dot{m} = \rho (D_h^2) \left(\frac{\text{Re} \bar{\mu}}{\rho D_h} \right) = \text{Re} \bar{\mu} D_h \quad (56)$$

Finally, the hydraulic diameter can then be solved for as a function of mass flow, the Reynold's Number, and the viscosity of the flow.

$$D_h = \frac{\dot{m}}{\text{Re } \bar{\mu}} \quad (57)$$

As mentioned, the flow of the air through the duct is modeled as laminar and fully developed. For this flow, the Reynold's Number was assumed to be 2300, the limit before the flow transitions to turbulent.

Similar to the conductivity of the air, the viscosity is also a function of temperature that increases non-linearly through the duct for a constant temperature wall design. Therefore, a mean viscosity was calculated for the air flow just as it was for the conductivity.

The hydraulic diameter was then calculated based off of the mass flow determined from Chapter II as well as the assumptions made for the flow. The flow parameters used and resulting size calculations are listed in Table 9.

Table 9. Collector Duct Flow Parameters and Hydraulic Diameter.

Parameter	Value	Units
Re	2300	[-]
\dot{m}	0.422	[kg/s]
$\bar{\mu}_{air}$	3.108E-5	[kg/s-m]
D_h	5.902	[m]
$\frac{L}{D_h}$	135.413	[-]

A single duct collector in this case would have a hydraulic diameter of 5.9 m, but just as the collector length, the hydraulic diameter of a single duct also reduces based on the number of ducts in the array. For this design, the length to hydraulic diameter ratio remains constant at approximately 135, regardless of how many ducts are stacked.

B. ALUMINUM REQUIREMENTS

1. Mass and Volume

In order to calculate the minimum amount of aluminum phase change metal required for the integrated TES, the total amount heat transfer from the collector must be determined.

$$Q = \dot{Q}t \quad (58)$$

The amount of aluminum required for TES is dependent upon how long the phase change metal would be expected to provide latent heat to the plant in the absence of the sun. The heat transfer rate from the collector was calculated in Chapter II and is a function of the rated power and efficiency of the cycle.

$$\dot{Q} = \frac{\dot{W}_{Net}}{\eta_{th}} \quad (59)$$

Substituting equation (59) for the heat transfer rate in equation (58), the new expression for the total heat transfer is expressed as follows:

$$Q = \frac{\dot{W}_{Net}}{\eta_{th}} t \quad (60)$$

For latent heat phase change, the total heat transfer is also a function of the mass of the phase change material and its latent heat of fusion.

$$Q = m_{Al} h_{f,Al} \quad (61)$$

In this case, the mass of the Aluminum required is expressed by the density and volume.

$$m_{Al} = \rho_{Al} V_{Al} \quad (62)$$

Combining equation (60) with (61), and substituting in equation (62), the minimum volume of Aluminum is expressed as a function of the rated power, efficiency, and the amount of time the phase change metal is expected to provide heating.

$$V_{Al} = \frac{\dot{W}_{Net} t}{\eta_{ih} \rho_{Al} h_{f,Al}} \quad (63)$$

The Andasol-1 power plant supplies heat from thermal energy storage for up to approximately eight hours [12], therefore the design of the aluminum phase change volume was determined as a comparable to that standard. Table 10. lists the values used to calculate the resulting volumetric requirement using equation (63).

Table 10. Minimum Aluminum Volumetric Requirement.

Parameter	Value	Units
\dot{W}_{Net}	50	[kW]
η	39	[%]
ρ_{Al}	2712	[kg/m ³]
$h_{f,Al}$	398000	[J/kg]
t	8	[hr]
V_{Al}	3.419	[m ³]

In summary, for a 50 kW rated plant operating within the limits defined in Chapter II, the minimum amount of Aluminum required to provide latent heating to the system is 3.4 m³.

2. Collector Duct Thickness

In the prototype design, each duct within the collector is wrapped in phase change aluminum. The minimum amount of Aluminum was determined in the previous section, therefore the additional duct thickness from the aluminum can be determined. For uniform thickness, the volume can be rewritten in terms of the number of ducts and the cross sectional area of the aluminum wrapping, remembering that the length and hydraulic diameter are inversely proportional to the number of ducts.

$$\frac{V_{Al}}{N} = A_{Al,duct} \frac{L}{N} = (A_o - A_i) \frac{L}{N} = \left(d^2 - \frac{D_h^2}{N^2} \right) \frac{L}{N} \quad (64)$$

Equation (64) can then be rearranged to solve for the new outer diameter of the duct to account for the added aluminum, as a function of the number of ducts.

$$d = \sqrt{\frac{V_{Al}}{L} + \frac{D_h^2}{N^2}} \quad (65)$$

For uniformity, the additional thickness can then be determined by subtracting the new outer diameter by the hydraulic diameter of the duct, and dividing that quantity by two.

$$i = \frac{d - \frac{D_h}{N}}{2} \quad (66)$$

For this system, the volume of the aluminum is constant regardless of how many ducts are stacked in an array, as it depends on the amount of heating and duration. The result, as seen in Table 11. is that the thickness of the aluminum wrapping increases when the collector is reduced in length by stacking ducts.

Table 11. Aluminum Thickness Compared to Number of Ducts.

Ducts [-]	Collector Length [m]	Hydraulic Diameter [mm]	Aluminum Thickness [mm]
10	79.92	590.20	1.81
50	15.98	118.04	8.46
100	7.99	59.02	14.54
200	4.00	29.51	21.12
500	1.60	11.80	27.33

Table 11. illustrates the disadvantage of spreading a fixed volume of Aluminum too thin for a small number of ducts. Stacking as many ducts as possible not only reduces the length of the collector, it also provides for a thicker layer of aluminum around the ducts, allowing for ease of machining and more uniform heat transfer.

C. HEAT FLUX

Of particular importance is the analysis of the heat flux for the prototype collector that can be used for sizing optimization. A central solar receiver is designed to focus the radiation from the sun on to a relatively small surface area. The expression for the heat flux is simply written as the ratio of the heat transfer rate to the heat transfer surface area.

$$q'' = \frac{q}{A_s} \quad (67)$$

The goal of central receiver design is to achieve as high of a heat flux as possible. Rodriguez-Sanchez et al. [24] showed how current receiver designs can achieve heat fluxes on the order of 10^5 and in some cases 10^6 W/m². While the prototype solar collector proposed is not expected to achieve a heat flux of that magnitude, it is still an important factor in size optimization.

Using MATLAB, the heat flux for the solar collector was first plotted as a function of the number of ducts, shown in Figure 14. See Appendix A for the MATLAB code. In this case, there was assumed to be no aluminum surrounding the ducts and they were stacked as a single array.

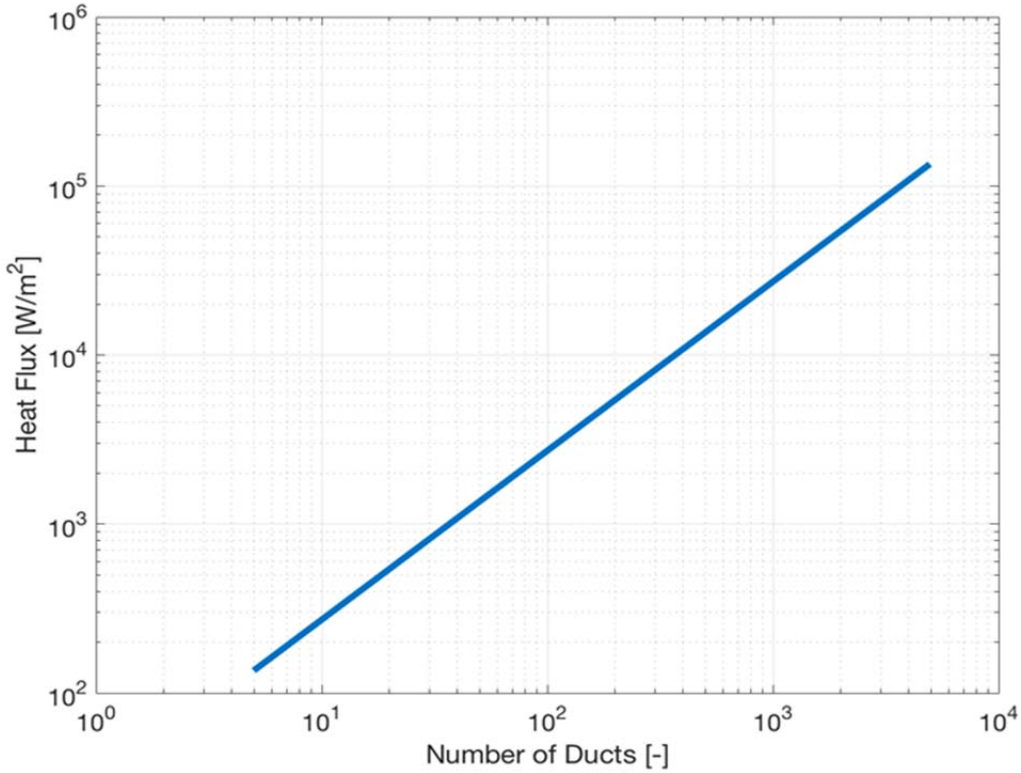


Figure 14. Heat Flux vs. Number of Ducts (Without Aluminum).

This figure illustrates how the heat flux rises linearly with the number of ducts on a logarithmic scale. Based on this scenario the following ducting numbers of Table 12. correlate with each approximate heat flux order of magnitude.

Table 12. Ducting Requirements for Heat Flux Orders of Magnitude.

Number of Ducts [-]	Approximate Heat Flux [W/m ²]
50	10 ³
500	10 ⁴
5000	10 ⁵

In reality, each duct is wrapped in aluminum. The minimum thickness calculations provided in Table 11. showed that the thickness of the aluminum increases around each duct as the number of ducts is increased. This leads to a rising total height of

the collector, offsetting the decrease in the surface area by reducing the length. Taking into consideration the added thickness of the aluminum, the heat flux was then plotted as a function of the number of ducts, shown in Figure 15.

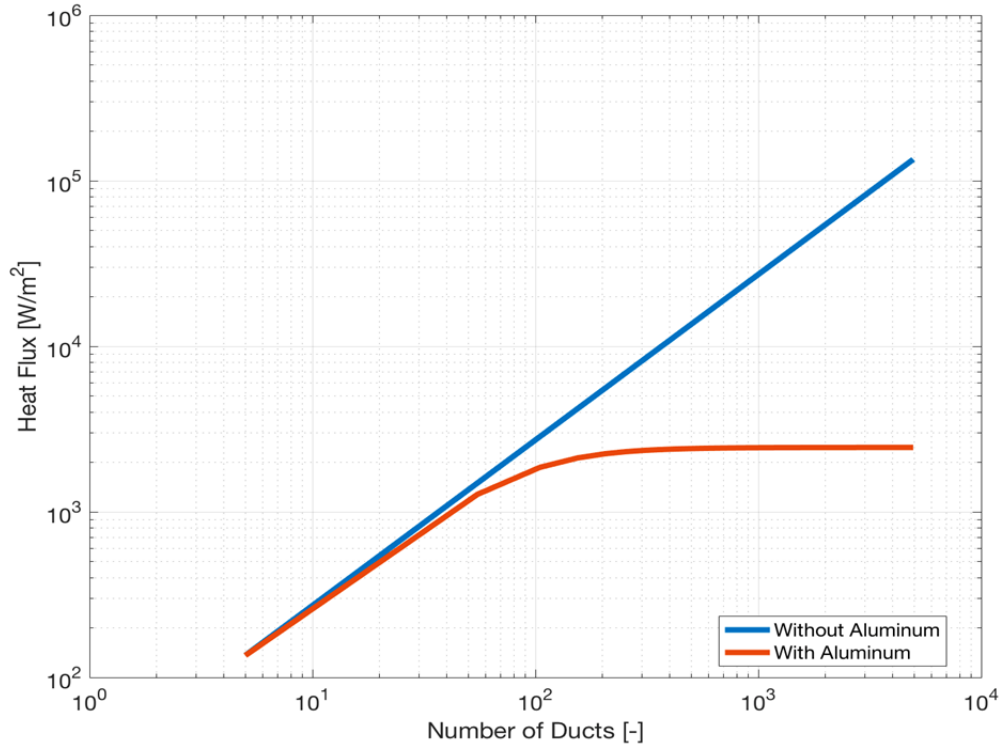


Figure 15. Heat Flux vs. Number of Ducts (With and Without Aluminum).

Figure 15 provides a more accurate representation of the heat flux behavior based on collector sizing, and illustrates how the heat flux actually approaches a limit of approximately 2450 W/m^2 . Because of the added thickness around each duct, there is eventually a loss of benefit in the collector height sizing that is particularly useful in further design refinement.

D. PRESSURE DROP

The prototype model presented in this thesis assumed a constant pressure through the solar collector, as shown in Chapter II, as a means of conducting an initial cycle analysis using a thermodynamic analysis. In reality, there is an expected pressure drop across the duct, especially when the length becomes shorter as a result of adding ducts.

An analysis of the collector flow was conducted using fluid dynamics as a means of quantifying the pressure drop in order to validate the assumption.

The expression of the pressure drop for a fully developed laminar flow in a non-circular duct accounts for the wall shear stresses that play a role in the loss of pressure.

$$\Delta P_{2-3} = \frac{32\mu L}{D_h^2} \left(\frac{u_{Max}}{2} \right) \quad (68)$$

The length to diameter ratio is constant at 135, and the hydraulic diameter in this case is a function of N. The maximum velocity is at the exit of the collector where the temperature is the highest, and is unknown. Equation (68) can then be rewritten as a function of the velocity and N.

$$\Delta P_{2-3} = 2160 \frac{N\mu u_3}{D_h} \quad (69)$$

The exit velocity is also found by expanding the mass flow equation in terms of an ideal gas.

$$\frac{P_3}{RT_3} Au_3 = \frac{P_2}{RT_2} Au_2 \quad (70)$$

For a constant area duct, the area on each side of the equation will cancel out, as well as the gas constant. Assuming a pressure drop across the collector, the outlet pressure can be expanded as a subtraction of the pressure drop from the inlet pressure. Equation (70) can then be rewritten in terms of the pressure drop.

$$\Delta P_{2-3} = P_2 \left(1 - \frac{T_3 u_2}{T_2 u_3} \right) \quad (71)$$

By combining equations (69) and (71), the velocity at the outlet can be calculated by solving the resultant quadratic formula.

$$2160 \left(\frac{N}{D_h} \right) \mu u_3^2 - P_2 u_3 + P_2 \frac{T_3}{T_2} u_2 = 0 \quad (72)$$

The quadratic constants were coded using MATLAB to solve the equation. See Appendix A for the MATLAB code used. The inlet velocity was solved as an input array based on the scaled mass flow and area as a function of N.

$$a = 2160 \frac{N}{D_h} \mu$$

$$b = -P_2$$

$$c = P_2 \frac{T_3}{T_2} u_2$$

The solution set of the exit velocity as a function of the number of ducts was then substituted back into equation (69) and plotted for analysis in Figure 16.

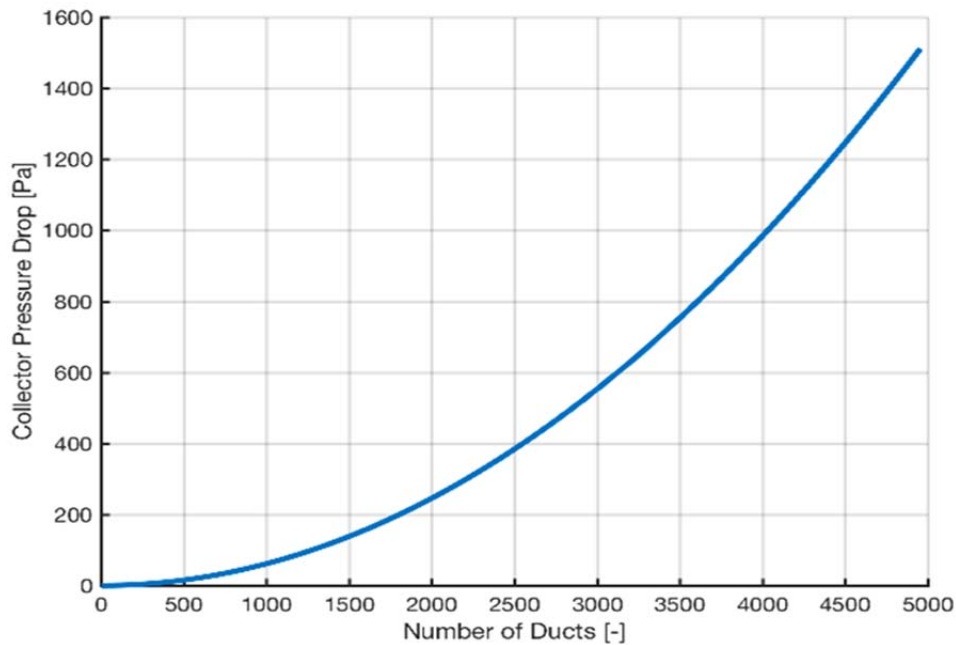


Figure 16. Collector Pressure Drop vs. Number of Ducts.

The pressure drop was plotted across a domain of up to 5000 ducts. As the number of ducts increased, the pressure drop rose at an exponential rate; however it is still very small relative to the collector's assumed pressure. The collector was assumed to operate at a constant 554 kPa, where it would require up to 4000 ducts to see a pressure drop of only 1 kPa. Based on this analysis, the assumption of a constant pressure process is a valid approximation.

THIS PAGE INTENTIONALLY LEFT BLANK

IV. OPTIMIZATION

In Chapter III, the basic sizing parameters of the solar collector for the 50 kW prototype plant were established using the operating limits as defined in Chapter II. The power of the plant, however, is a function of mass flow as well as the collector temperature rise that is also a function of mass flow. For a fully developed flow in a duct, exhibiting a constant wall temperature, the mean temperature of the fluid rises non-linearly as it approaches the wall temperature, seen in Figure 17.

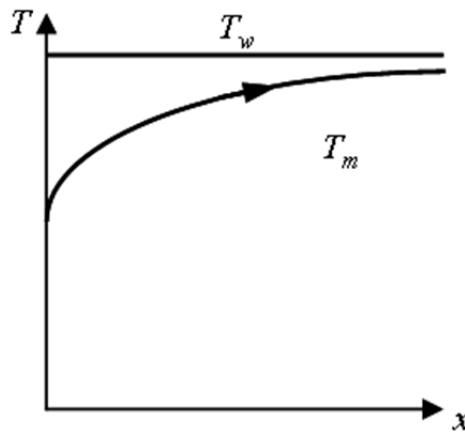


Figure 17. Mean Temperature Profile for Fully Developed Flow, Constant Temperature Wall. Source: [25]

The steepness of this curve depends on the mass flow rate of the fluid. A higher mass flow will yield a lower temperature rise, but a lower mass flow yields a lower power. This lends to the idea that there is an optimum mass flow where the power is maximized as it relates to the temperature rise of the air across the collector.

An optimization study was conducted analytically to establish an operating curve for the plant as a function of mass flow. A similar analysis was conducted using numerical methods to capture the real effects of air. These results were compared to see how the plant would behave under a range of flows.

A. ANALYTICAL MODEL

The temperature of the air exiting the collector was a fixed limit as discussed in Chapter II, but in reality, this temperature increases and decreases as a function of mass flow. Capturing this phenomenon analytically relies on the relationship between thermodynamics and the heat transfer properties of the collector duct. When equations (49) and (50) are combined, the logarithmic temperature profile is expressed as a function of the flow properties and duct geometry.

$$\ln\left(\frac{T_w - T_2}{T_w - T_3}\right) = \frac{4Nu_D \bar{k}L}{\dot{m}c_p} \quad (73)$$

The inverse log of both sides of the equation results in an exponential function, containing the mass flow term that can be used to scale the temperature profile.

$$\frac{T_w - T_2}{T_w - T_3} = \exp\left(\frac{4Nu_D \bar{k}L}{\dot{m}c_p}\right) = \alpha = f(\dot{m}) \quad (74)$$

For this analysis, the mean conductivity is again assumed to be a fixed average although in reality it changes as a function of temperature. The length can be expressed as the value calculated in Chapter III for a single duct collector, as the number of ducts that scale both the length and flow offset each other. The collector inlet temperature is then expressed in terms of the scaling function, wall temperature, and outlet temperature.

$$T_2 = (1 - \alpha)T_w + \alpha T_3 \quad (75)$$

As discussed in Chapter II, from equation (21) the maximum work occurs when the collector inlet temperature equals the square of the compressor inlet temperature and collector outlet temperature.

$$T_2 = \sqrt{T_1 T_3}$$

Substituting equation (21) into equation (75) produces a new expression for the collector outlet temperature that is assumed to be unknown.

$$T_3 = (1-\alpha)^2 \frac{T_w^2}{T_1} + 2(\alpha - \alpha^2) \frac{T_w T_3}{T_1} + \alpha^2 \frac{T_3^2}{T_1} \quad (76)$$

By collecting like terms, equation (76) can then be rearranged in the form of a second order polynomial equation, where the scaling function contains the mass flow term.

$$T_3^2 + \left[2\left(\frac{1}{\alpha} - 1\right)T_w - \frac{T_1}{\alpha^2} \right] T_3 + \frac{(1-\alpha)^2}{\alpha^2} T_w^2 = 0 \quad (77)$$

Equation (77) is then solved for the collector outlet temperature for each value of mass flow across a specified domain using the quadratic formula and associated quadratic constants.

$$T_3 = \frac{-b \pm \sqrt{b^2 - 4ac}}{2a} \quad (78)$$

$$a = 1$$

$$b = \left[2\left(\frac{1}{\alpha} - 1\right)T_w - \frac{T_1}{\alpha^2} \right]$$

$$c = \frac{(1-\alpha)^2}{\alpha^2} T_w^2$$

The quadratic formula was solved for the collector outlet temperature as a function of mass flow. See Appendix B for the code executed in MATLAB to solve the equation.

Having solved for the collector outlet temperature, the plant power can then be calculated using equation (32) for ideal gases that expresses the net work in terms of temperature states.

$$\dot{W}_{Net} = \dot{m}(w_T + w_C) = \dot{m}c_p \left[(T_3 - T_4) + (T_1 - T_2) \right]$$

Recalling again that for maximum work, the compressor outlet temperature and the turbine outlet temperature are equal for the design prototype of the smallest size, the

power equation can be rewritten in terms of the compressor inlet temperature and collector outlet temperature that was just solved.

$$\dot{W}_{Net} = \dot{m}c_p \left[(T_3 - \sqrt{T_1 T_3}) + (T_1 - \sqrt{T_1 T_3}) \right] = \dot{m}c_p (T_3 + T_1 - 2\sqrt{T_1 T_3}) \quad (79)$$

The compressor inlet temperature again is a fixed uncontrollable constant based on the atmospheric conditions, but similar to the methods of Chapter II, it can be assumed based on an average of seasonal variation. Substituting the fixed limits into equation (79), as well as the solution for the collector outlet temperature, the power can then be plotted as a function of mass flow. The resulting operating curve for up to 2 kg/s of flow is shown in Figure 18.

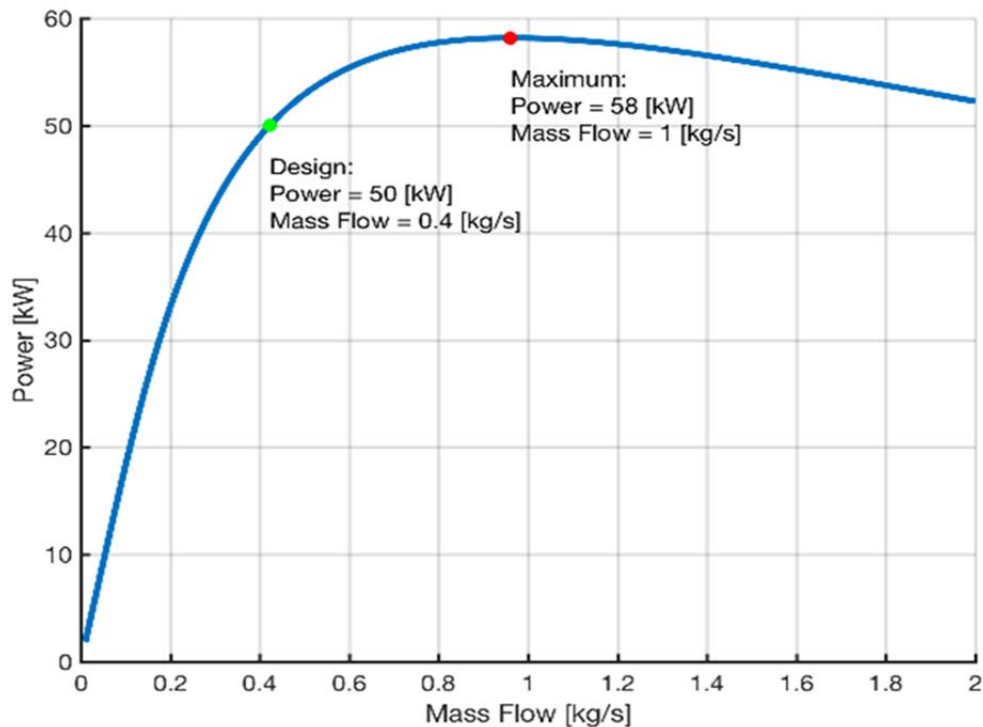


Figure 18. Analytical Solution of Power vs. Mass Flow for a 50 kW Plant.

The analytical solution of the plant power as a function of mass flow yields a maximum power of the 50 kW plant design. Based on the operating curve, the previously calculated mass flow from Chapter II correlates with the design power of 50 kW on the

curve. The analysis, however, shows that the power can be maximized by increasing the mass flow to nearly 1 kg/s. Table 13. provides a summary of the exact calculations for both design and maximum power conditions.

Table 13. Design and Maximum Power Calculations for a 50 kW Plant.

	Mass Flow [kg/s]	Power [kW]
Design	0.42	50.00
Maximum	0.96	58.18

The analytical analysis represents the potential to exceed design power by 16%. In this case, the lowered collector temperature difference is offset by the increased flow through the duct. Figure 19 shows how the collector temperature difference decreases in an exponential decay as the mass flow in increased.

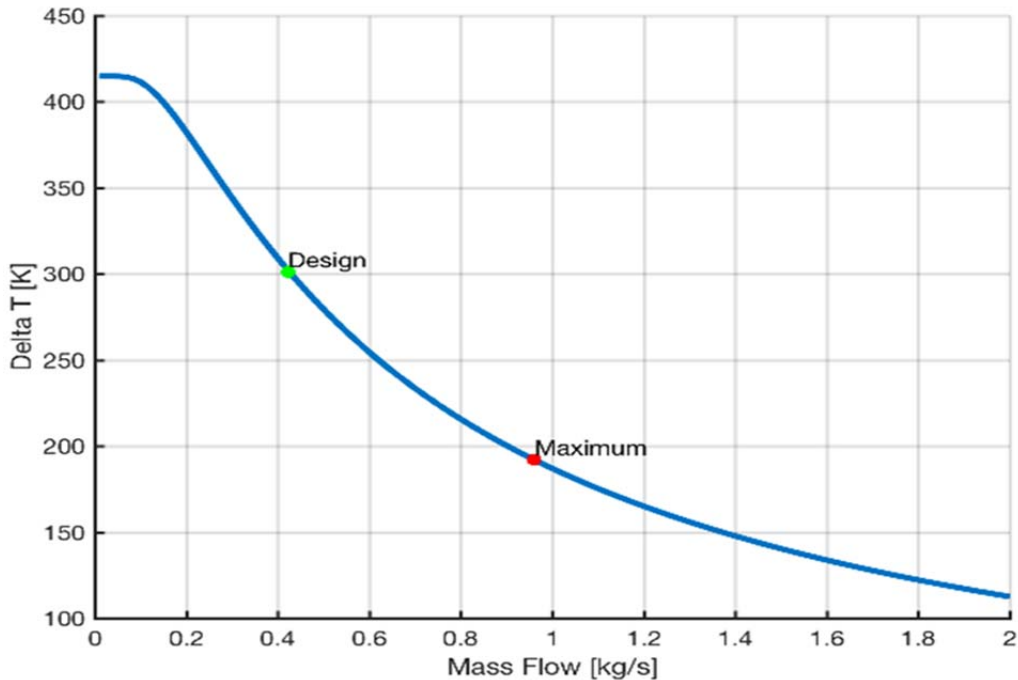


Figure 19. Analytical Solution of Collector Temperature Difference vs. Mass Flow for a 50 kW Plant.

The initial design prototype produced a basic operating collector temperature difference of approximately 301 K, but that difference can drop as low as 192 K when maximum power is preferred. The analysis shows that the plant could support a significant increase in flow relative to design for more power.

The plant efficiency was also plotted against the same domain of mass flow to observe the difference between design and maximum power efficiencies, as shown in Figure 20.

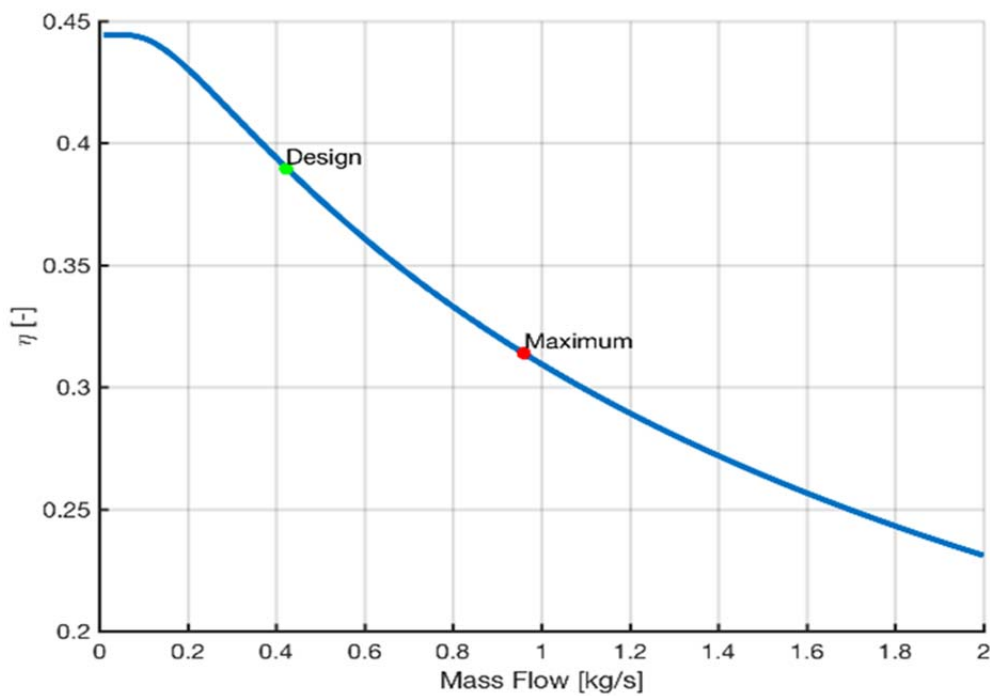


Figure 20. Analytical Solution of Thermal Efficiency vs. Mass Flow for a 50 kW Plant.

From Chapter II, the thermal efficiency of the plant modeled at 50 kW was calculated at 39%, but at maximum power, the thermal efficiency drops to 31%. This observation is particularly useful for the operational considerations of the plant. Solar thermal plants aim to maximize power over efficiency, so a higher mass flow would be preferred, especially during the day when the plant is powered by the sun. However, during night time operations or inclement weather conditions, the thermal energy stored

by the phase change aluminum must be conserved. The reduced flow in this case is preferred to minimize the power in a way that meets demands up to design limits but maximizes the duration of the phase change thermal storage capacity.

Finally, the heat exchanger effectiveness was analyzed to observe the performance of the collector across the operating range of mass flows. The heat exchanger effectiveness is expressed as a percentage ratio based on the maximum heat of the collector.

$$\varepsilon = \frac{q}{q_{Max}} \quad (80)$$

The maximum heat from the collector is achieved when the collector outlet temperature equals the wall temperature. For the constant wall temperature duct model, the effectiveness of the heat exchanger is maximized when the mass flow is nearly zero, which is not ideal as the power is then minimized. Similar to the efficiency analysis, the heat exchanger effectiveness drops as a function of mass flow, as illustrated in Figure 21.

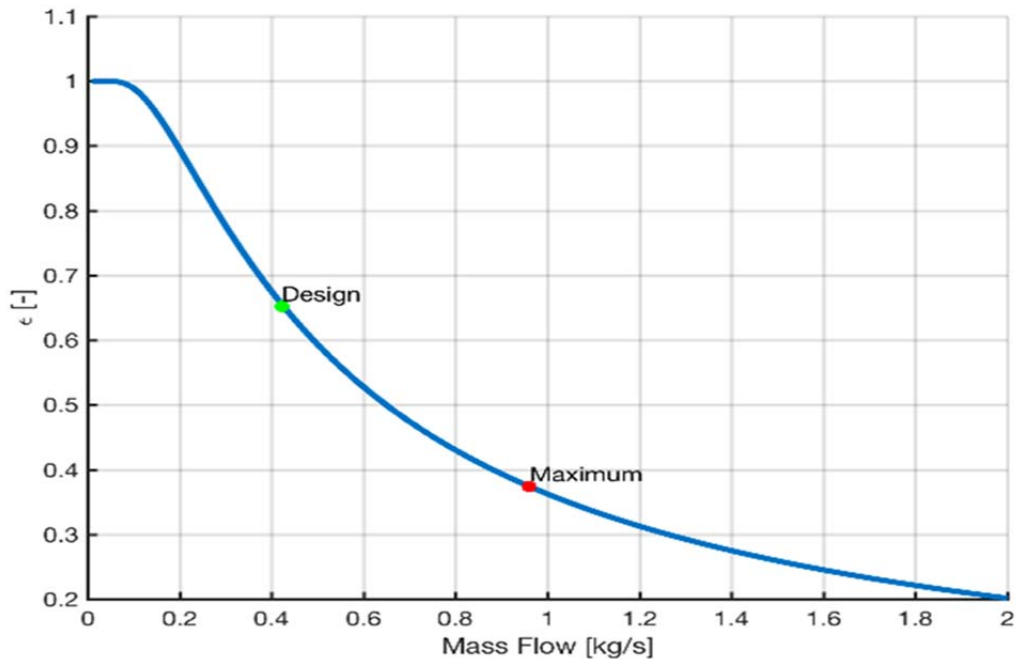


Figure 21. Analytical Solution of Heat Exchanger Effectiveness vs. Mass Flow for a 50 kW Plant.

For the design parameters, the heat exchanger effectiveness is 0.65, but drops to 0.37 when maximum power is achieved. This operating range shows how the heat exchanger should perform during day or night operation to maximize the use of the molten aluminum thermal storage.

B. NUMERICAL MODEL

The analytical model was useful in determining approximate curves to describe the behavior of the plant and solar collector. As stated previously, some broad assumptions were required to simplify the optimization model in a way that could be solved analytically. The flow was modeled as laminar and fully developed. The corresponding Nusselt number for a cross-sectional duct could then be used to define the heat transfer coefficient in the heat equation for the constant temperature wall duct. Additionally, both the thermal conductivity and viscosity of the flow were assumed to be fixed constants, calculated as mean values based on the inlet and outlet temperatures of the duct. In reality, as previously discussed, these values vary with temperature, which can change the profile through the duct.

In order to better understand how the real flow through the duct would behave, a model was constructed to simulate similar conditions to the design while removing the assumptions of the temperature dependent flow parameters. ANSYS-CFX software was used to numerically solve for the flow behavior, using a model constructed with SolidWorks.

1. Model Construction

A single duct was created using SolidWorks software. By modeling a single duct, the behavior can be scaled accordingly for a multiple duct system. The length to hydraulic diameter ratio remains constant regardless of how many ducts are stacked in the solar collector. Therefore, the dimensions of the duct are irrelevant, so long as the geometric ratio is 135, and the mass flow rate through the duct is scaled accordingly. Figure 22 provides an illustration of the model, which represents the air duct under consideration.



Figure 22. SolidWorks Drawing of Single Duct Model.

For the prototype duct, the length and hydraulic diameter were specified at 400 m and 2.95 m respectively. This model would correspond to a two-duct collector of a 50 kW plant. The geometry was then imported into ANSYS-CFX software for a full-scale analysis of the flow.

The first step of the analysis was to create a working mesh by which the model can be numerically solved. The resulting generated mesh, as shown in Figure 23 has a total of 28764 elements and 39200 nodes (see Appendix C).

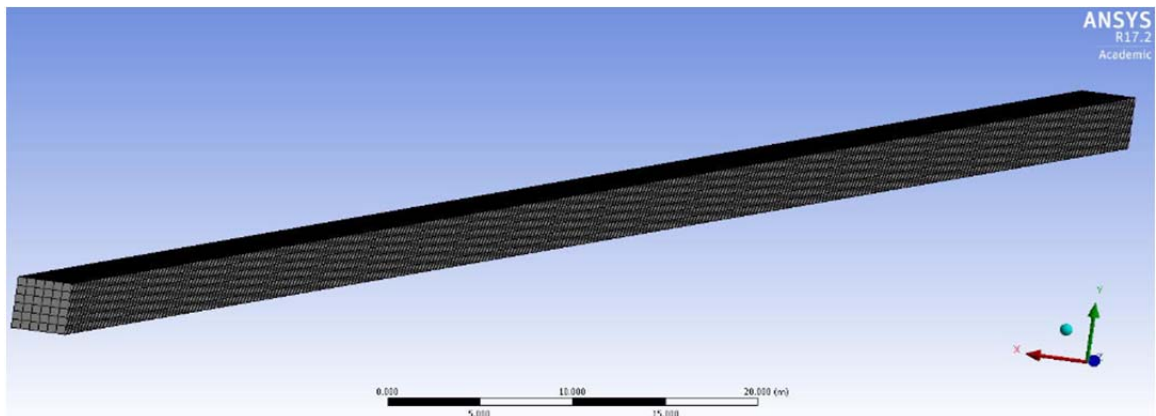


Figure 23. ANSYS-CFX Mesh for Single Duct Model.

2. Boundary Conditions

The next step of the solution process was to establish the fluid domain and boundary conditions for the model. The fluid model for this analysis was selected such that the air behaved as an ideal gas and that the flow was laminar, but incorporated real effects in order to achieve more realistic results. In doing so, the effects of changing viscosity and conductivity were included. This real effect of the flow could not be easily captured analytically, but is accounted for numerically using Sutherland's law that is expressed mathematically for both flow properties.

$$\varphi = \varphi_{ref} \left(\frac{T}{T_{ref}} \right)^{\frac{3}{2}} \frac{T_{ref} + S}{T + S} \quad (81)$$

In this formula, the flow parameter changes as a function of temperature relative to a reference point. The "S" refers to Sutherland's constant and is represented in units of Kelvin. By selecting this option, the program ANSYS-CFX invokes the relationship throughout the solution process.

Table 14. Sutherland's Constant and Reference Properties.

Property	Value	Units
S	110.4	[K]
T_{ref}	273.15	[K]
μ_{ref}	$1.72(10^{-5})$	[kg/m-s]
k_{ref}	$2.43(10^{-2})$	[W/m-K]

The duct has a total of six boundaries: inlet, outlet, and four walls. The boundary conditions at the inlet and outlet were specified as mass flow, scaled for a two-duct 50 kW model (0.211 kg/s). In order to resolve continuity, however, a temperature or pressure must be specified at the inlet mass flow boundary. The inlet temperature in this case was first specified as the same temperature calculated in Chapter II (472.377 K).

Each wall boundary for this model was established as a constant temperature wall, equal to the melting temperature of Aluminum (933 K). These wall boundaries were also expressed as no slip boundaries, where the velocity of the flow at the wall is zero. Figure 24 illustrates the default domain and boundaries for the fluid model.

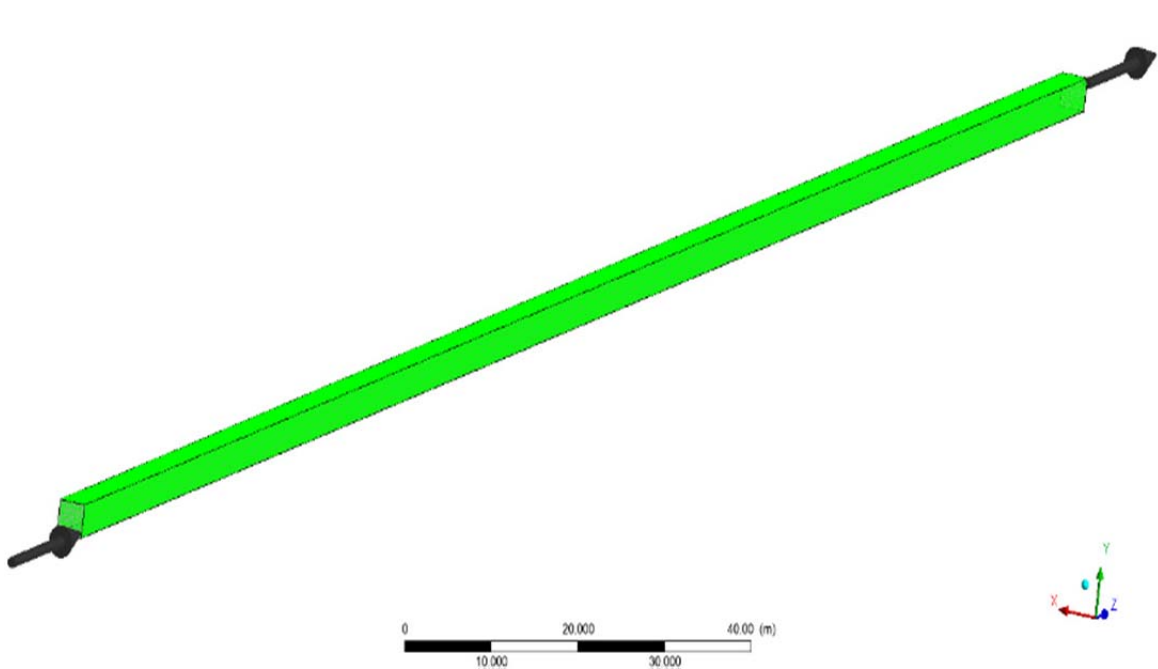


Figure 24. ANSYS-CFX Default Domain with Boundaries for Single Duct Model.

The model had a convergence target of 10^{-5} with the maximum number of iterations set to 500 with automatic time stepping.

3. Initial Run

The model was run once to check the flow behavior and properties at the outlet compared to the analytical calculations. Figure 25 is the plot of the convergence of mass and momentum for the initial run.

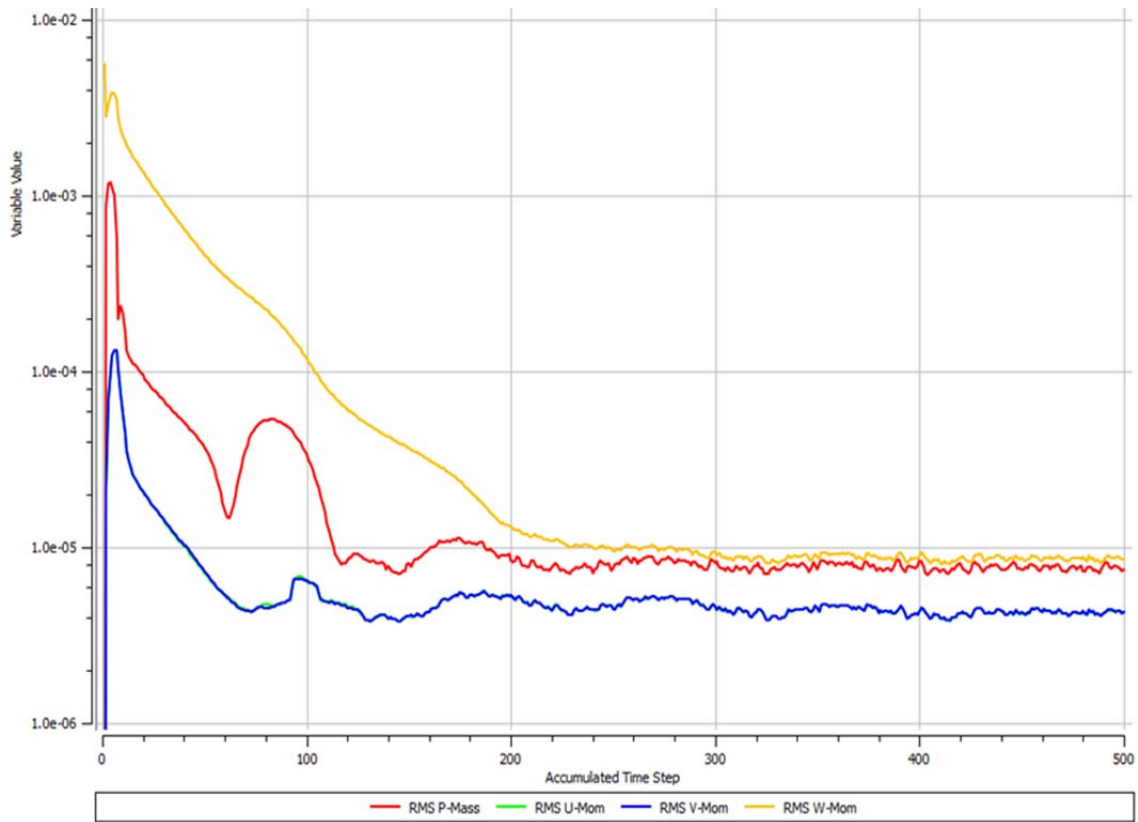


Figure 25. ANSYS-CFX Mass and Momentum Solution Convergence for Single Duct Model.

According to the plot, the mass and momentum equations were resolved with good convergence. The results of the simulation were then observed to check the flow properties at the duct outlet.

The first parameter checked was the temperature of the air at the outlet of the duct to compare with the value calculated in Chapter II. Figure 26 illustrates the temperature profile at the outlet of the duct.

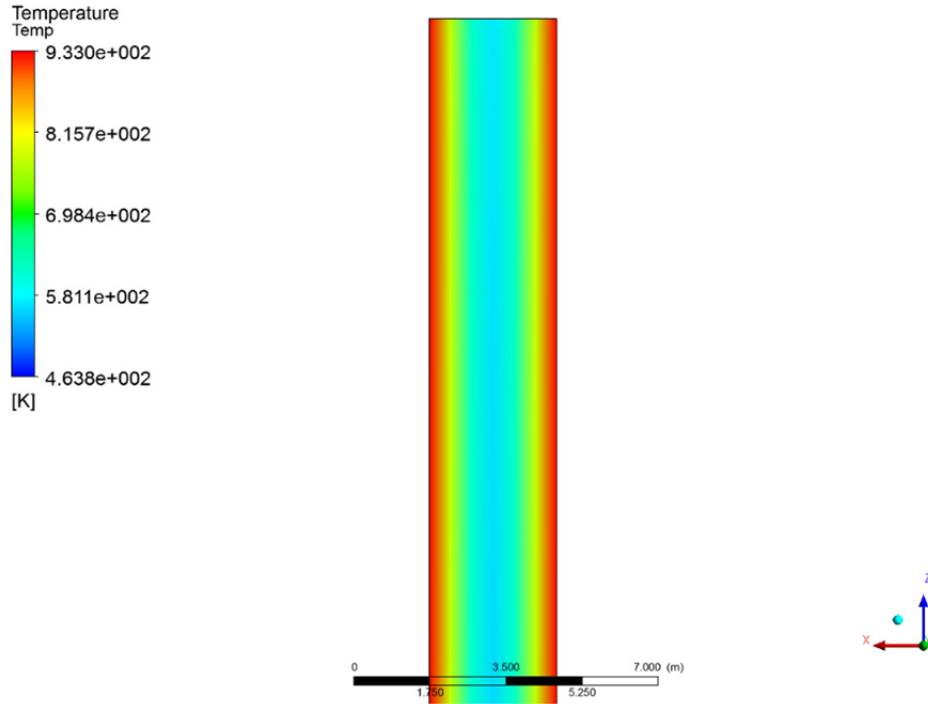


Figure 26. Collector Duct Outlet Temperature Profile.

The average temperature at this location was calculated to be 742 K. This value was slightly smaller than the temperature upper limit defined in Chapter II, which was an approximation based on an assumed reduction from the wall temperature (772 K). The numerical solution indicates a 20% reduction as opposed to the assumed 17% reduction previously defined, which shows that the analytical assumptions are reasonable.

An important assumption about the flow in the analytical modeling process was that of the Reynold's Number that was fixed at 2300, representing the limit before a flow transitions to turbulent. In order to validate that assumption, the Reynold's Number was checked at the outlet of the duct where the velocity was expected to be a maximum. Figure 27 shows the velocity profile of the flow at the duct outlet.

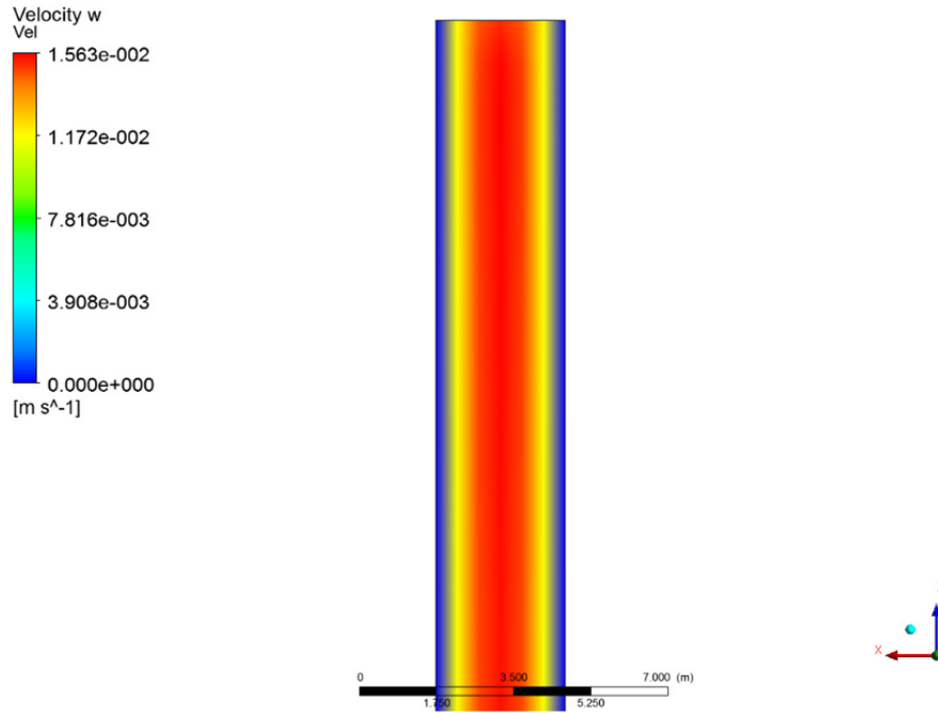


Figure 27. Collector Duct Outlet Velocity Profile.

The Reynold's Number was computed using an expression in CFX, based on the average velocity of the flow at the outlet and equals 2620 for this model. This value is slightly higher than the assumed value, and just inside the transition region, but again shows that the analytical assumptions were reasonable.

In Chapter III, the pressure drop in the collector was analyzed analytically as a function of the number of ducts. Based on that analysis, the pressure drop increased exponentially as a function of N . For collectors with two ducts, the pressure drop was found to be $2.46(10^{-4})$ Pa (see Appendix A). The pressure drop in the numerical model was quantified by observing the minimum and maximum pressures of the flow in the duct that correlate with the inlet and outlet of the duct, respectively, and was found to be $4.60(10^{-4})$ Pa (see Appendix C).

4. Optimization

Having established satisfactory results from the initial simulation run, the model was then analyzed using the Optimization tool in ANSYS, (see Appendix D). This

feature allows the user to specify a range of design inputs, in this case mass flow, instead of just one. The software runs multiple simulations across evenly spaced values in that range and stores the resulting output parameter(s) specified by the user. For this model, the three output parameters of significance were the collector outlet temperature, the collector temperature difference, and the resulting plant power.

a. Collector Outlet Temperature

In order to capture a similar comparison numerically, the inlet temperature of the collector duct boundary was specified as an expression, using the same relationship defined by equation (21) for maximum work. This resulted in ANSYS-CFX calculating the inlet temperature iteratively throughout the solution process. After 25 simulations, the outlet temperature was recorded (see Appendix E) and plotted in excel with the analytical solution. Figure 28 illustrates the comparison of the outlet temperature as a function of mass flow between the analytical and numerical models.

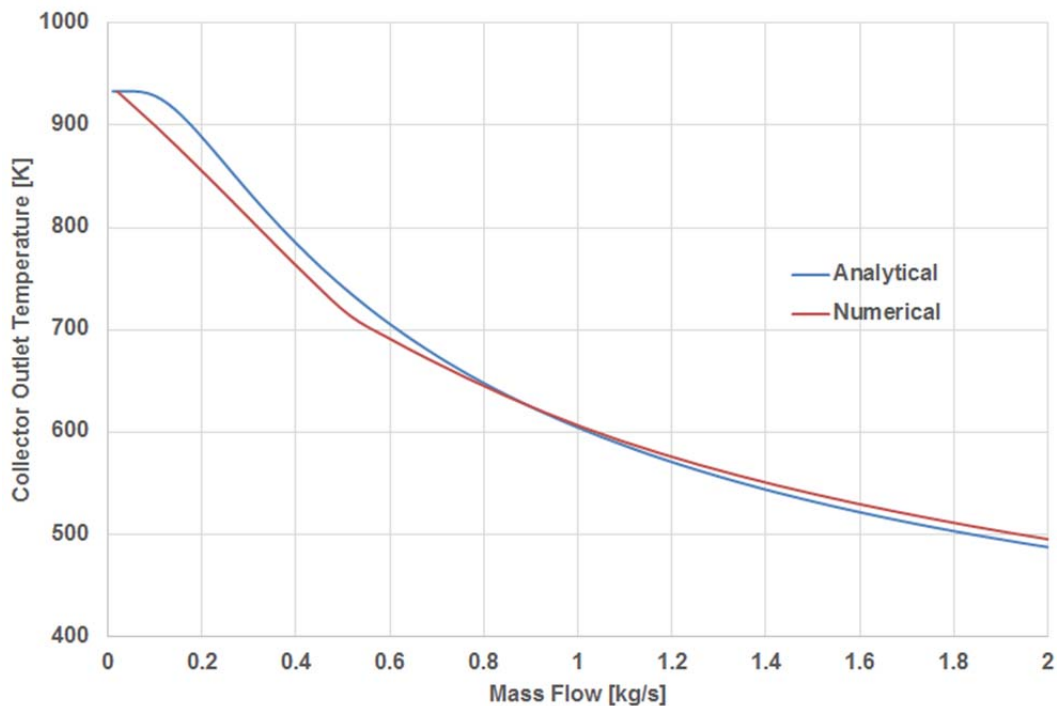


Figure 28. Comparison of Analytical and Numerical Solutions for Collector Outlet Temperature vs. Mass Flow.

Based on the plot, the results between both analysis methods were very similar, with the maximum error occurring at a mass flow value of approximately 0.1 kg/s.

b. Collector Temperature Difference

Similarly, the optimization tool was used to establish a curve for the collector temperature difference as a function of mass flow. Figure 29 illustrates comparison of both analytical and numerical models.

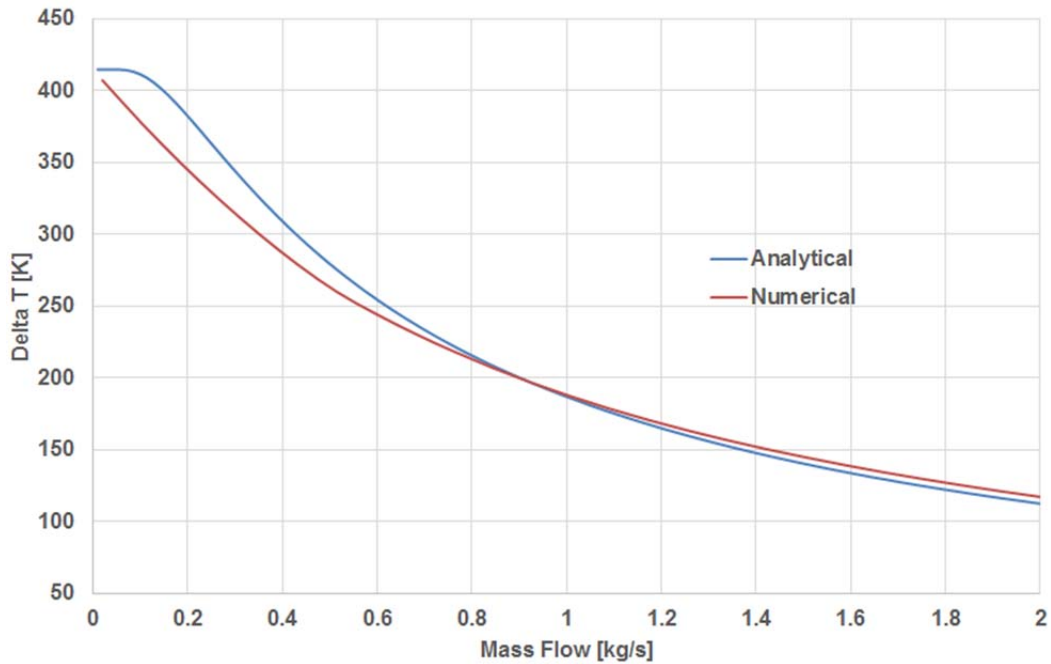


Figure 29. Comparison of Analytical and Numerical Solutions for Collector Temperature Rise vs. Mass Flow.

The results were again very similar in this case, with the maximum error also occurring at a mass flow value of approximately 0.1 kg/s.

c. Power

Most importantly, the plant power was observed using the optimization tool to compare with the analytical model when more real effects of the flow were invoked. In this case, the output parameter, power, was expressed as equation (79), such that the

numerical solution of the power only relied on the compressor inlet temperature (fixed) and the numerical solution of the collector outlet temperature as a function of mass flow. Figure 30 shows the resulting comparison between both the analytical and numerical curves.

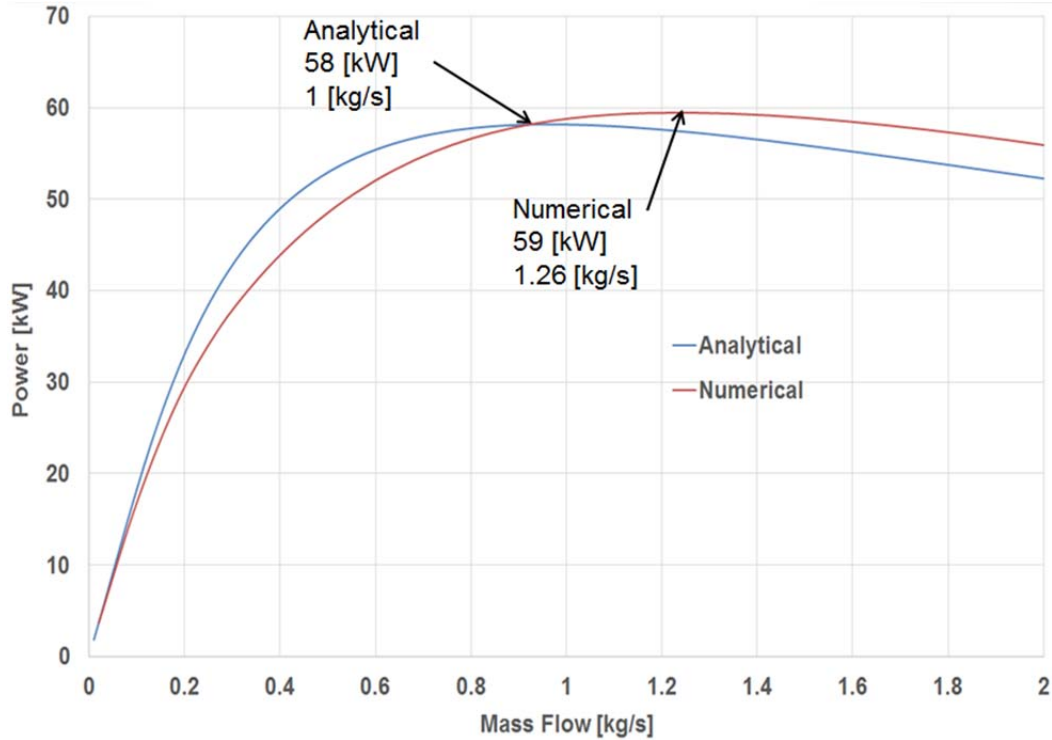


Figure 30. Comparison of Analytical and Numerical Solutions for Power vs. Mass Flow.

The analytical model, which assumed a constant average viscosity and conductivity, yielded a maximum power of 58 kW corresponding to a mass flow of approximately 1 kg/s. For the numerical model, the optimization showed that the maximum power of 59 kW could actually be achieved at a higher mass flow, approximately 1.26 kg/s. In general, the curve shapes were very similar, with the calculated maximum power values having only an approximate 1 kW difference. Table 15. shows a summary of the exact calculations from each model.

Table 15. Maximum Power and Pressure drop Based on Analytical and Numerical Solutions

Model	Mass Flow [kg/s]	Maximum Power [kW]	Pressure Drop [10⁻⁴ Pa]
Analytical	0.96	58.18	2.46
Numerical	1.26	59.46	4.62

In summary, the numerical model was intended to provide a more exact solution to compare against the analytical solution, which made more broad assumptions of the flow. The comparison of both models indicated that the assumptions and approximations made to enable an analytical solution were fairly accurate and could be used for extremely fast approximations.

V. DISCUSSION

Thermal Energy Storage systems in use today are very complex and require the pumping and circulation of multiple fluids to power solar thermal plants during non-daylight hours. These complexities can add additional operational burden, increased plant maintenance, and drive down overall plant efficiency. The purpose of this thesis was to establish a new design centered on simplicity, completely removing any pumping of hot liquid to foster the automatic transition between solar power supply and thermal energy storage. Many plants today operate on a Rankine cycle, but the prototype design in this thesis is based off of a Brayton cycle, so that air is the only moving fluid, further simplifying the plant.

In order to only have only one moving fluid for this plant, the thermal energy storage integrated into the collector for this design utilized the latent heat of phase change of aluminum as this minimized the volumetric requirements of the material. Other metals may be possible but Aluminum was suitable for operation when a Brayton cycle is used, because of its ready availability and relative low cost.

The prototype design model presented in this thesis intended to establish some basic operating limits and sizing specifications, as well as minimum volumetric requirements of the aluminum phase change metal. The assumptions of the collector flow were the largest contributor to the geometric design. For the 50 kW prototype, the Reynold's Number was assumed to be 2300 based on those assumptions. As stated in Chapter III, the hydraulic diameter is a function of mass flow, which scales proportionally with plant power. If the prototype were scaled up, the resulting collector height would not be feasible. A 50 MW plant, for example, would have a minimum height of 5900 m. In order to reduce the collector height for a larger plant, the flow should not be modeled as laminar. By increasing the Reynold's Number to turbulent flow, the minimum collector height as well as the length could be dramatically reduced. Another option would be to change the material to a higher temperature metal.

The model intended to estimate the minimum volumetric requirements of aluminum to sustain up to eight hours of power without the sun. This calculation required that the boundaries encasing the aluminum were infinitesimally thin and rigid. In reality, the aluminum would be wrapped with a non-corrosive material, preferably of a high conductivity to maximize the heat transfer.

Solar central receivers in operation and under design achieve extremely high heat fluxes. The prototype design in this thesis achieved a maximum heat flux on the order of 10^3 , limited by the aluminum wrapping. The analysis in Chapter III showed how the thickness of the aluminum around the ducts increases as the ducts are stacked, although the length and hydraulic diameters are reduced by a factor of N . The limit assumed some customizable losses from the aperture and mirror farm, which can be explored further to seek ways to improve the heat flux for this design.

VI. CONCLUSION

The design is a new concept; therefore, a basic thermodynamic analysis was used to conduct a complete cycle analysis of the system to establish operating limits necessary to design the collector. The upper temperature limit was established based on the melting temperature of Aluminum. By fully integrating latent heat thermal storage into the collector, the efficiency loss would be very minimal, limited only to heat losses to the atmosphere. These losses are easily mitigated with proper insulation technologies.

The collector was sized based on the limits defined from the cycle analysis. The collector duct geometry was selected based on the idea of stacking multiple ducts, which reduces the length and hydraulic diameters as the ducts are stacked in a column. Stacking ducts also increases the heat flux by minimizing the heat transfer surface area in the collector. The model was assumed to have no pressure drop, which was validated by analytical and numerical methods, that showed very little pressure drop.

The plant behavior as it pertains to mass flow was analyzed using both analytical and numerical methods. Using the equations from thermodynamics and heat transfer, the plant power and performance characteristics were calculated and plotted as a function of mass flow to see how these parameters behave under different conditions. The results showed that the design power could actually be exceeded by increasing the mass flow to a certain extent. Other performance characteristics were also analyzed to establish operating bands of the plant between day time and night time. The power and temperature calculations were compared to a numerical model which incorporated more real effects of the air and flow. The results from both models showed some similarities, and the assumptions made in the analytical model were validated as good approximations.

THIS PAGE INTENTIONALLY LEFT BLANK

VII. RECOMMENDATIONS

The research conducted in this thesis has hopefully established a foundation on which the prototype plant can be further developed. In an effort to guide the continued effort in this design study, the following recommendations are provided:

1. Analyze larger scale plant design
2. Revise flow model for larger collector sizing
3. Investigate suitable materials to encase the phase change metal around the ducts, such as high conductivity ceramics
4. Investigate modifications to the cycle such as a bottoming Rankine cycle to improve the plant efficiency

THIS PAGE INTENTIONALLY LEFT BLANK

APPENDIX A. MATLAB CODE FOR ANALYSIS OF PRESSURE DROP AND HEAT FLUX OF 50 KW PLANT

```

% LT Collin Roof, Thesis
%% Collector Pressure Drop and Heat Flux

Power = 50000;           % [W] Rated Power
nu = 0.39;               % [N/A] Thermal Efficiency
Q = Power/nu;           % [W] Collector heat xfer
P1 = 101325;            % [Pa] Compressor inlet pressure
T1 = 288.15;            % [K] Compressor inlet temperature
Tw = 933;               % [K] Collector wall temperature
f = 0.83;               % [N/A] Collector outlet reduction
T3 = f*Tw;              % [K] Collector outlet temperature
T2 = sqrt(T1*T3);       % [K] Collector inlet temperature
gamma = 1.4;            % [N/A] Air specific heat ratio
P2 = P1*(T2/T1)^(gamma/(gamma-1)); % [Pa] Collector inlet pressure
mu3 = ((1.458e-6)*T3^(3/2))/(T3+110.4); % [kg/ms] Collector out viscosity
% (Sutherland's Law)
R = 287;                % [kJ/kgK] Air Gas Constant
D = 5.902;              % [m] Single Duct Diameter
L = 799.206;           % [m] Single Duct Length
C = L/D;                % [N/A]

N = 5:50:5000;         % [N/A] Number of Ducts
mdot = 0.422./N;       % [kg/s] Mass Flow/duct
d = D./N;              % [m] Diameter/duct
l = L./N;              % [m] Length/duct
A = d.^2;              % [m^2] Area/duct
As = N.*l.*d;          % [m^2] Heat xfer surface area
V2 = (R*T2/P2).*mdot./A; % [m/s] Inlet velocity/duct
Qf = Q./As;            % [W/m2] Heat flux

% Quadratic Constants
a = 16*C*(mu3./d);
b = -P2;
c = P2*(T3/T2).*V2;

% Solve Quadratic Equation for V3 (Collector Outlet)
for i = 1:length(N)
    V3(:,i) = roots([a(i) b c(i)]);
end

% Removing erroneous root
V3 = V3(2,:);

% Plug V3 back into formula for Pressure Drop
dP = ((16*C*mu3)./d).*V3; % [Pa] Collector Pressure Drop

% Plot Pressure Drop vs. Number of Ducts
figure(01)
set(gca,'fontsize',15, 'linewidth', 2)
hold on
plot(N, dP, 'LineWidth',4)
xlabel('Number of Ducts [-]')
ylabel('Collector Pressure Drop [Pa]')
grid on

% Plot Heat Flux vs. Number of Ducts
figure(02)
loglog(N, Qf, 'LineWidth',4)
set(gca,'fontsize',15)
hold on
xlabel('Number of Ducts [-]')
ylabel('Heat Flux [W/m^2]')
grid on

```

THIS PAGE INTENTIONALLY LEFT BLANK

APPENDIX B. MATLAB CODE FOR ANALYTICAL OPTIMIZATION OF 50 KW PLANT

```

%% LT Collin Roof, Thesis, Solar Plant Optimization, 50kW Plant
%% Introduction

% The following script optimizes mass flow of the solar collector Brayton
% cycle for maximum power.
%
% Assumptions:
% 1) Air - Ideal Gas
% 2) Duct(s) - Constant area square cross section, L/a = constant
% 3) Fully developed flow, Nu provided from text, Re = 2300
% 4) Average constant conductivity through duct
% 6) Ideal, Open Cycle - Compressor and Turbine processes
% reversible/adiabatic
% 7) Design Power - 50 [kW]

clear all
close all
clc

%% Setup

T1 = 288.15; % [K] Compressor Inlet Temperature
P1 = 101.325; % [kPa] Compressor Inlet Pressure
cp = 1.005; % [kJ/kg-K] Specific Heat Capacity of Air
gamma = 1.41; % [N/A] Specific Heat Ratio of Air
R = 0.287; % [kJ/kg-K] Gas Constant of Air
Tw = 933.45; % [K] Wall Temperature (Melting temperature of Al...
% and max operating temperature of cycle)
P4 = P1; % [kPa] Turbine Outlet Pressure
Nu = 2.98; % [N/A] Nusselt Number for Square X-Section Duct
k = 4.746e-5; % [kW/m-K] Average Conductivity of Air through duct
L = 799.206; % Length of a single duct

%% Initialization

% Set domain for Mass Flow
mdot = linspace(0.01,2,135); % [kg/s] Mass Flow

% Coefficient function of mdot from heat equation
alpha = exp((4*Nu*k*L/cp)./mdot);

% Quadratic Solver for T3 using max power relationship with T2
a = 1;
b = ((2.*(alpha-alpha.^2).*Tw./T1)-1)./((alpha.^2)./T1);
c = (((1-alpha).^2).(Tw^2)./T1)./((alpha.^2)./T1);

% Root solver loop
for i = 1:length(mdot)
    T3(:,i) = roots([a b(i) c(i)]);
end

% Removing 2nd root array as not realistic
T3 = T3(1,:);

% Solving for T2 using max power relationship
T2o = sqrt(T1.*T3); % Optimizer T2 (Varies with T3)

% Delta T through duct
dT = T3-T2o;

% Cycle Power as a function of Mass Flow, Max Power
P = mdot.*cp.*T1.*((T3./T1)-2.*sqrt(T3./T1)+1);
[M I] = max(P);

```

```

% Heat Exchanger Effectiveness
epsilon = (dT)./(Tw - T2o);

% Cycle Efficiency
eta = P./(mdot.*cp.*dT);
%% Results/Figures

% Delta T Through Duct as a Function of Mass Flow
figure(01)
set(gca,'fontsize',15, 'linewidth', 2)
hold on
plot(mdot, dT(1,:), 'LineWidth',4)
plot(0.422, dT(29), 'g', 'markersize', 30)
hold on
plot(mdot(I), dT(I), 'r', 'markersize', 30)
hold on
text(0.422, dT(29), sprintf(['Design']),...
    'VerticalAlignment','bottom', 'HorizontalAlignment','Left',...
    'fontsize',15)
hold on
text(mdot(I), dT(I), sprintf(['Maximum']),...
    'VerticalAlignment','bottom', 'HorizontalAlignment','Left',...
    'fontsize',15)
xlabel('Mass Flow [kg/s]')
ylabel('Delta T [K]')
%title('Collector Delta T vs. Mass Flow')
grid on

% Power as a function of mass flow
figure(02)
set(gca,'fontsize',15, 'linewidth', 2)
hold on
plot(mdot, P(1,:), 'LineWidth',4)
hold on
plot(mdot(I), M, 'r', 'markersize', 30)
hold on
text(mdot(I), M, sprintf(['\nMaximum:\nPower = 58 [kW]\nMass Flow = 1 [kg/
s]']),...
    'VerticalAlignment','top', 'fontsize',15)
hold on
plot(0.422, 50, 'g', 'markersize', 30)
text(0.422, 50,...
    sprintf(['\nDesign:\nPower = 50 [kW]\nMass Flow = 0.4 [kg/s]']),...
    'VerticalAlignment','top', 'fontsize',15)
hold on
xlabel('Mass Flow [kg/s]')
ylabel('Power [kW]')
%title('Cycle Power vs. Mass Flow')
grid on

% Heat exchanger effectiveness as a function of mass flow
figure(03)
set(gca,'fontsize',15, 'linewidth', 2)
hold on
plot(mdot, epsilon, 'LineWidth',4)
hold on
plot(0.422, epsilon(29), 'g', 'markersize', 30)
hold on
plot(mdot(I), epsilon(I), 'r', 'markersize', 30)
hold on
text(0.422, epsilon(29), sprintf(['Design']),...
    'VerticalAlignment','bottom', 'HorizontalAlignment','Left',...
    'fontsize',15)
hold on
text(mdot(I), epsilon(I), sprintf(['Maximum']),...
    'VerticalAlignment','bottom', 'HorizontalAlignment','Left',...
    'fontsize',15)
xlabel('Mass Flow [kg/s]')
ylabel('\epsilon [-]')

```

```

%title('Heat Exchanger Effectiveness vs. Mass Flow')
grid on

% Cycle efficiency as a function of mass flow
figure(04)
set(gca,'fontsize',15, 'linewidth', 2)
hold on
plot(mdot, eta, 'LineWidth',4)
hold on
plot(0.422, eta(29), '.g', 'markersize', 30)
hold on
plot(mdot(I), eta(I), '.r', 'markersize', 30)
hold on
text(0.422, eta(29), sprintf(['Design']),...
    'VerticalAlignment','bottom', 'HorizontalAlignment','Left',...
    'fontsize',15)
hold on
text(mdot(I), eta(I), sprintf(['Maximum']),...
    'VerticalAlignment','bottom', 'HorizontalAlignment','Left',...
    'fontsize',15)
xlabel('Mass Flow [kg/s]')
ylabel('\eta [-]')
%title('Cycle Efficiency vs. Mass Flow')
grid on

%% Temperature Distribution Through Single Duct, Fixed Mass Flows

% Analyzing the Temperature Profile Through the Duct for Mass FLOws

T2 = 472.491;      % [K] Collector Inlet Temperature

mdot1 = [0.01 0.42 0.96 1.5 2]'; % [kg/s] Mass Flow Samples

x = linspace(0,800,1000); % [m] Duct Length (Dependent Variable)
l = x/800; % [N/A] Normalized Length

alpha = exp(((4*Nu*k/cp)./mdot1).*x); % [N/A] Scaling Function

T = (1-1./alpha)*Tw + (1./alpha)*T2; % [K] Temperature Across Duct

% Results/Plot

figure(05)
set(gca,'fontsize',15, 'linewidth', 2)
hold on
plot(l,T(1,:), l,T(2,:), '-g', l,T(3,:), '-r', l,T(4,:), l,T(5,:),...
    'LineWidth',4)
xlabel('Normalized Duct Length [-]')
ylabel('Average Temperature [K]')
h=legend('0.010 [kg/s]', '0.422 [kg/s] (Design)',...
    '0.960 [kg/s] (Maximum)', '0.150 [kg/s]',...
    '0.200 [kg/s]')
set(h, 'Position',...
    [0.219433992346939 0.572591553287982 0.286607142857143 0.204761904761905])
%title('Average Temperature Distribution Through Single Duct')
grid on

```

THIS PAGE INTENTIONALLY LEFT BLANK

APPENDIX C. ANSYS-CFX SOLUTION REPORT FOR 50KW PLANT



Title

Solar Collector Single Duct

Author

LT Collin Roof

Date

2017/05/23 20:45:37

Contents

[1. File Report](#)

[Table 1](#) File Information for CFX 1

[2. Mesh Report](#)

[Table 2](#) Mesh Information for CFX 1

[Table 3](#) Mesh Statistics for CFX 1

[3. Physics Report](#)

[Table 4](#) Domain Physics for CFX 1

[Table 5](#) Boundary Physics for CFX 1

[4. Solution Report](#)

[Table 6](#) Boundary Flows for CFX 1

[Table 7](#) Forces and Torques for CFX 1

[5. Pictures](#)

[Figure 1](#) Pressure Profile

[Figure 2](#) Temperature Profile

[Figure 3](#) Velocity Profile

1. File Report

Table 1. File Information for CFX 1

Case	CFX 1
File Path	H:\MyDocs\Thesis\Model\SingeDuct(Scaled)_files\dp0\CFX-1\CFX\Fluid Flow CFX_061.res
File Date	22 May 2017
File Time	10:25:13 PM
File Type	CFX5
File Version	17.2

. Mesh Report

Table 2. Mesh Information for CFX 1

Domain	Nodes	Elements	Tetrahedra	Wedges	Pyramids	Hexahedra	Polyhedra
Default Domain	39200	28764	0	0	0	28764	0

Table 3. Mesh Statistics for CFX 1

Domain	Minimum Face Angle	Maximum Face Angle	Maximum Edge Length Ratio	Maximum Element Volume Ratio	Connectivity Range	
Default Domain	90 [degree]	90 [degree]	1.01691	1.00006	1	8

3. Physics Report

Table 4. Domain Physics for CFX 1

Domain - Default Domain	
Type	Fluid
Location	B30
<i>Materials</i>	
Air Ideal Gas	
Fluid Definition	Material Library
Morphology	Continuous Fluid
<i>Settings</i>	
Buoyancy Model	Non Buoyant
Domain Motion	Stationary
Reference Pressure	5.5491e+02 [kPa]
Heat Transfer Model	Total Energy
Include Viscous Work Term	Off
Turbulence Model	Laminar

Table 5. Boundary Physics for CFX 1

Domain	Boundaries	
Default Domain	Boundary - Inlet	
	Type	INLET
	Location	Inlet
	<i>Settings</i>	
	Flow Direction	Normal to Boundary Condition
	Flow Regime	Subsonic
	Heat Transfer	Static Temperature
	Static Temperature	T2
	Mass And Momentum	Mass Flow Rate
	Mass Flow Rate	MassFlow
	Mass Flow Rate Area	As Specified

Boundary - Outlet	
Type	OUTLET
Location	Outlet
<i>Settings</i>	
Flow Regime	Subsonic
Mass And Momentum	Mass Flow Rate
Mass Flow Rate	MassFlow
Mass Flow Rate Area	As Specified
Boundary - Bottom	
Type	WALL
Location	Bottom
<i>Settings</i>	
Heat Transfer	Fixed Temperature
Fixed Temperature	9.3300e+02 [K]
Mass And Momentum	No Slip Wall
Boundary - Side1	
Type	WALL
Location	Side1
<i>Settings</i>	
Heat Transfer	Fixed Temperature
Fixed Temperature	9.3300e+02 [K]
Mass And Momentum	No Slip Wall
Boundary - Side2	
Type	WALL
Location	Side 2
<i>Settings</i>	
Heat Transfer	Fixed Temperature
Fixed Temperature	9.3300e+02 [K]
Mass And Momentum	No Slip Wall

Boundary - Top	
Type	WALL
Location	Top
<i>Settings</i>	
Heat Transfer	Fixed Temperature
Fixed Temperature	9.3300e+02 [K]
Mass And Momentum	No Slip Wall

4. Solution Report

Table 6. Boundary Flows for CFX 1

Location	Type	Mass Flow	Momentum		
			X	Y	Z
Bottom	Boundary	0.0000e+00	4.3131e-10	-2.7280e-01	-6.8225e-04
Inlet	Boundary	2.1000e-01	-2.4106e-14	3.7373e-14	1.2185e-03
Outlet	Boundary	-2.1000e-01	1.3553e-07	1.6927e-07	1.5106e-03
Side1	Boundary	0.0000e+00	-2.7280e-01	3.0748e-10	-6.8225e-04
Side2	Boundary	0.0000e+00	2.7280e-01	3.3885e-10	-6.8225e-04
Top	Boundary	0.0000e+00	4.1045e-10	2.7280e-01	-6.8225e-04

Table 7. Forces and Torques for CFX 1

Location	Type	X	Y	Z
Bottom	Pressure Force	0.0000e+00	2.7280e-01	0.0000e+00
	Viscous Force	-4.3132e-10	5.6631e-07	6.8225e-04
	Total Force	-4.3132e-10	2.7280e-01	6.8225e-04
	Pressure Torque	-7.2782e+01	0.0000e+00	-3.8641e-08
	Viscous Torque	-1.0248e-03	-1.6459e-07	-6.4290e-10
	Total Torque	-7.2783e+01	-1.6459e-07	-3.9284e-08
Side1	Pressure Force	2.7280e-01	0.0000e+00	0.0000e+00
	Viscous Force	5.6630e-07	-3.0748e-10	6.8225e-04
	Total Force	2.7280e-01	-3.0748e-10	6.8225e-04
	Pressure Torque	0.0000e+00	7.2782e+01	5.6216e-08
	Viscous Torque	1.1879e-07	1.0248e-03	3.9457e-10
	Total Torque	1.1879e-07	7.2783e+01	5.6611e-08
Side2	Pressure Force	-2.7280e-01	0.0000e+00	0.0000e+00
	Viscous Force	-5.6761e-07	-3.3885e-10	6.8225e-04
	Total Force	-2.7280e-01	-3.3885e-10	6.8225e-04
	Pressure Torque	0.0000e+00	-7.2782e+01	-4.8739e-08
	Viscous Torque	1.2992e-07	-1.0253e-03	-5.9973e-10
	Total Torque	1.2992e-07	-7.2783e+01	-4.9338e-08
Top	Pressure Force	0.0000e+00	-2.7280e-01	0.0000e+00
	Viscous Force	-4.1046e-10	-5.6760e-07	6.8225e-04
	Total Force	-4.1046e-10	-2.7280e-01	6.8225e-04

	Pressure Torque	7.2782e+01	0.0000e+00	3.9689e-08
	Viscous Torque	1.0253e-03	-1.6161e-07	6.2895e-10
	Total Torque	7.2783e+01	-1.6161e-07	4.0318e-08

5. Pictures

Figure 1. Pressure Profile

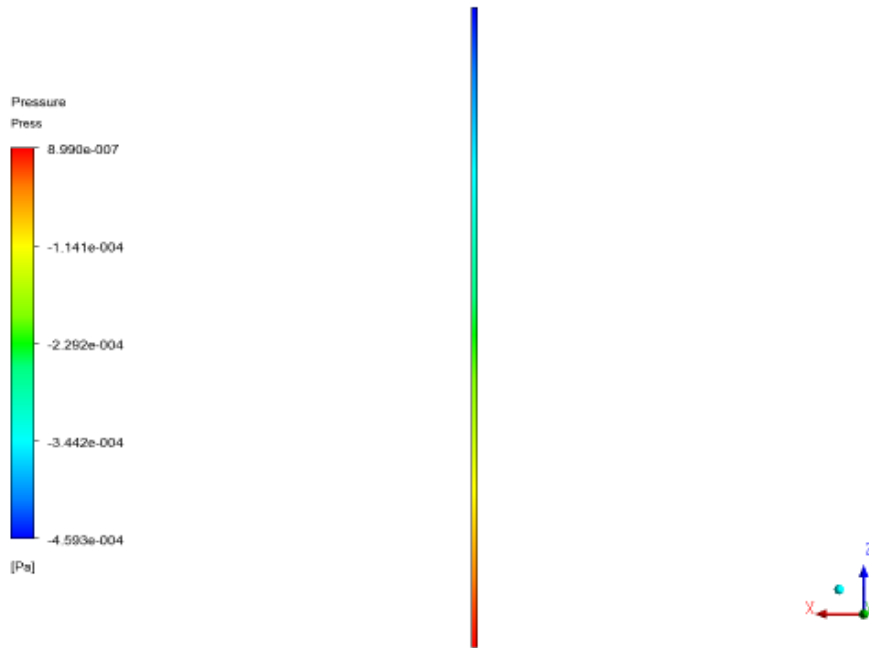


Figure 2. Temperature Profile

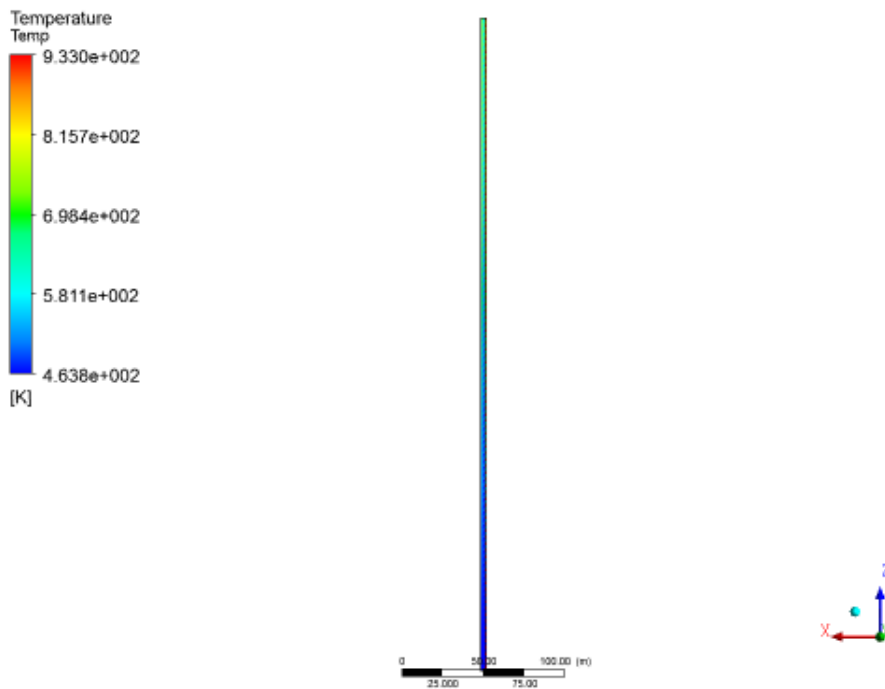
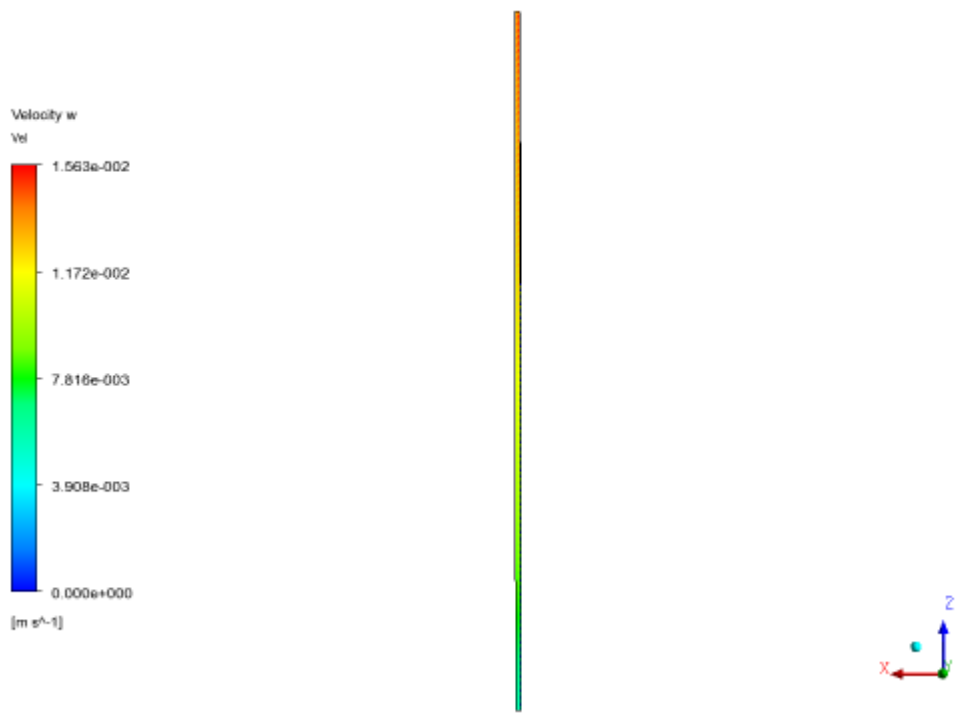


Figure 3. Velocity Profile



THIS PAGE INTENTIONALLY LEFT BLANK

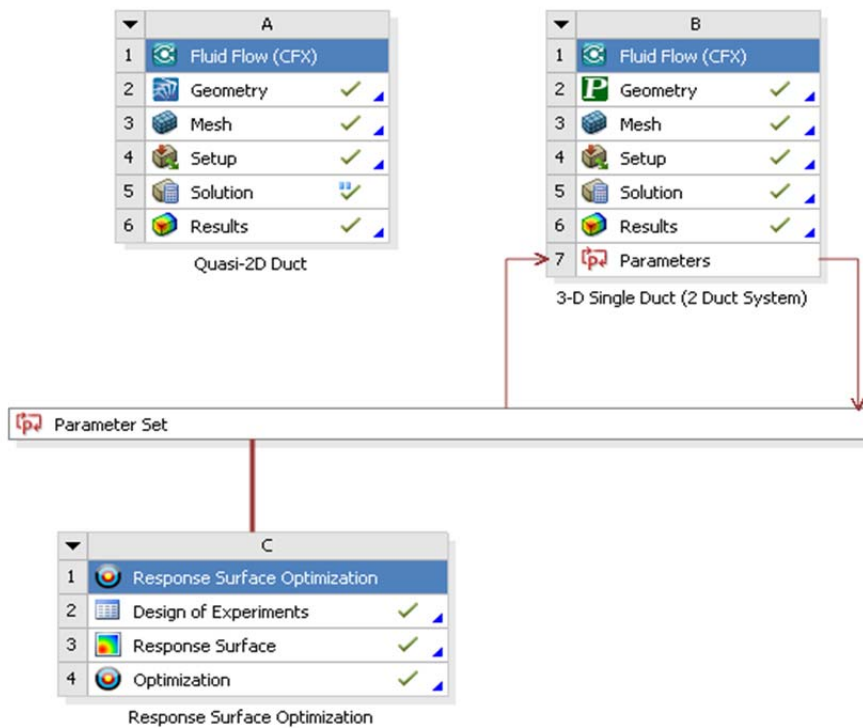
APPENDIX D. ANSYS-CFX OPTIMIZATION REPORT FOR 50KW PLANT



Summary

Project:	SingleDuct(Scaled)
Date:	5/23/2017
Time:	8:19:37 PM
Product Version:	Release 17.2
Last Saved Version:	Release 17.2

Project Schematic View



Files

Name	Size	Type	Date Modified	Location
 SingleDuct(Scaled).x_t	5 KB	Geometry File	12/2/2016 10:22:51 AM	H:\MyDocs\Thesis\Model
 CFX1.cmdb	6 MB	CFX Mesh File	2/20/2017 5:07:51 PM	dp0\CFX\MECH
 CFX.mshdb	6 MB	Mesh Database File	2/20/2017 5:07:54 PM	dp0\global\MECH
 SingeDuct(Scaled).wbj	484 KB	Workbench Project File	5/23/2017 12:24:36 AM	H:\MyDocs\Thesis\Model

Design Points

Name	P5 - MassFlow	P2 - DeltaT	P3 - Power	P4 - T3	Retained	Retained Data State	Report	Note
Units	kg s ⁻¹	K	W	K				
DP 0 (Current)	0.21	282.91	22653	747.21	yes	✓		
DP 1	0.6184							Created from Response Surface

Outline of All Parameters

ID	Parameter Name	Value	Unit
 Input Parameters			
  3-D Single Duct (2 Duct System)			
 P5	MassFlow	0.21	kg s ⁻¹
 Output Parameters			
  3-D Single Duct (2 Duct System)			
 P2	DeltaT	282.91	K

 P3	Power	22653	W
 P4	T3	747.21	K

Response Surface Optimization

Design of Experiments

The Design of Experiments is the initial step building a Response Surface over the design space. This section describes the selected input parameters and their variation range, the chosen Design of Experiments type, and the generated Matrix of Experiments.

Parameters

The explored design space is defined by the range of variation of the following 1 input parameters.

ID	Name	Classification	Lower Bound	Upper Bound
P5	MassFlow	Continuous	0.01 [kg s ⁻¹]	1 [kg s ⁻¹]

Design of Experiments Properties

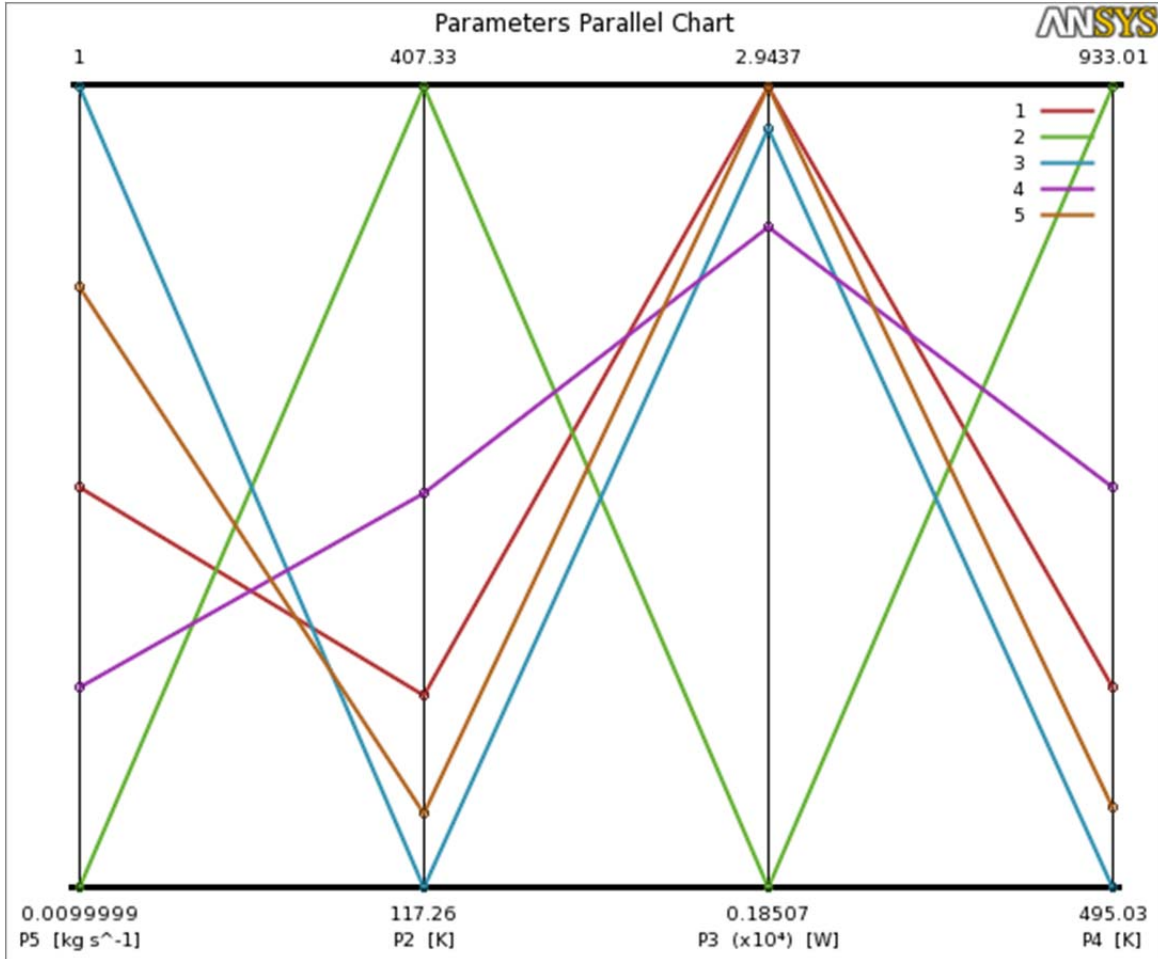
Property	Value
Design of Experiments Type	Central Composite Design
Design Type	Auto Defined

Matrix of Experiments

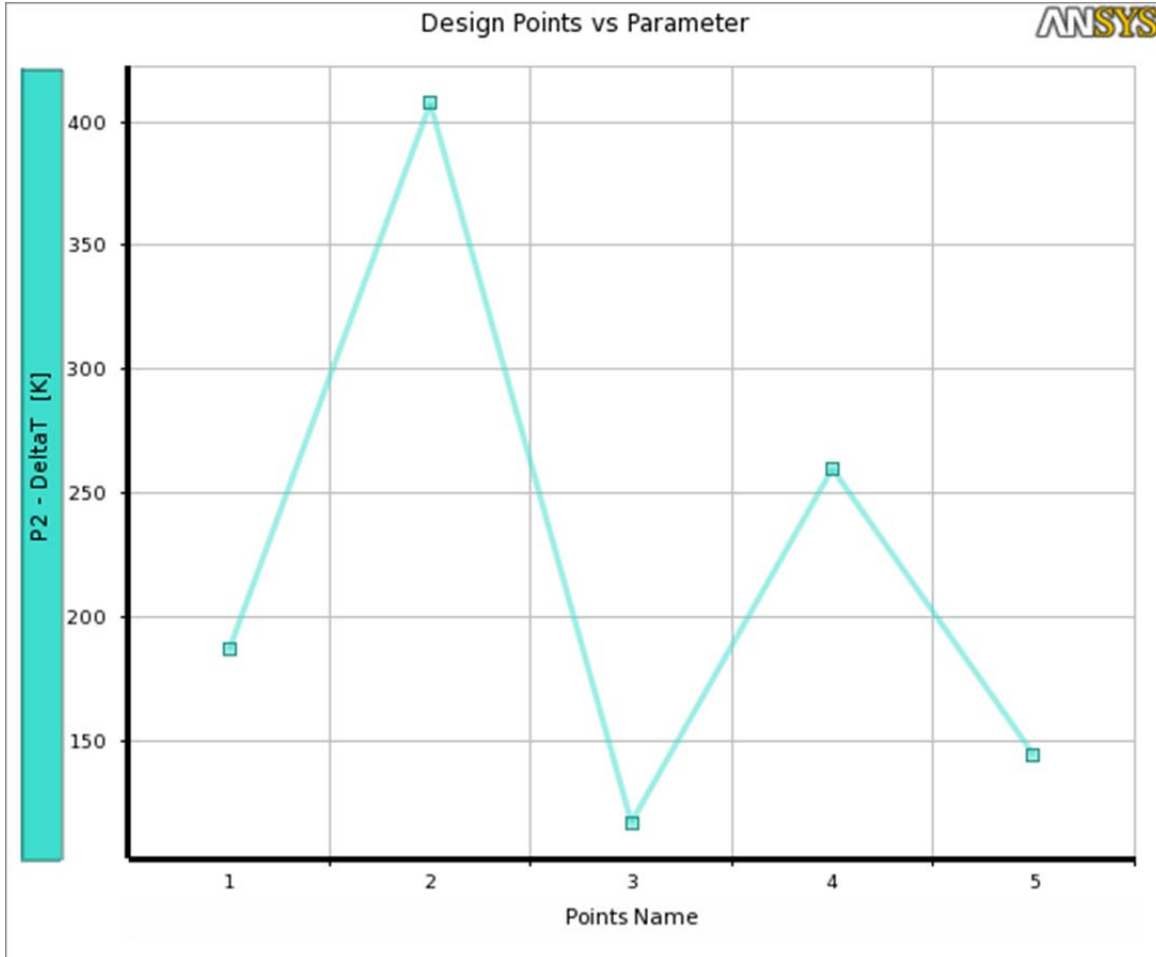
All of the 5 points are up-to-date.

[The full Matrix of Experiments is provided in the Appendices.](#)

Parameters Parallel Chart



Design Points vs Parameter Chart



Response Surface

The Response Surface is a meta-model built from the Design of Experiments for an efficient exploration of the design space. This section describes the selected type of meta-model, including its properties, the obtained quality, and the generated Response Points and charts.

Response Surface Properties

Property	Value
Response Surface Type	Genetic Aggregation
Random Generator Seed	0
Maximum Number of Generations	12

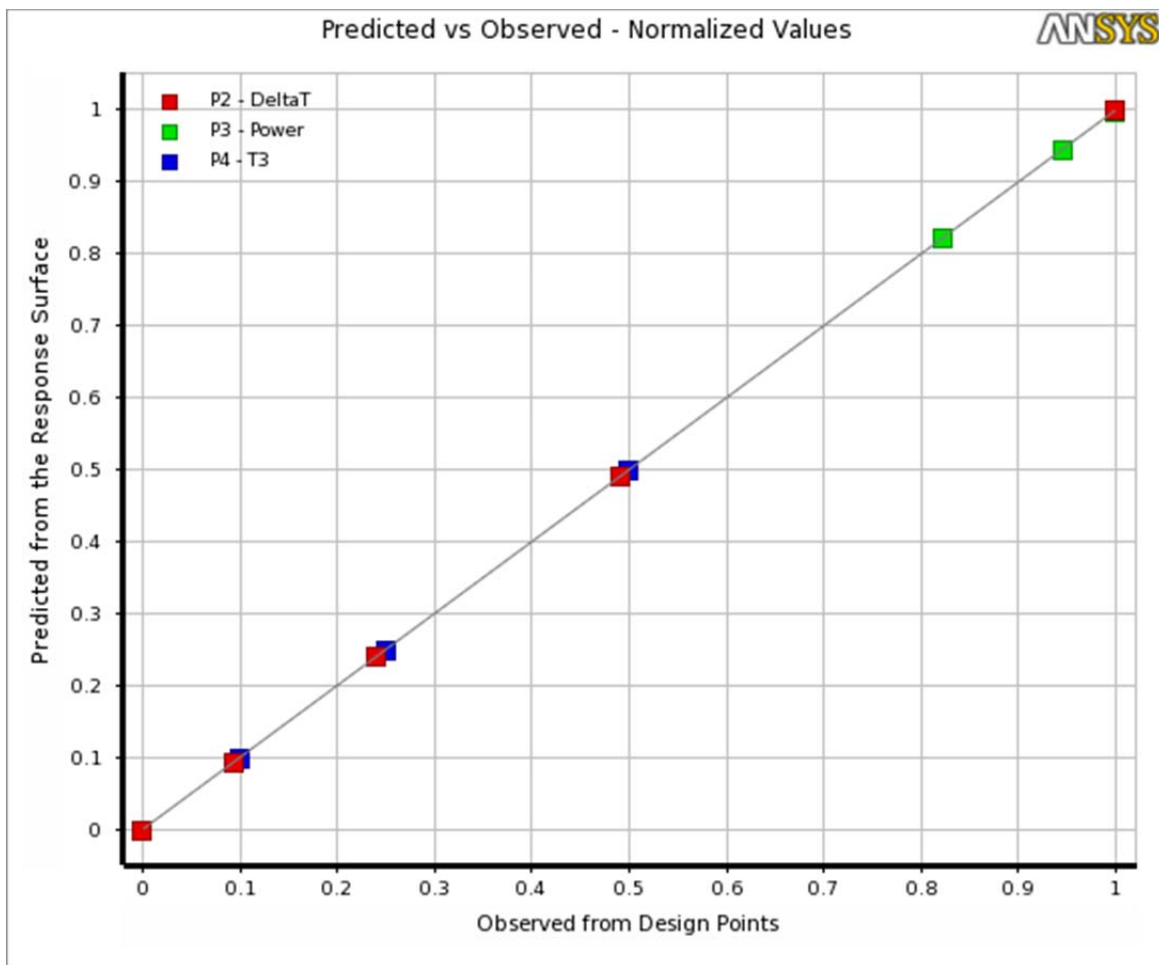
Display Level	Final
Generate Verification Points	No

Goodness of Fit

The Goodness of Fit report provides charts and metrics to understand how each output parameter is approximated by the response surface.

Details of ‘Goodness Of Fit’

Predicted vs Observed Scatter Chart



	P2 - DeltaT	P3 - Power	P4 - T3
Coefficient of Determination (Best Value = 1)			
Learning Points	★ ★ ★ ₁	★ ★ ★ ₁	★ ★ ★ ₁

Cross-Validation on Learning Points	 1	 1	 1
Root Mean Square Error (Best Value = 0)			
Learning Points	7.8215E-05	4.4538E-05	7.1423E-06
Cross-Validation on Learning Points	0.00037587	0.00033711	1.3094E-05
Relative Maximum Absolute Error (Best Value = 0%)			
Learning Points	 0	 0	 0
Cross-Validation on Learning Points	 0.00066882	 6.1964E-06	 1.0682E-05
Relative Average Absolute Error (Best Value = 0%)			
Learning Points	 0	 0	 0
Cross-Validation on Learning Points	 0.00022649	 1.7665E-06	 6.3594E-06

Minimum and maximum values

This section reports the minimum and maximum values for each output parameter. These values are approximations found by the Min-Max Search on the Response Surface.

Name	Minimum value	Maximum value
P2 - DeltaT (K)	117.26	407.33
P3 - Power (W)	1850.7	29731
P4 - T3 (K)	495.04	933

[The input parameter values corresponding to the minimum and maximum values are provided in the Appendices.](#)

Response Points

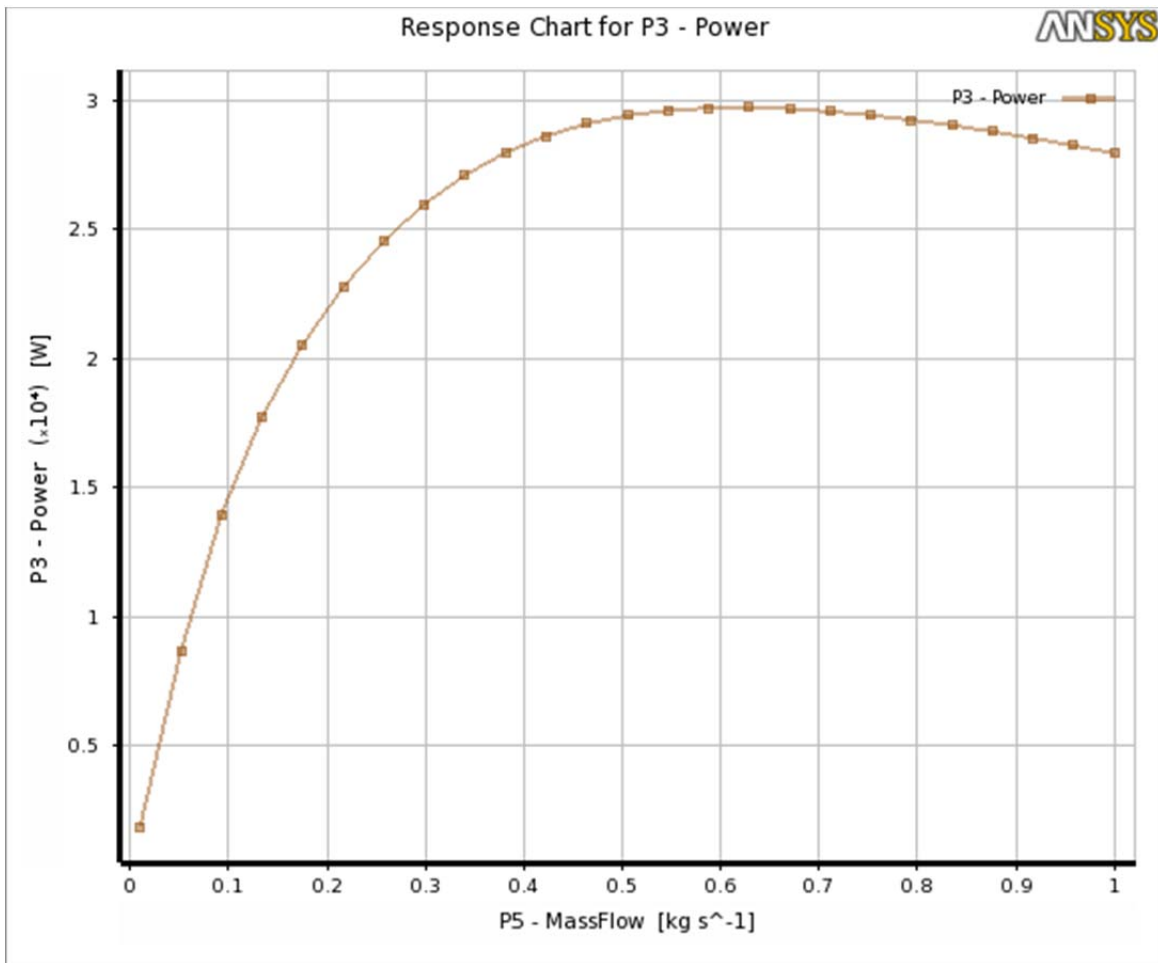
The Response Points provide the output parameter values obtained by evaluating the Response Surface. This section lists all the Response Points and their associated charts.

Name	P5 - MassFlow (kg s ⁻¹)	P2 - DeltaT (K)	P3 - Power (W)	P4 - T3 (K)	Report
------	-------------------------------------	-----------------	----------------	-------------	--------

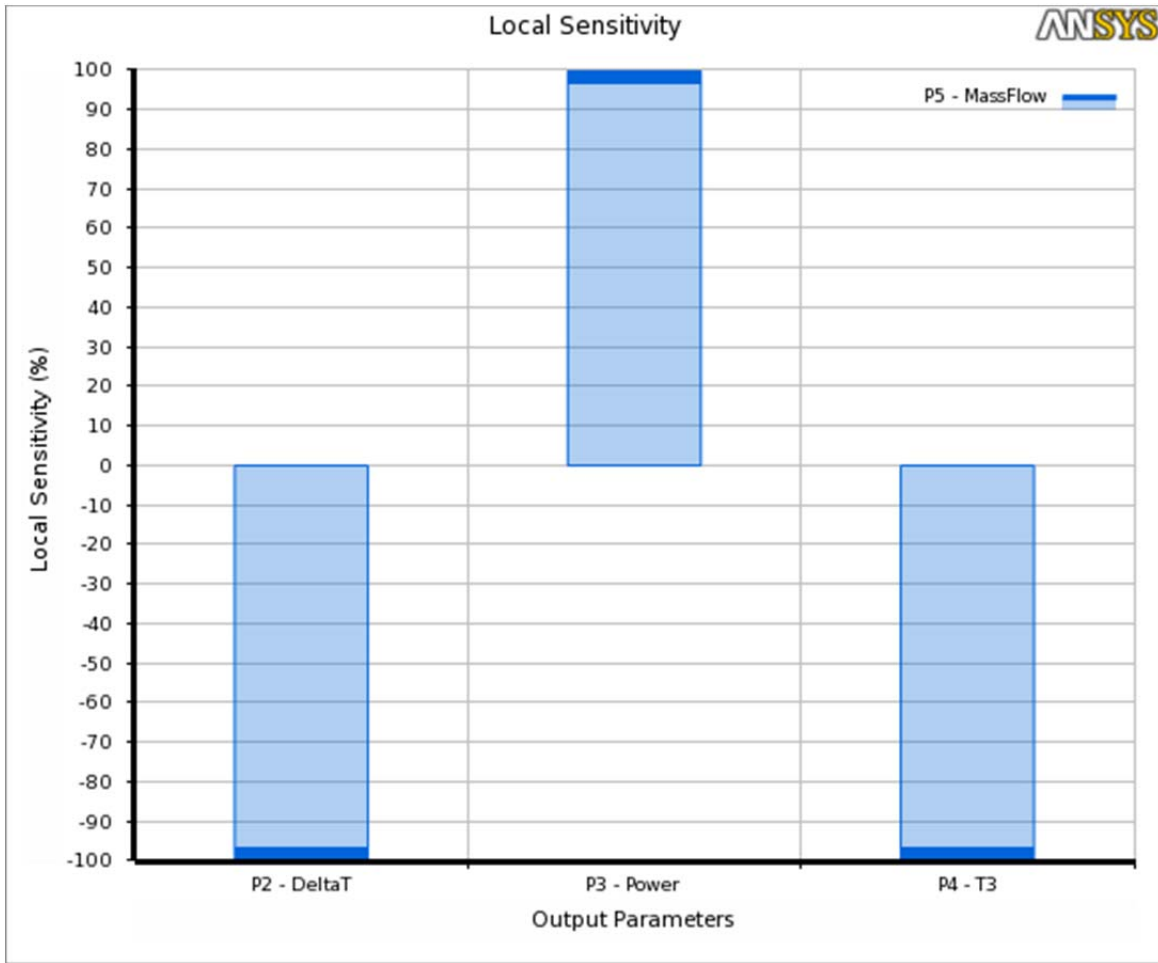
Response Point	0.505	187.07	29424	604.63	
----------------	-------	--------	-------	--------	--

Details of 'Response Point'

Response Chart

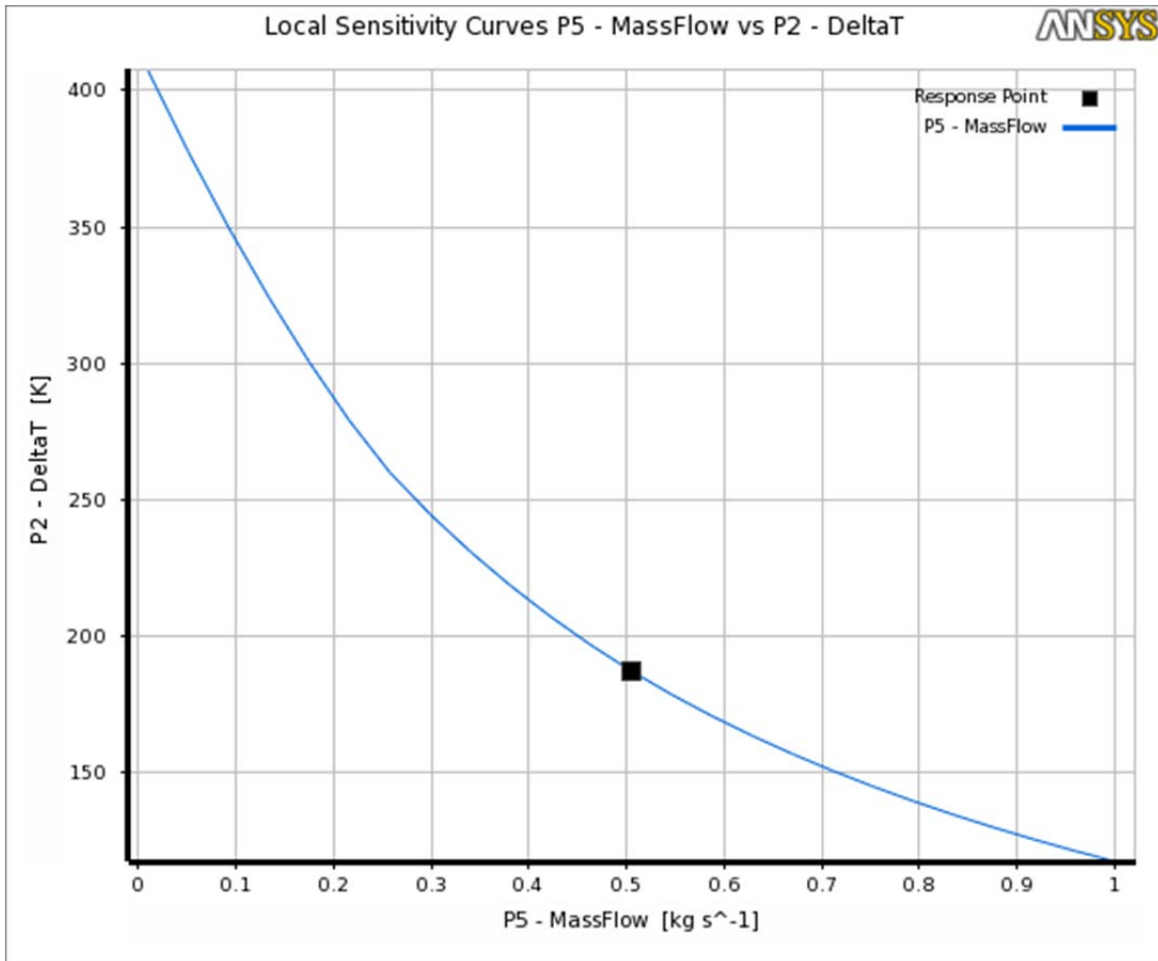


Local Sensitivity Chart

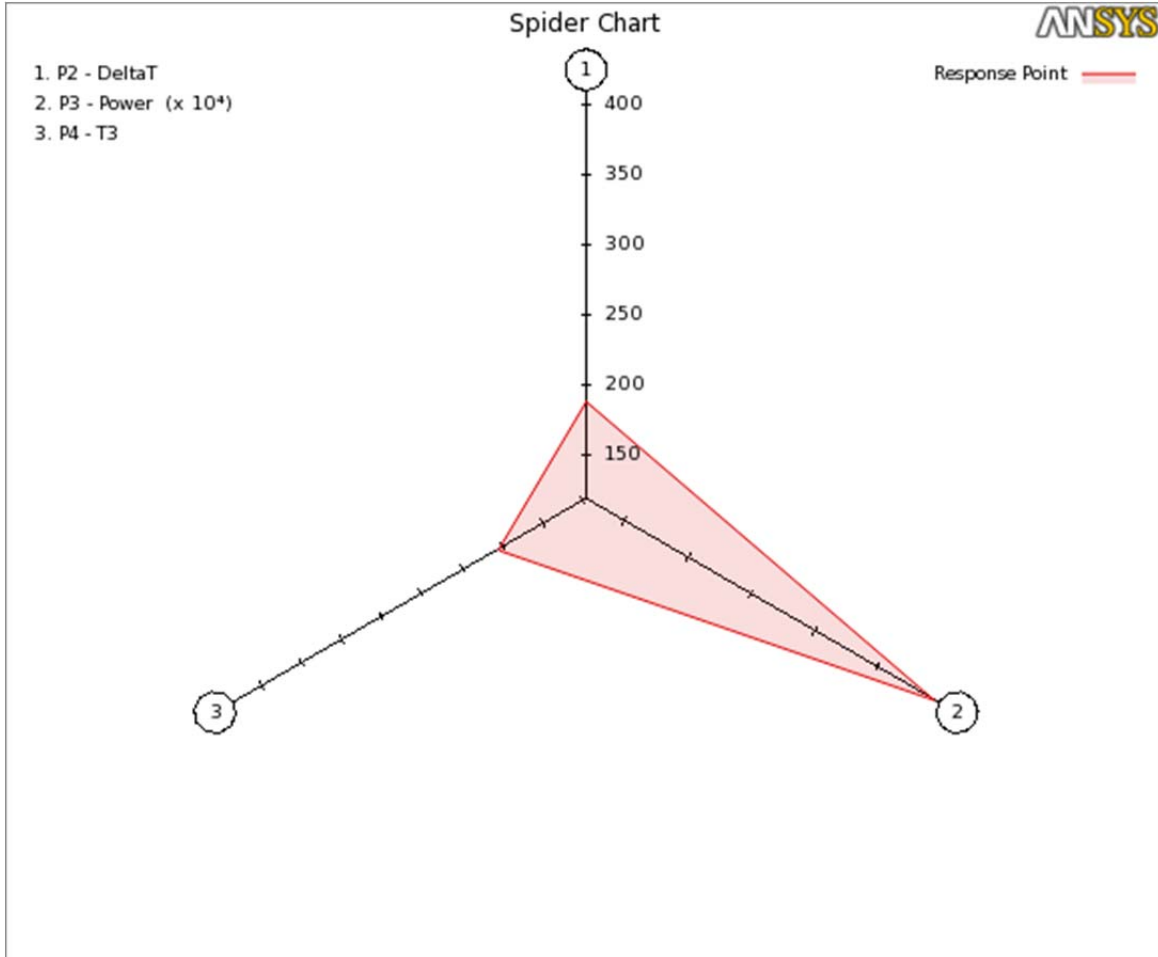


Local Sensitivity Curves Chart

Axes Range = Use Min Max of the Output Parameter



Spider Chart



Optimization

The Optimization is based on Response Surface evaluations. This section describes the chosen Optimization type and the generated candidates and charts.

Parameters

The explored design space is defined by the range of variation of the following 1 input parameters.

ID	Name	Classification	Lower Bound	Upper Bound
P5	MassFlow	Continuous	0.01 [kg s ⁻¹]	1 [kg s ⁻¹]

Properties

Property	Value
Method Name	Screening
Verify Candidate Points	No
Number of Samples	1000
Maximum Number of Candidates	3

Definition

Objectives and constraints of the optimization study

P5 - MassFlow (kg s ⁻¹)		P3 - Power (W)
Domain	[0.01;1]	
Objective		Maximize

Description

Optimization Method	
Screening	The Screening optimization method uses a simple approach based on sampling and sorting. It supports multiple objectives and constraints as well as all types of input parameters. Usually it is used for preliminary design, which may lead you to apply other methods for more refined optimization results.
Configuration	Generate 1000 samples and find 3 candidates.
Status	Converged after 1000 evaluations.

Status

Property	Value
Converged	Yes
Number of Evaluations	1000
Number of Failures	0
Size of Generated Sample Set	1003

Number of Candidates	3
----------------------	---

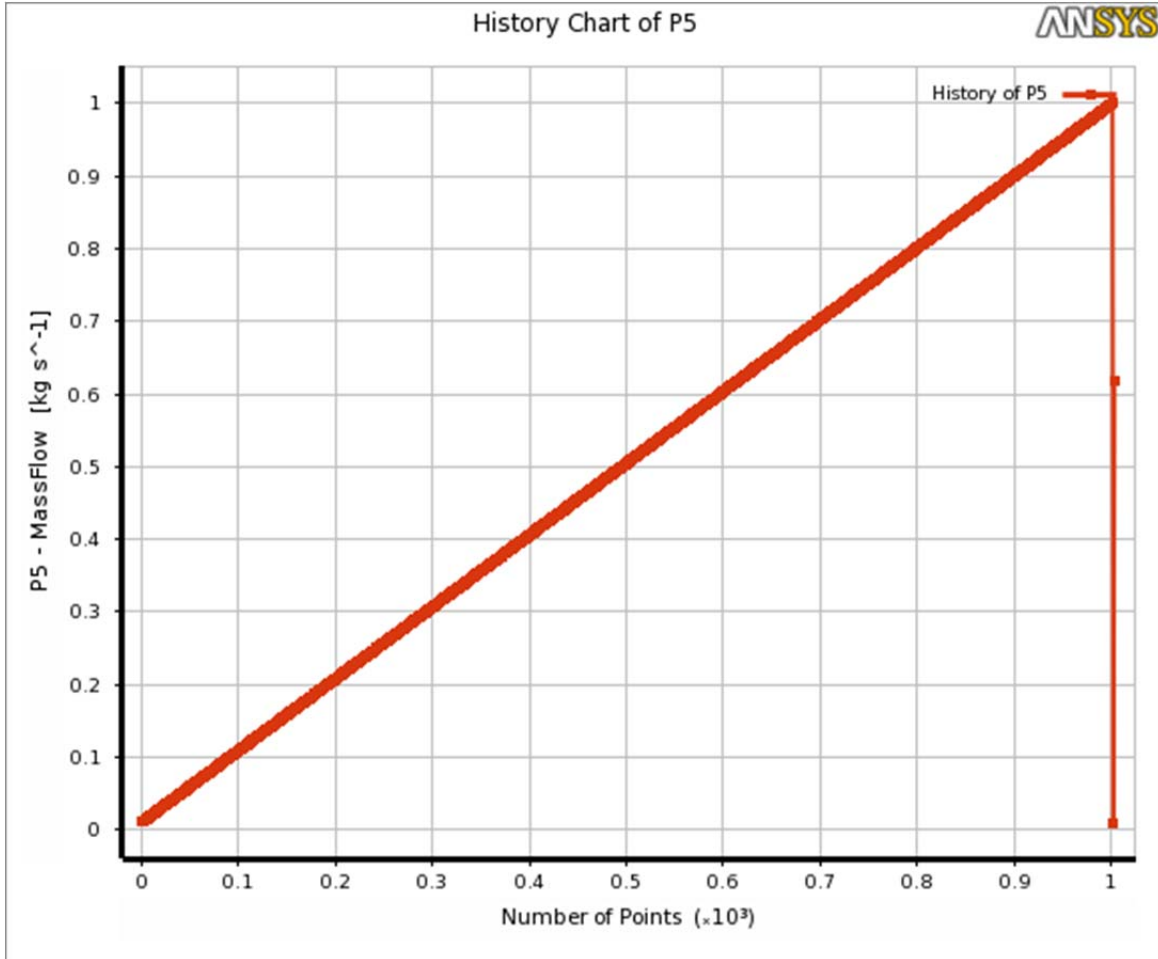
Candidates

Candidates of the optimization study

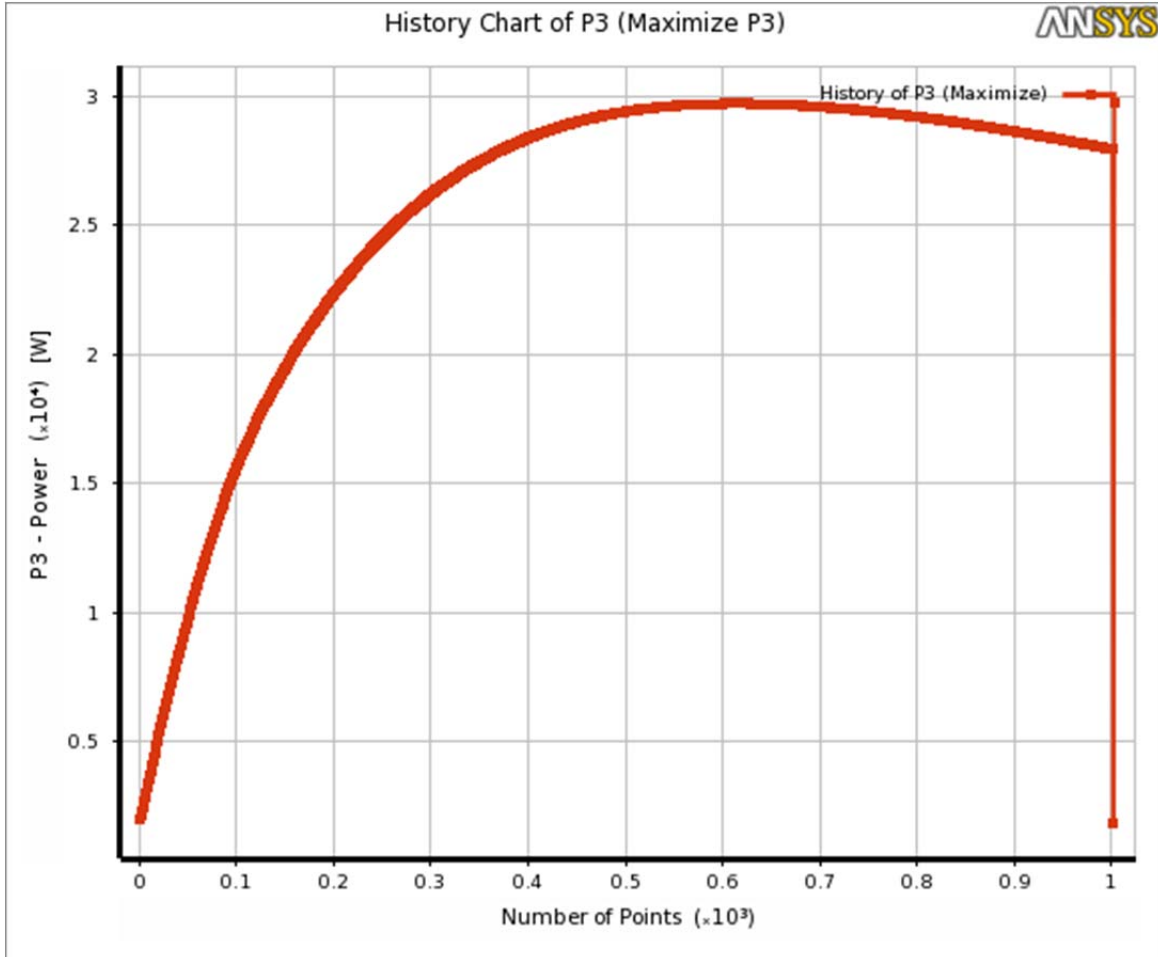
	P5 - MassFlow (kg s ⁻¹)	P2 - DeltaT (K)	P3 - Power (W)	P4 - T3 (K)	Report
Candidate Point 1	0.6176	165.24	 29731	570.75	
Candidate Point 2	0.67875	155.31	 29664	555.37	
Candidate Point 3	0.74013	146.41	 29484	541.51	

[The table of Rating Values is provided in the Appendices.](#)

History Chart

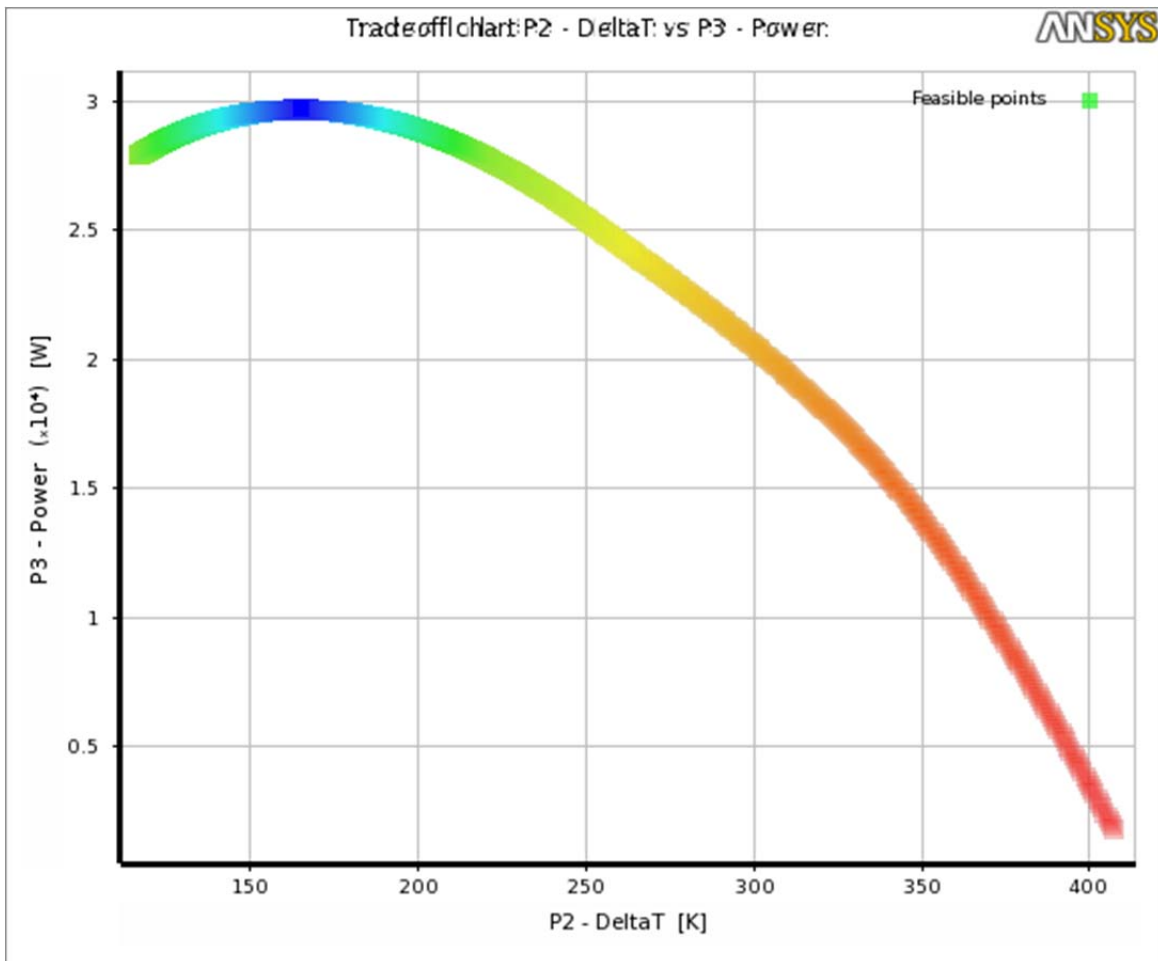


History Chart



Tradeoff Chart

Number of Pareto Fronts to Show = 995/995

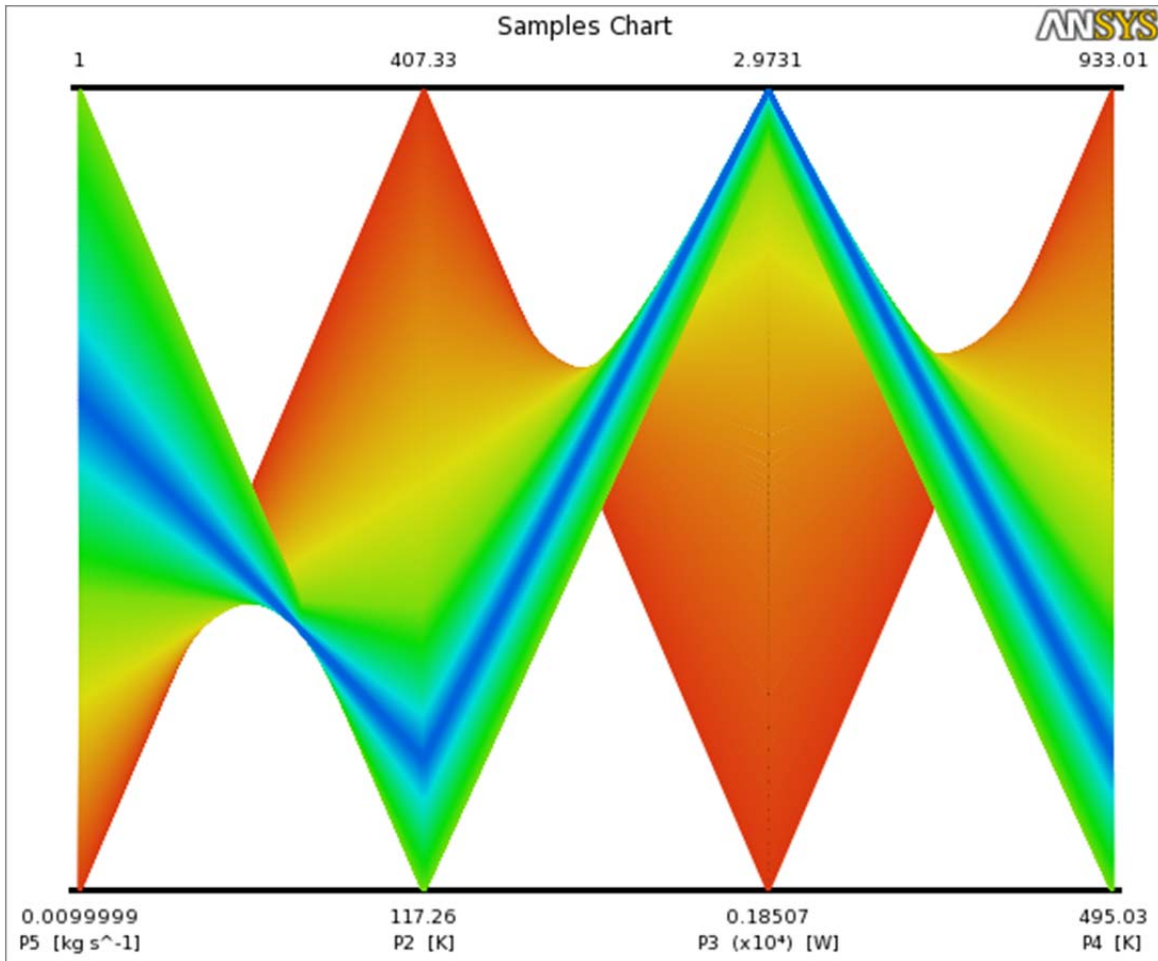


Samples Chart

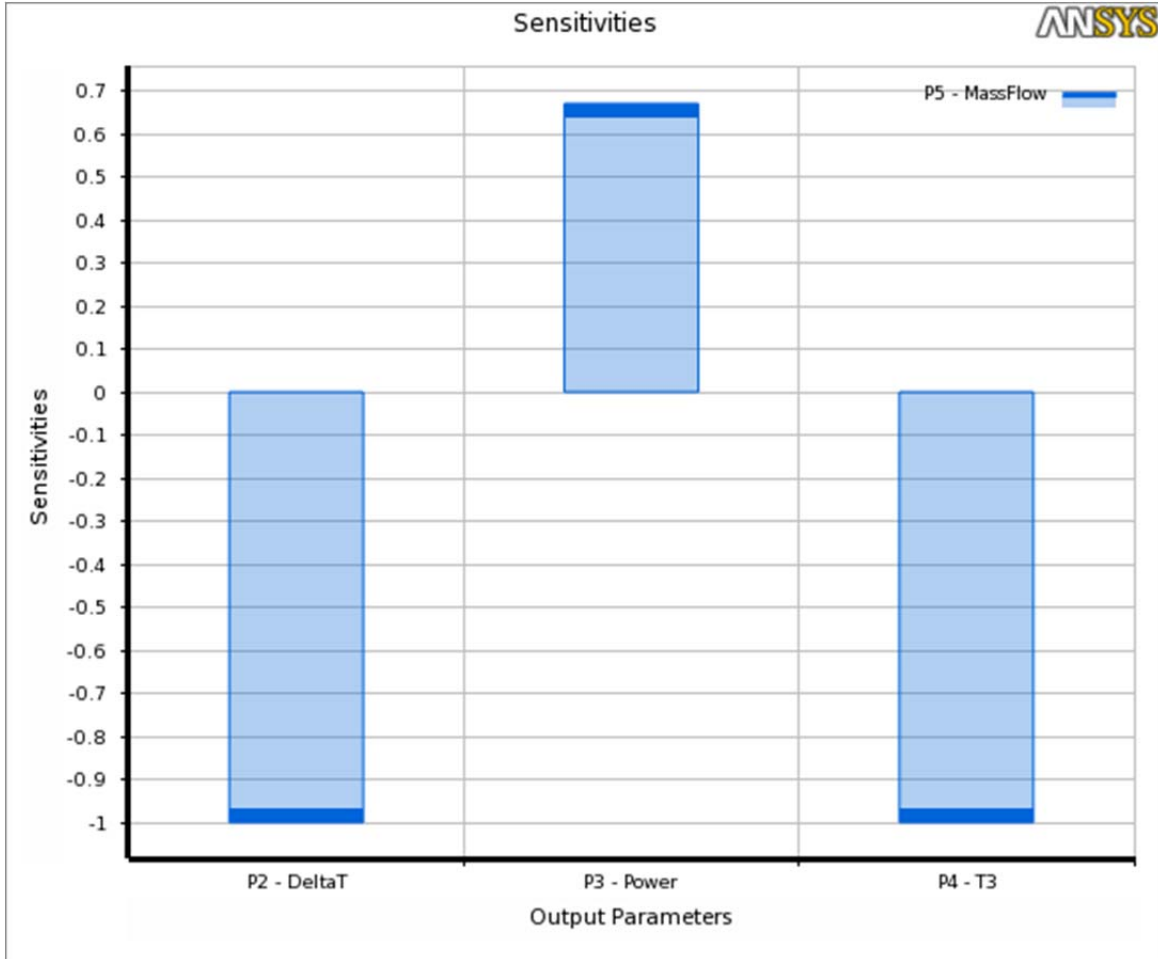
Mode = Pareto Fronts

Coloring method = per Pareto Front

Number of Pareto Fronts to Show = 995/995

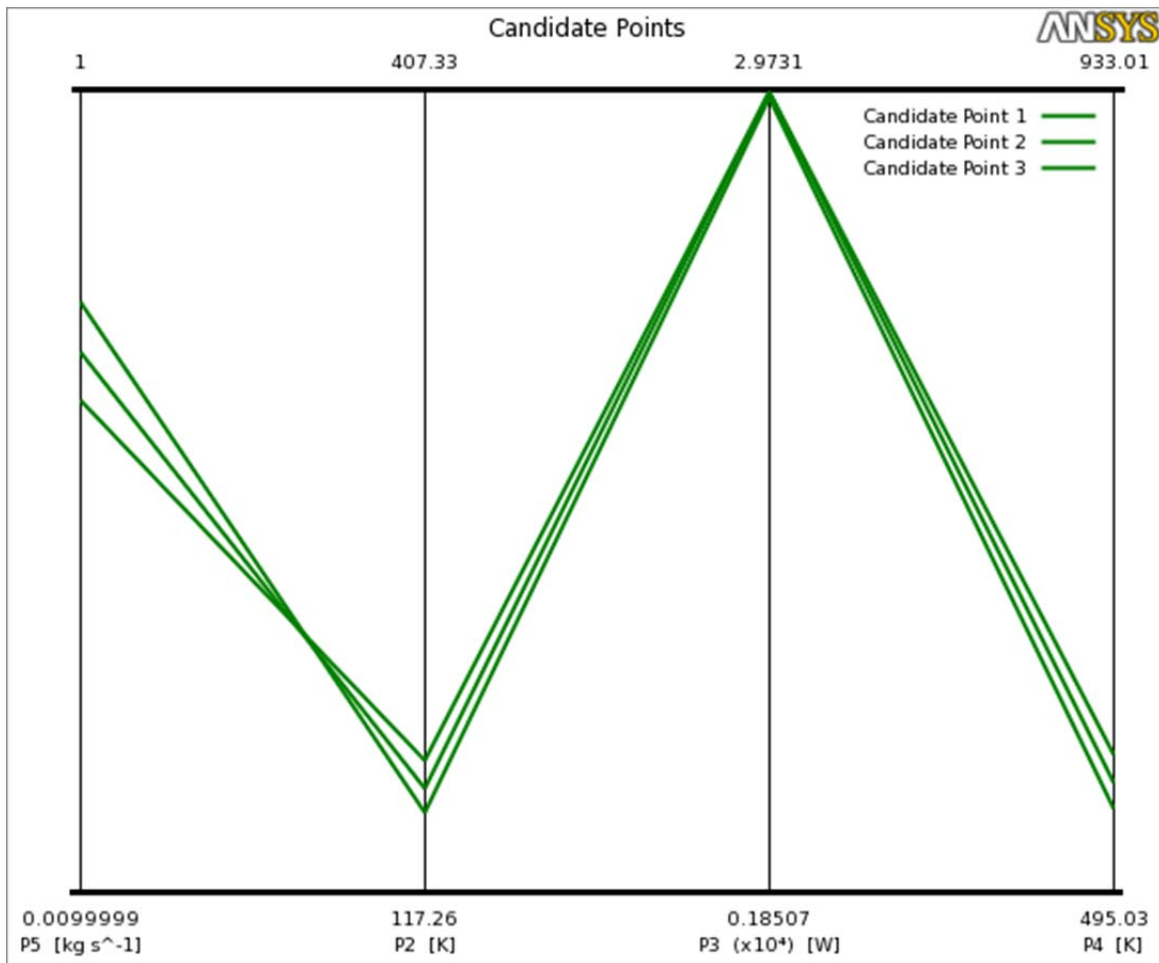


Sensitivities Chart



Candidates Chart

Coloring method = per Candidate



Appendix

Matrix of Experiments (Response Surface Optimization system)

Name	P5 - MassFlow (kg s ⁻¹)	P2 - DeltaT (K)	P3 - Power (W)	P4 - T3 (K)	Report
1	0.505	187.07	29424	604.63	
2	0.01	407.33	1850.7	933	
3	1	117.26	27959	495.04	
4	0.2575	260.01	24557	713.76	
5	0.7525	144.73	29437	538.88	

Output Parameter Minimums (Response Surface Optimization system)

Name	P5 - MassFlow (kg s ⁻¹)	P2 - DeltaT (K)	P3 - Power (W)	P4 - T3 (K)
P2 - DeltaT	1	117.26	27959	495.04
P3 - Power	0.01	407.33	1850.7	933
P4 - T3	1	117.26	27959	495.04

Output Parameter Maximums (Response Surface Optimization system)

Name	P5 - MassFlow (kg s ⁻¹)	P2 - DeltaT (K)	P3 - Power (W)	P4 - T3 (K)
P2 - DeltaT	0.01	407.33	1850.7	933
P3 - Power	0.6176	165.24	29731	570.75
P4 - T3	0.01	407.33	1850.7	933

Table of Rating Values (Response Surface Optimization system)

P3 - Power (W)	
Objective	Maximize
	[27407 ; 29731]
	[22761 ; 27407]
	[18114 ; 22761]
	[13467 ; 18114]
	[8820.7 ; 13467]
	[4174 ; 8820.7]
	[1850.7 ; 4174]

APPENDIX E. ANSYS-CFX OPTIMIZATION RAW DATA FOR 50KW PLANT

Mass Flow [kg/s]	T3 [K]	dT [K]	Power [kW]
0.02	933	407.3290384	3.701339955
0.1025	898.6047457	377.5018905	17.23358692
0.185	862.0005805	349.7800669	27.90234773
0.2675	824.1123246	324.113039	35.49245444
0.35	785.8689574	300.4774403	41.08261961
0.4325	748.3235337	278.9230139	45.53495101
0.515	713.7579984	260.0088857	49.11380011
0.5975	691.6929407	244.6514758	51.97397773
0.68	671.6875067	230.9024898	54.22868854
0.7625	652.98166	218.3910802	55.96955214
0.845	635.536148	206.9727605	57.27484372
0.9275	619.3964533	196.5559324	58.21355049
1.01	604.6250075	187.0721207	58.84759985
1.0925	591.2289457	178.4503371	59.23398199
1.175	579.0219231	170.574234	59.42401775
1.2575	567.8161804	163.3392515	59.45684005
1.34	557.4652728	156.6625267	59.3618072
1.4225	547.8526508	150.4770975	59.1614127
1.505	538.8839875	144.7279626	58.87320006
1.5875	530.4818445	139.3693151	58.51106224
1.67	522.5818596	134.3625463	58.08614696
1.7525	515.1299579	129.6747742	57.60750197
1.835	508.0802721	125.2777347	57.08254418
1.9175	501.3935634	121.1469344	56.51740676
2	495.0360063	117.2609916	55.91720001

THIS PAGE INTENTIONALLY LEFT BLANK

LIST OF REFERENCES

- [1] Schwartz, M. et al., 2012, “Department of Defense Energy Initiatives: Background and Issues for Congress,” Cong. Research. Serv., Washington, DC, Rep. R42558.
- [2] Feldman, R., 2014, “Renewable Energy for Military Installations: 2014 Industry Review,” Amer. Council. On Renew. Ener., Washington, DC
- [3] Mabus, R., 2012, “Strategy for Renewable Energy,” U.S. Depart. of the Navy, Washington, DC
- [4] Solar Energy Industries Association, 2013, “Enlisting the Sun: Powering the U.S. Military with Solar Energy 2013,” Washington, DC
- [5] McGinn, D., 2016, “Microgrids: Macro Benefits for our Navy Bases,” <http://navylive.dodlive.mil/2016/05/02/microgrids-macro-benefits-for-our-navy-bases/>
- [6] Office of the Secretary of the Navy, 2012, Renewable Energy Projects, <http://greenfleet.dodlive.mil/energy/shore/renewable-energy-projects/>
- [7] National Renewable Energy Laboratory, 2012, Dynamic Maps, GIS Data, and Analysis Tools, <http://www.nrel.gov/gis/solar.html>
- [8] IRENA and IEA-ETSAP, 2013, “Technology Brief 4: Thermal Energy Storage,” <https://www.irena.org/DocumentDownloads/Publications/IRENA-ETSAP%20Tech%20Brief%20E17%20Thermal%20Energy%20Storage.pdf>
- [9] Solar Reserve, n.d., Molten Salt Energy Storage, <http://www.solarreserve.com/en/technology/molten-salt-energy-storage>
- [10] Herrmann, U. and Kearney, D., 2002, “Survey of Thermal Energy Storage for Parabolic Trough Power Plants,” *J. Sol. Energy Eng.*, **124(2)**, pp. 145–152.
- [11] Hinke, T., 2014, “Hot Thermal Storage in a Variable Power, Renewable Energy System,” M.S. thesis, Mech. Eng., Naval Postgraduate School, Monterey, CA.
- [12] National Renewable Energy Laboratory, 2017, Concentrating Solar Power Projects: Andasol-1, https://www.nrel.gov/csp/solarpaces/project_detail.cfm/projectID=3
- [13] Skumanich, A., 2011, CSP: Developments in Heat Transfer and Storage Materials, <http://www.renewableenergyfocus.com/view/17095/csp-developments-in-heat-transfer-and-storage-materials/>

- [14] Abutayeh, M. et al., 2016, “A Case Study of Augmenting Solar Power Generation With Thermal Energy Storage,” in *ASME 2016 10th International Conference on Energy Sustainability*, Charlotte, NC, pp. 1–8.
- [15] Roman, C. and Fireteanu, V., 2011, “An Overview on Solar Energy, Molten Salts and Electromagnetic Pumping Technologies,” <http://ieeexplore.ieee.org/stamp/stamp.jsp?arnumber=5874692>
- [16] Gil, A. et al., 2015, “Design of a 100 kW Concentrated Solar Power on Demand Volumetric Receiver With Integral Thermal Energy Storage Prototype,” in *ASME 2015 Power Conference*, San Diego, CA, pp. 1–7.
- [17] Li, X. et al., 2013, “Metallic Composites Phase-Change Materials for High-Temperature Thermal Energy Storage,” in *ASME 2013 7th International Conference on Energy Sustainability*, Minneapolis, MN, pp. 1–5.
- [18] Kotze, J. and von Backstrom, T., 2013, “High Temperature Thermal Energy Storage Utilizing Metallic Phase Change Materials and Metallic Heat Transfer Fluids,” *J. Sol. Energy Eng.*, **135**(3), pp. 1–6.
- [19] Jiang, Y. et al., 2016, “A New Phase Change Material for High Temperature Thermal Energy Storage,” in *ASME 2016 10th International Conference on Energy Sustainability*, Charlotte, NC, pp. 1–6.
- [20] Borgnakke, C. and Sonntag, R., 2009, *Fundamentals of Thermodynamics*, Seventh ed., Hoboken, J. Wiley & Sons, Inc.
- [21] ME Mechanical, 2016, Brayton Cycle, <https://me-mechanicalengineering.com/brayton-cycle/>
- [22] Greitzer, E. et al., n.d., 3.7: Brayton Cycle, <http://web.mit.edu/16.unified/www/SPRING/propulsion/notes/node27.html>
- [23] Incropera, F. et al., 2007, *Introduction to Heat Transfer*, Fifth ed., Hoboken, J. Wiley & Sons, Inc., pp. 456–498.
- [24] Rodriguez-Sanchez, M. et al., 2013, “New Designs of Molten-Salt Tubular-Receiver for Solar Power Tower,” *Energy Pro.*, **49**, pp. 504–513.
- [25] Global Digital Central, n.d., File:Fig5.4.png, [Online], Available <http://www.thermalfluidscentral.org/encyclopedia/index.php/File:Fig5.4.png>. Accessed Jun. 1, 2017.

INITIAL DISTRIBUTION LIST

1. Defense Technical Information Center
Ft. Belvoir, Virginia
2. Dudley Knox Library
Naval Postgraduate School
Monterey, California